Abstract

Title of Dissertation: BLACK HOLE DYNAMICS AND GRAVITATIONAL RADIATION IN GALACTIC NUCLEI

Vanessa Michelle Lauburg, Doctor of Philosophy, 2009

Dissertation directed by: Professor M. Coleman Miller
Department of Astronomy

In this dissertation, we present new channels for the production of gravitational radiation sources: mergers of black holes in the nuclear star clusters found in many small galaxies, and mergers and tidal separations of black hole binaries in galaxies that host supermassive black holes. Mergers between stellar-mass black holes will be key sources of gravitational radiation for ground-based detectors. However, the rates of these events are highly uncertain, because we can not observe these binaries electromagnetically. In this work, we show that the nuclear star clusters found in the centers of small galaxies are conducive environments for black hole mergers. These clusters have large escape velocities, high stellar densities, and large numbers of black holes that will have multiple close encounters, which often lead to mergers. We present simulations of the three-body dynamics of black holes in this environment and estimate that, if many nuclear star clusters do not have supermassive black holes, tens of events per year will be detectable with Advanced LIGO. Larger galaxies that host supermassive black holes can produce extreme-mass ratio inspiral (EMRI) events, which are important sources for the future space-based detector, LISA. Here, we show that tidal separation of black hole binaries by supermassive black holes will produce a distinct class of EMRIs with near-zero eccentricities, and we estimate that rates from tidal separation could be comparable to or larger than those from the

traditionally-discussed two-body capture formation scenario. Before tidal separation can occur, a binary encounters multiple stars as it sinks through the nucleus toward the supermassive black hole. In this region, velocities are high, and interactions with stars can destroy binaries through ionization. We investigate wide ranges in initial mass function and internal energy of the binaries, and find that tidal separations, mergers, and ionizations are all likely outcomes for binaries near the galactic center. Tidally separated binaries will contribute to the LISA detection rate, and mergers will produce ∼tens of events per year for Advanced LIGO. We show, therefore, that galactic nuclei are promising hosts of gravitational wave sources for both LISA and LIGO.

BLACK HOLE DYNAMICS AND GRAVITATIONAL RADIATION IN GALACTIC NUCLEI

by

Vanessa Michelle Lauburg

Dissertation submitted to the Faculty of the Graduate School of the
University of Maryland at College Park in partial fulfillment
of the requirements for the degree of
Doctor of Philosophy
2009

Advisory Committee:

Professor M. Coleman Miller, chair
Doctor Richard F. Mushotzky
Professor Christopher S. Reynolds
Professor Derek C. Richardson
Professor Gregory W. Sullivan

Preface

This dissertation consists of six chapters including an introduction and two additional background chapters. Chapter 4 appeared in *The Astrophysical Journal* as "Mergers of Stellar-Mass Black Holes in Nuclear Star Clusters" (Miller & Lauburg 2009), and Chapter 5 was published in *The Astrophysical Journal* as "Binary Encounters with Supermassive Black Holes: Zero-Eccentricity LISA Events" (Miller et al. 2005).

To Jamie.

Acknowledgements

I am very grateful to my advisor, Cole Miller, for all of the encouragement and guidance he has given me over the years. His unending enthusiasm for science and his keen insight have been invaluable to me in my thesis work. Since my first semester in graduate school, I have admired him as a teacher, and I hope that my future students will learn as much from me as I have from him.

I would also like to thank Richard Mushotzky, Chris Reynolds, Derek Richardson, and Greg Sullivan for serving on my thesis committee.

Thanks to Doug Hamilton, Derek Richardson, and Kayhan Gültekin for always being willing to talk about my research, and for their ideas and assistance.

I am thankful to Stan Whitcomb, Jay Marx, Fred Raab, and everyone in the LIGO groups at Caltech and Hanford. Meeting with all of you, seeing your facilities, and giving the seminars that you arranged were true highlights in my graduate career.

Thanks to my family for being so wonderful, fun, and caring. I especially want to thank my mom, who supports me without fail, and whose generosity and kindness I admire; and my dad, who introduced me to the Beatles, who is funny and loving, and very good at math! Thanks also to my grandparents, Odice, Susie, Marjorie, and Robert.

Thanks to my friends who are all funny, smart, and good-looking. In particular, I want to mention my graduate classmates Stacy, Stephanie, Misty, Laura, Huaning, Carl, and Franziska, as well as other astronomy-related friends: Frances, Megan, Lisa, Rick, Hez, Jen, Matthew, Rob, Ashley, Katie, Mike, Kelly, Rahul, Daniel, Claudia, and Steve.

Also, thanks to Beren, Wyvin, Jorge, Shadow, Talegamp, and Lia. You know who you are.

Lastly, I'd like to thank Jamie. He always says something unexpected to make me laugh and reassures me when I feel low. Also, his beard is very fetching.

Contents

List of Tables

List of Figures

Chapter 1

Introduction

"Galileo, with an opera-glass, discovered a more splendid series of celestial phenomena than anyone since."

—Ralph Waldo Emerson, from *Self-Reliance*

1.1 Painting the Big Picture with a New Brush

Galileo, upon turning his spyglass to the night sky, discovered a fundamentally new way to examine the universe. His telescope not only uncovered a wealth of detail in objects studied for eons by naked-eye astronomers, but paved the way to the discovery of new classes of objects that would in turn intrigue future generations. Now, some 400 years later, gravitational radiation detectors are poised to afford us another rare opportunity to view the cosmos through a fresh set of eyes. With these instruments we will expand our knowledge of known sources, and, undoubtedly, be surprised by many that we have not yet imagined. We will confirm our understanding of well-studied processes, such as the decaying orbits of binary pulsars, gain insight into elusive aspects of galaxy formation, and, perhaps, find echos

left over from the formation of the universe itself. In these ways and many others, the detection and study of gravitational waves will act in concert with electromagnetic observations, but for one class of object in particular gravitational radiation provides the only means of direct detection: black holes.

Black holes are at once simple and mysterious. While they can be described completely by just their mass and spin, understanding the relationship between black holes and their host environments and even providing conclusive proof of their existence pose difficult challenges for scientists. Electromagnetic observations are limited because they only provide information about the ways in which a black hole interacts with its surroundings, be it the pull of its gravity on nearby stars, or the vast amounts of energy produced in an accretion disk. While these studies allow for estimates of a black hole's properties, the best possible result can still only provide an incomplete picture. Gravitational waves will soon take us out of the realm of indirect observation of black holes and allow us to "see" them once and for all. By forcing black holes out of hiding, detectors such as LISA and LIGO will not only give us insight into the formation and demographics of these objects, but will also test Einstein's theory of general relativity in the limit of very strong gravity.

Through a series of rigorous tests, general relativity has been demonstrated to be the most robust theory of gravity to date. In an early confirmation, general relativity was shown to produce correct calculations of the precession of the orbit of Mercury, for which the Newtonian theory was known to give results that were too small. This was followed closely by a famous test during a solar eclipse in 1919, in which Arthur Eddington showed that light is bent by the gravity of the Sun at an angle that is accurately predicted by Einstein's theory. More recently, the double pulsar originally discovered by Hulse and Taylor in 1974, PSR B1913+16, has provided indirect evidence of gravitational radiation. The orbits of the pulsars not only

undergo relativistic precession, but are also losing energy by the amount predicted to result from gravitational wave emission to within 0.05% (Kramer et al. 2006). In a practical application, global positioning satellites must frequently make corrections to their internal clocks as a result of general relativistic effects (Ashby 2003). These tests demonstrate that general relativity gives accurate corrections to Newtonian gravity in a variety of physical scenarios, but in relatively weak gravitational fields the divergence between the two theories is not large. It is in the limit of strong gravity that general relativity separates itself, for in this regime things get truly bizarre, and neither space nor time behave in the way to which we are accustomed. Black holes can only be understood in a general relativistic framework. From their basic nature as the extreme of curved spacetime, to their effect on light, to the way in which they spiral together and merge, they are excellent laboratories with which to test relativistic predictions, and the gravitational radiation produced by black holes is the only means of directly testing relativity in the limit of strong gravity.

While gravitational radiation is produced by extremely energetic events, these "ripples in spacetime" are incredibly weak. Detection itself constitutes a great challenge, requiring distance measurements accurate to better than one part in 10^{21}. In addition, the identification of many sources will rely on comparison of measured signals to theoretical waveforms derived from detailed source models. Therefore, our best bet of detecting gravitational radiation is to have a comprehensive knowledge of its sources in advance. Binaries composed of compact objects, such as white dwarfs and neutron stars, are abundant potential sources for LIGO and other ground-based detectors, and a considerable effort has gone into determining their associated detection rates. Electromagnetic observations of these binaries have provided insight into their populations and orbital properties, which is invaluable in the calculation of waveforms. Black holes are not as cooperative. While mergers of black hole

binaries are among the most promising potential sources of gravitational radiation, their expected waveforms and detection rates are much more difficult to predict than those of their white dwarf and neutron star counterparts because black holes are electromagnetically invisible. Some signals, originating from nearby sources or resulting from mergers of massive black holes, will register high enough above the noise to make themselves known with minimal effort on the part of data analysts, but for many classes of potential black hole sources a theoretical framework is an essential precursor to signal detection. For this reason, comprehensive study of possible sources is extremely important for the overall success of detectors. A key aspect of this study is the identification and analysis of potential host environments.

Compact object binaries form by several mechanisms, however only a fraction of them will emit detectable gravitational waves. The strength of the radiation produced by these binaries and the time required for the pair to merge depend strongly how closely the compact objects approach one another in their orbits, with very close binaries emitting stronger signals and spiraling in more rapidly. In situ formation occurs when a binary remains intact after both of its member stars leave the main sequence. If such a binary is born with a wide separation and remains isolated, then its orbit will remain relatively unchanged. In less secluded regions, interactions with passing stars can alter the binary's orbit. If a close dynamical encounter causes the binary members to pass each other closely, then their gravitational wave emission will increase, making a merger possible. Therefore, environments in which many close dynamical encounters occur are expected to be efficient producers of gravitational wave sources.

Globular clusters are one such environment. Boasting large numbers of stars and high densities, globular clusters are known to facilitate close interactions. Because the stellar populations of globulars tend to be older than those in a galactic disk,

sufficient time has passed for a significant number of stars to have evolved into compact objects. Neutron stars and black holes, in particular, are significantly more massive than the remaining main sequence population, and they sink rapidly to the center of the cluster. The resulting over-abundance of compact objects in the dense cluster center increases the probability that neutron stars and black holes will interact dynamically. For those already in binaries, close encounters can enable them to shrink and eventually emit detectable radiation. Close interactions benefit single compact objects as well, by promoting exchanges. This allows lone black holes and neutron stars to swap into binaries, making it much more likely that they will become gravitational radiation sources.

Much like globular clusters, galactic nuclei have large number densities and contain abundant reservoirs of compact objects. The dense environments of galactic nuclei foster close encounters between stellar-mass black hole binaries and stars, which often lead to mergers. This is an important source for LIGO and other ground-based detectors. Supermassive black holes (SMBHs) lurk at the centers of most large galaxies, where they are likely to capture low-mass objects such as stellar-mass black holes onto close orbits that will lead to mergers. As they spiral in, stellar-mass black holes act as test particles, producing gravitational wave signals that map the rotating spacetime around the supermassive black hole. These extreme mass ratio inspirals are among the most important target sources for LISA, the planned space-based detector. Galactic nuclei, therefore, are excellent settings for the study of gravitational radiation, producing sources in both low- and high-frequency regimes.

With gravitational wave detectors in development and coming online, the near future holds fantastic opportunities. We will rediscover objects of previous study, understand working theories with newfound rigor, and undoubtedly discover aspects

of the universe that have long been invisible. Gravitational waves carry a vast amount of information that is waiting to be explored, and the study of potential sources is a key step in ensuring our success on this frontier. With this dissertation, we use numerical simulations to investigate new potential formation channels for sources of gravitational radiation: tidal separation of binaries by supermassive black holes and induced mergers of stellar-mass black holes in the centers of galaxies.

In §1.2 of this introductory chapter, we discuss gravitational waves, and in §1.3 we consider the dynamics of dense stellar systems. §1.4 follows with analysis of double black hole mergers in small galaxies, and in §1.5 we consider the production of LISA and LIGO sources in larger galaxies. Finally, §1.6 outlines the remainder of this dissertation.

1.2 Gravitational Waves and Detectors

In reenvisioning gravity as the curvature of spacetime, Einstein was able to clear up several unresolved issues with the established theory, including the problem of "action at a distance." In Newton's theory of gravity, the effects of a changing gravitational field are felt instantaneously by all observers. This aspect of Newton's work troubled some of his peers. In general relativity, however, there is a reciprocal relationship between matter, which curves spacetime, and the curvature of spacetime, which determines the motion of that matter. As an object moves it causes the curvature of spacetime to change, which in turn alters the path of matter. The communication of a change in a gravitational field does not arrive instantly everywhere in the universe, but rather propagates outward at the speed of light in the form of gravitational radiation.

A gravitational wave is a distortion of spacetime, which is generated by the ac-

celeration of mass that is in an asymmetric configuration. As this distortion propagates, it affects matter by changing the separation of objects that are floating freely in space. Gravitational waves are transverse, and have two polarization modes, h_+ and $h_\times$, the linear combination of which yields the dimensionless strain amplitude, $h(t)$. This strain is a measure of the strength of a gravitational wave, and is given by

$$h(t) = 2\frac{\delta L}{L} \quad . \tag{1.1}$$

Here δL is the change in position of two masses separated by a distance, L. To see the effects of this radiation it is useful to imagine how a passing gravitational wave distorts a ring of freely floating masses. Figure 1.1 (Schutz 1996) shows the distortion of a circle of test masses caused by each linear polarization mode. The $h_\times$ mode is offset from h_+ by 45°. This figure illustrates to scale the warpage caused by a wave with an amplitude of $h(t) = 0.2$, but in reality gravitational waves are not nearly this strong. In fact, a relatively strong signal from the merger of a double neutron star binary in a nearby galaxy cluster would have an amplitude of $\sim 10^{-20}$ (Thorne 1996). This is such a tiny disturbance that it would only cause masses separated by 10 km to oscillate by about one tenth of a proton radius. Measuring extremely small displacements to this level of precision is the goal that must be accomplished by gravitational wave detectors.

There are two classes of interferometric gravitational radiation detectors in various stages of development: ground-based detectors, such as LIGO, and the space-based detector LISA. The frequency of gravitational radiation produced by a source is inversely proportional to its mass, therefore detectors that operate in a certain frequency range will be attuned to sources with a particular set of masses. Figure 1.2 compares the sensitivity curves of LISA and LIGO, indicating the types of objects that will be observable which each detector. Ground-based detectors are

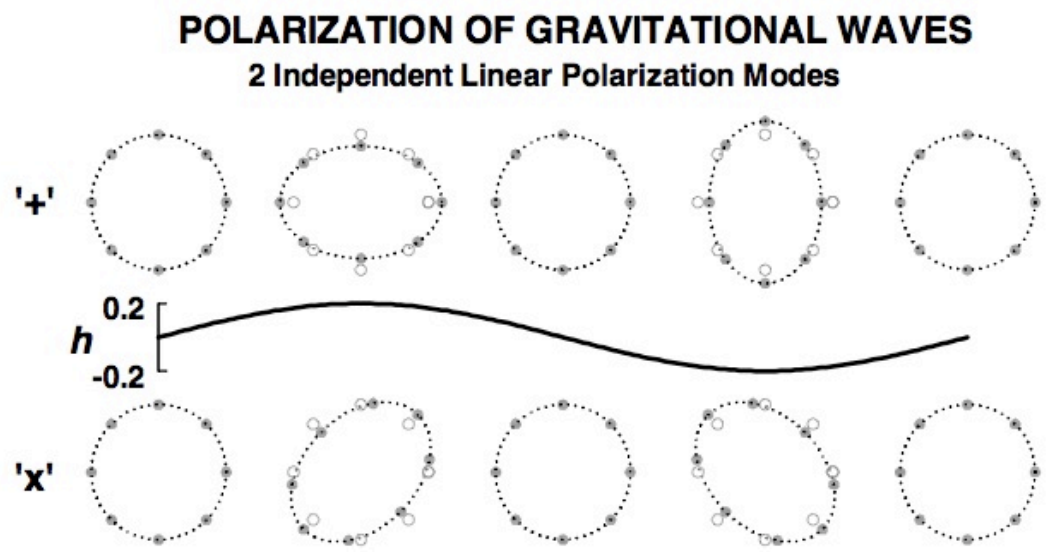

Figure 1.1: (Schutz 1996) Two polarization modes of gravitational radiation.

sensitive to higher-frequency, lower-mass sources, such as merging neutron stars and stellar-mass black holes, while LISA will be more responsive to supermassive black hole binaries. The shapes of the sensitivity curves are determined by the restrictions imposed in large part by a variety of noise sources, and one of the primary challenges for detector developers is finding ways to overcome these limits.

While they differ greatly in scale and setting, LISA and LIGO have similar basic designs. Both instruments are laser interferometers, and each is configured with long arms, which house a laser at the vertex and test masses situated at the ends. An incident gravitational wave will change the length of one arm with respect to the other, which will produce an interference pattern when the laser light is recombined. LIGO consists of two L-shaped detectors in two sites in the United States separated by $\sim$3000 km, each with arms measuring 4 km in length, and a third 2 km detector at the Washington State site. While three detectors might seem redundant, multiple locations will provide information about source positions, and will also confirm that signals originate from gravitational waves rather than some

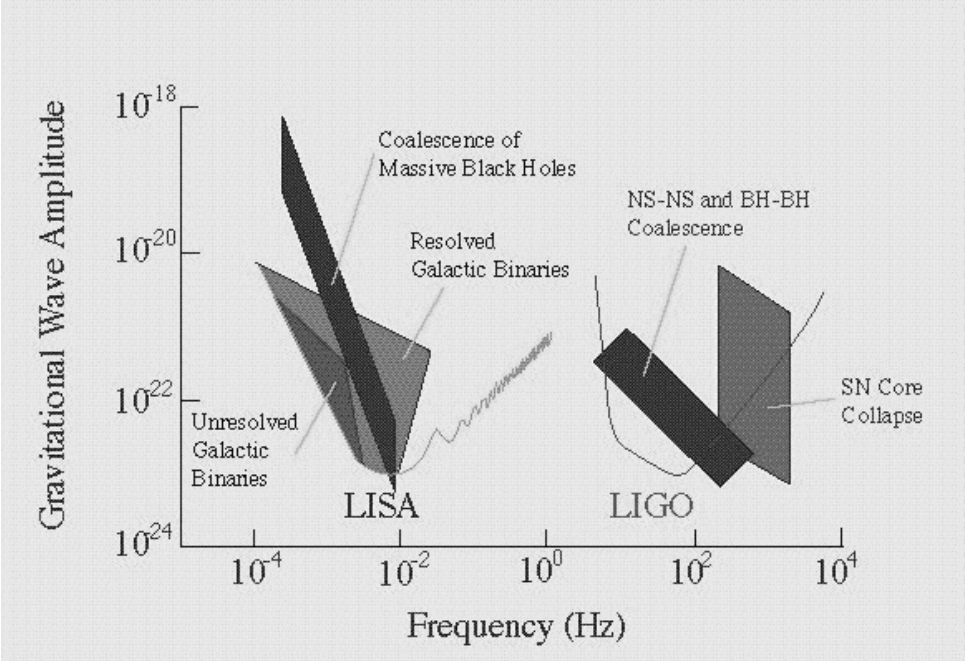

Figure 1.2: Sensitivity curves of the LISA and LIGO detectors. LISA will operate at low frequencies, where signals from supermassive black holes will fall. LIGO and other ground-based detectors are sensitive to high-frequency signals such as those produced by neutron star and stellar-mass black hole coalescences. The curves are shaped in part by noise sources which limit the sensitivities of the instruments. (Source: www.srl.caltech.edu)

Earth-bound noise source. When LISA flies, it will be composed of 3 independent spacecraft forming an equilateral triangle of $\sim 5 \times 10^6$ km on a side. Because it is comprised of three sets of arms, LISA is actually designed to be three interferometers in one, which will work in concert to determine source positions. The sensitivities of LISA and LIGO are limited on the high-frequency end by shot noise that results from the finite number of photons in the laser beams. LIGO must also contend with thermal noise in its mirrors, which affects the middle of its frequency range, as well as seismic noise at the low-frequency end. LISA will be removed from seismic disturbances, but will be buffeted by solar outflows and cosmic rays.

LIGO is a multi-stage project. After decades of planning and five years of construction, operation began at the two sites in 2002. The initial goal for the detectors was to take data for one full year at the design sensitivity, which would detect sig-

nals with $h(t) \sim 10^{-22}$. This goal was met with the fifth scientific run (S5), which concluded in 2007. No detections were made, but non-detection sets a new upper limit for signals for nearby sources such as the Crab pulsar. After S5, the 4 km instruments were taken out of service in order to begin a series of upgrades that will eventually lead to Advanced LIGO. As an intermediary step, dubbed Enhanced LIGO, an upgraded laser and improved readout will boost LIGO sensitivity by a factor of 2. The planned science run with this configuration will be a useful testing ground for Advanced LIGO technology. The development of Advanced LIGO is a collaboration with two European detectors, Virgo and GEO 600, and will require the replacement of all of the major LIGO components, save the vacuum system. The upgrades will include a more powerful and more stable laser, improved optics, and a more robust system for seismic isolation. These improvements will give Advanced LIGO a tenfold increase in sensitivity over its predecessor, which translates into an increase in the volume of detection by a factor of 10^3, as illustrated by Figure 1.3. When Advanced LIGO is commissioned in 2014, it is expected to detect hundreds of signals per year.

Because it is still in a developmental phase, LISA has a longer timeline before it will begin to take data. Building a detector composed of three independent spacecraft that will fly in formation while measuring disturbances to one part in 10^{23} is an extremely ambitious undertaking. While being in space has the clear benefits of a natural vacuum and absence of seismic disturbances, conducting precise measurements over 10^6 km armlengths is difficult. Many challenges arise because the arm lengths of the interferometer are not fixed, partially because Earth's gravity introduces perturbations to the system (Shaddock 2008). The motions of the spacecraft cause the laser frequency to be Doppler shifted, which produces noise. Each spacecraft houses a freely floating test mass, which it must shield from exter-

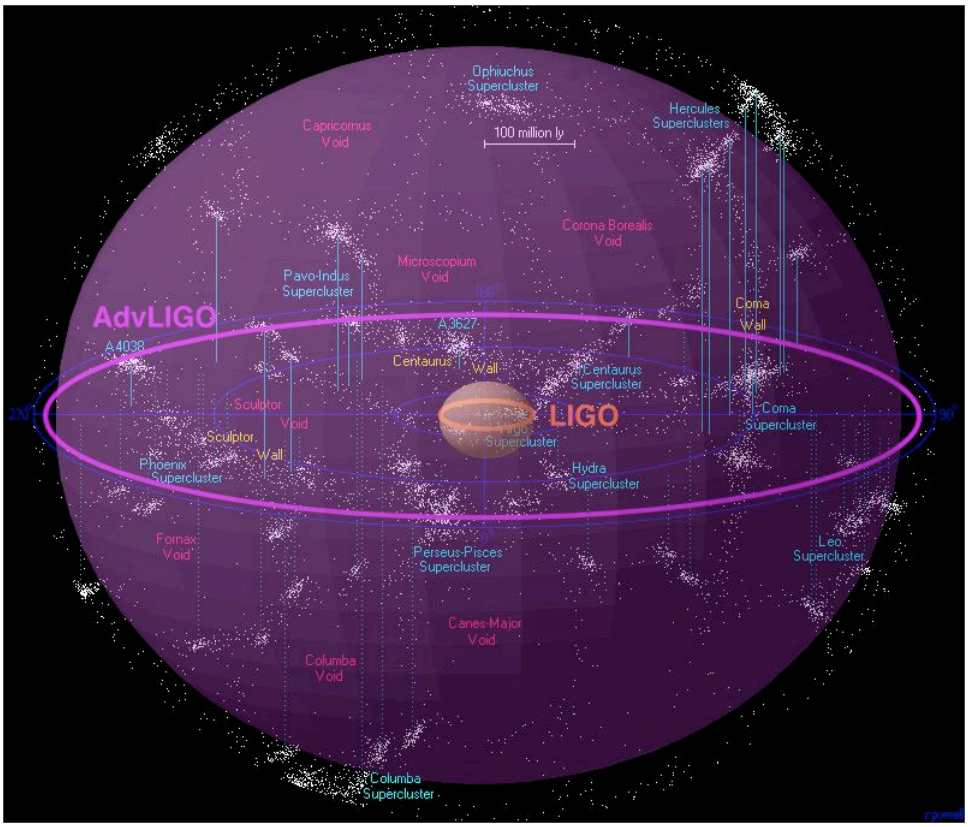

Figure 1.3: Illustration of the detectable regions for initial LIGO and Advanced LIGO. Advanced LIGO, which is scheduled to begin operation in 2014, will see to ten times the distance, and therefore 10^3 times the volume of the initial LIGO configuration (Source: www.ligo.caltech.edu).

nal disturbances. Unwanted acceleration of these proof masses creates noise at low frequencies. To minimize this, actuators will keep the test masses centered while microNewton thrusters will correct the spacecraft trajectory by counteracting accelerations due to the solar wind. Teams in Europe and in the U.S., at Goddard Space Flight Center, for instance, continue to develop and test these technologies. A planned precursor mission, LISA Pathfinder, will test the capabilities of the test mass housing and related hardware, and it is scheduled for launch in 2010. LISA is estimated to follow in 2018-2025.

Following the path to gravitational wave detection that has been set by general relativistic theory does not stop at the development of detectors. Once measure-

ments are made, the task of isolating and identifying individual signals in the data will begin. Gravitational wave detectors are not pointed instruments, rather they will measure sources from across the sky, and the resulting data will contain a combination of many sources. Strong signals will be straightforward to find, but for weaker sources the prospects of detection greatly improve if the properties of the signals are predicted in advance. This is achieved by creating theoretical waveforms corresponding to sources with a wide range of properties and then searching the data for matches. LIGO data will be abundant, and this method of matched filtering will improve the effective sensitivity of the instrument by a factor of ten (Thorne 1996). For LISA, all of the data taken over a run of two years will fit on a single CD, with many signals occupying the same ranges of frequency. Theoretical waveforms will be used to produce templates that will then be compared to the data, allowing for sources with similar properties to be isolated from the din. The computation of waveforms requires analysis of sources and their potential hosts, such as galactic centers. In later chapters, we will focus on two main classes of galaxies: small galaxies with nuclear star clusters at their centers and larger galaxies that are known to host massive black holes. In the case of nuclear star clusters, we show that stellar-mass black holes are often induced to merge, producing LIGO sources. We also demonstrate that binaries in larger galaxies can become sources for both LISA and LIGO.

1.3 Dynamics in Star Clusters

Galactic centers are fairly compact regions with $\sim 10^6 - 10^7$ stars and number densities that can exceed 10^6 pc^{-3}, making them excellent environments for close encounters. We can demonstrate this with a quick calculation. Consider a binary

with a relatively moderate semimajor axis, $a \sim 1$ AU, in a galactic nucleus with $n \sim 10^6$ pc^{-3}. If the average speed in such a nucleus is $v = 100$ km s^{-1}, then the encounter rate is

$$\tau^{-1} = n\Sigma v = \text{few} \times 10^{-9}\text{yr}^{-1} \quad , \tag{1.2}$$

where $\Sigma \sim \text{a}^2$ is the cross section of the binary. From this, we expect the binary to interact once every few hundred million years. Let's compare this to the social schedule that this binary would have if it lived in a galactic region similar to our solar neighborhood. Here, $n \sim 1$ pc^{-3}, and relative velocities are slower, $v \sim 20$ km s^{-1}, and the interaction rate is

$$\tau^{-1} = \text{few} \times 10^{-16}\text{yr}^{-1} \quad . \tag{1.3}$$

In the solitary environment of the galactic disk, a binary remains unperturbed by encounters, having $\sim$ one interaction per 10^5 Hubble times. Therefore, when it comes to the frequency of dynamical encounters, binaries in dense clusters are at a distinct advantage.

The large scale dynamics of such systems take place over the course of a relaxation time,

$$t_{\text{rel}} \approx \frac{N}{8\text{lnN}} t_c \quad . \tag{1.4}$$

Here the crossing time is $t_c = R/v$ for a nucleus of radius R (Binney & Tremaine 1987). The relaxation time is the timescale in which energy distribution occurs within the nucleus, and in this time a star will have its velocity changed by of order itself. In this work, we will primarily consider small-to-moderate galaxies. For instance, a nuclear star cluster in a small galaxy typically has $N \sim 10^6$, $v \sim 50$ km s^{-1}, and $R \sim 1$ pc, which gives $t_{\text{rel}} \sim 10^8$ yr. Such a short relaxation time ensures not only that these systems are in rough dynamic equilibrium, but also that individual stars will have had ample opportunity to interact with one another. Larger galaxies

with $N \sim 10^7$ stars in their central $R \sim 3$ pc, will have larger stellar velocities on average. For $v \sim 100$ km s^{-1}, the relaxation time is $t_{\rm rel} \sim 10^9$ yr. While this larger galaxy, with its $\sim 10^{11}$ stars, will not have relaxed as a whole, its central few parsecs will have undergone several relaxation times. From Eqn (1.2), we know that a binary in such a nucleus will have a few interactions over the course of a billion year relaxation time. Therefore, we see that central regions of both small and mid-sized galaxies are conducive to multiple dynamical encounters between stars. This treatment assumes stars of equal mass. More realistic scenarios that incorporate a range in masses show that more massive objects sink to the centermost region of a galaxy long before their lighter counterparts.

Massive objects such as stellar-mass black holes (BHs) will sink through the field of lower mass stars that populate the galactic nucleus, while lighter objects tend to move further out (e.g., Freitag et al. 2006). The time required for an object of mass M to sink to the center is given by its local relaxation time, $t_{\rm rel}(r)$, which is (Spitzer 1987)

$$t_{\rm rel}(r) = \frac{0.339}{\ln \Lambda} \frac{\sigma^3(r)}{{\rm G}^2 m_* M n(r)} \quad , \tag{1.5}$$

where m_* is the average mass of field stars, and $\ln \Lambda \sim 10$ is the Coulomb logarithm. The more massive an object, the more quickly it sinks. For instance, the relaxation time of a 1.4 $M_\odot$ neutron star is about 14 times longer than that of a BH with $M \sim 20$ $M_\odot$. In fact, simulations that track black holes in a population of lighter stars find that BHs sink to the center very rapidly, and come to dominate the innermost region of the nucleus (Freitag et al. 2006). Binaries, also being more massive than the average star, will sink quickly as well. Therefore, galactic centers will contain much larger fractions of compact objects and binaries than a galactic disk, making it likely that BHs will not only interact frequently, but will have multiple encounters with other BHs, neutron stars, and binaries. Numerical results

have determined that if a close encounter between a single object and a binary results in an exchange, then the final binary tends to consist of the two most massive objects (Heggie 1975). As a result, interactions tend to swap BHs into binaries. When these binaries are formed, they are typically too widely separated to produce significant gravitational radiation. Whether they ever become gravitational wave sources depends on the outcome of subsequent dynamical interactions.

The result of an encounter depends in large part on how the kinetic energy of the single object compares to the internal energy of the binary. In a nucleus with stars of average mass, m_*, and velocity dispersion, σ, a binary with binding energy E is considered hard if

$$\frac{|E|}{m_*\sigma^2} > 1 \quad , \tag{1.6}$$

and soft if

$$\frac{|E|}{m_*\sigma^2} < 1 \quad . \tag{1.7}$$

Typically, a hard binary will shrink, or harden, while a soft binary will widen further, or soften, as a result of a close encounter (Heggie 1975). While this has been determined numerically, there is a qualitative argument that offers insight into this trend. Consider a binary-single interaction between three equal-mass objects. If the binary is hard, then the initial speed of the single object is less than the binary's orbital speed. At the end of the encounter, the single typically leaves with a speed roughly equal to the initial orbital speed of the binary. It has, therefore, gained energy, which means that the binary is more tightly bound, and its semimajor axis has decreased. In contrast, when the binary is soft the initial speed of the single object is greater than the orbital speed. In fact, for a very soft binary, the orbital speed is so slow that one can approximate that it is stationary as the single object passes. The effect felt by the binary is then dominated by the pull of the single object on the closest binary member. The high-velocity interloper will attempt to

equilibrate its energy with the binary member, hence increasing its orbital speed. As a result, the binary is less bound, and widens (Binney & Tremaine 1987). The process of hardening has a substantially different effect on the fate of a binary than that of softening. When a binary hardens, its cross section decreases and it is less likely to have another interaction. The opposite is true for a softened binary, for which a subsequent encounter becomes more likely. Each time a soft binary has an encounter it is likely to grow softer, and its interaction cross section increases. This runaway process heightens the probability that the binary will be ionized, leaving both of the binary members and the interloping star unbound. For this reason, it is reasonable to assume that soft binaries in dense environments do not survive for long.

Observations of dense star systems support the picture that binaries have frequent dynamical encounters. In the galactic disk, the fraction of stars in binaries is $f_b \sim 0.7$, or approximately one binary for each single star. These stars must be born in binaries, because number densities are too low for them to have come together dynamically. It is reasonable to assume that the mechanism of star formation is similar in dense clusters such as globulars, which would lead to a comparable percentage of binaries, however, far lower values of f_b, from 0.05-0.2, are observed in these systems (e.g. Albrow et al. 2001). Close encounters with stars are likely to blame for this discrepancy. One means by which interactions deplete the population is by eliminating soft binaries though repeated softening and eventual ionization. Also, in an encounter with a hard binary, the binary shrinks and receives a recoil kick that can easily exceed the escape velocity of a globular cluster. These kicks add energy to central region of the system by increasing the velocities of single stars, which is the primary mechanism that keeps the cores of globular clusters from collapsing. In addition, low-mass x-ray binaries, are more abundant in globulars than in the galactic

disk. These are close binaries in which a neutron star accretes from a companion, resulting in x-ray emission, and their relative abundance in globulars indicates that dynamical encounters greatly increase their formation. These observations provide a basis with which to estimate gravitational wave detection rates from neutron star binaries, but no such observational anchor exists in the case of black hole binaries. Instead, BH merger rate estimates largely depend on population synthesis models.

1.4 Black Hole Mergers in Dense Star Clusters: LIGO Sources

While population synthesis simulations produce results for neutron star binaries that are consistent with merger estimates based on observations of known double neutron stars, their predicted rates for double black hole (BH-BH) mergers vary from 1 per year to 500 per year with Advanced LIGO (Belczyński et al. 2007). Though it is known that stars are often born in binaries, and that a large fraction of binaries contain stars of similar mass, it is not known whether a massive binary star will in turn evolve into a BH-BH binary in isolation. The main source of uncertainty lies in the common envelope phase of evolution. This occurs after one of the stars has become a black hole, and the other enters the red giant phase. The giant is so large that its black hole companion is engulfed, which produces a drag on its orbit and can cause the BH to merge with the core of the star. Depending on the details of the common envelope model used, in-situ formation of BH-BH binaries that are small enough to merge by gravitational radiation within a Hubble time might be greatly inhibited, hence the uncertainty in the LIGO rates. The distribution of BH-BH binaries that survive the common envelope phase is flat across a range of low masses, as seen in Figure 1.4. Therefore, these models predict that mergers

of isolated BH-BH binaries will involve low mass BHs, which is in contrast with BH-BH mergers formed by dynamical interactions in dense systems.

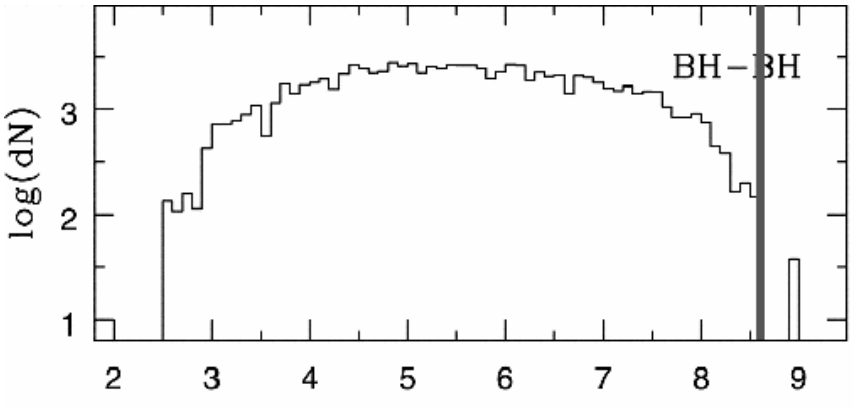

Figure 1.4: Distribution of close BH-BH binaries produced by population synthesis simulations (Belczyński et al. 2007). The horizontal axis is M_{chirp} – a particular combination of the two masses of the binary members. The vertical line shows M_{chirp} for two 10 $M_\odot$ BHs, which demonstrates that BH-BH mergers from this mechanism are of low mass.

If mergers of BH-BH binaries formed in isolation are suppressed by the common envelope phase, then it is likely that merger rates are dominated by dynamical encounters in dense clusters. In addition to decreasing the semimajor axis of a hard binary, interactions with stars also tend to cause the eccentricity of the pair to wander. The strength of the gravitational radiation emitted by the binary depends on the distance of the closest approach, or pericenter, of the binary members, therefore a change in eccentricity can have a significant effect. The timescale for a binary with masses m_1 and m_2, semimajor axis a, and eccentricity e to merge by gravitational radiation is given by (Peters 1964)

$$t_{\rm insp} \approx 6 \times 10^{17}\ {\rm yr} \frac{(1\ {\rm M}_\odot)^3}{m_1 m_2 (m_1+m_2)} \left(\frac{a}{1\ {\rm AU}}\right)^4 (1-e^2)^{7/2} \quad . \tag{1.8}$$

For example, if $m_1 = m_2 = 10\mathrm{M}_\odot$, $a = 0.1\mathrm{AU}$ and $e = 0.9$, then $t_{\mathrm{insp}} \sim 90$ Myr. Figure 1.5 illustrates how such dynamically-triggered mergers might take place.

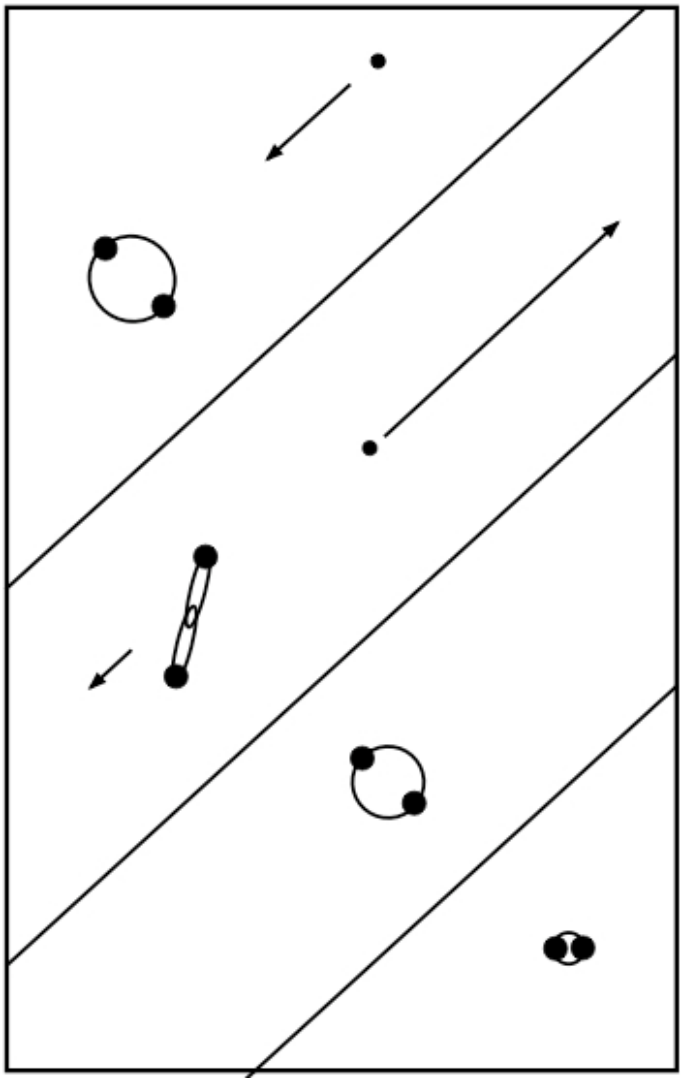

Figure 1.5: Illustration of a dynamically-induced merger. After a close encounter with a star, the binary pericenter decreases, which increases gravitational wave emission. It then spirals together and eventually merges.

While globular clusters are ideal environments for fostering close interactions, it is not clear that they are able to retain their black hole populations. Observations of BHs in globular clusters are rare, but this fact could simply be because they are invisible unless they have a partner from which to accrete. However, the low escape speeds of globulars suggest that BH populations are not simply hiding. Each

successive hardening of the binary imparts a recoil that can exceed the modest 40-50 km s^{-1} escape velocities that are typical for massive globular clusters. In fact, simulations show that the vast majority of binaries will be ejected from globulars before they have the opportunity to merge (Portegies Zwart & McMillan 2000; Sigurdsson & Hernquist 1993). Additionally, BHs might be ejected from clusters by the kicks that they receive at birth from supernovae. At least one known BH x-ray binary has been observed to have a 100 km s^{-1} supernova kick (Mirabel et al. 2002), which is sufficient to eject it from any globular cluster with ease. In contrast to globulars, galactic nuclei are conducive to close encounters, abundant in compact objects, and have escape velocities large enough to withstand both natal BH kicks and three-body recoil.

There is increasing evidence that a large fraction of small galaxies have nuclear star clusters (NSCs) in their centers, and that many NSCs may not host massive black holes. Surveys suggest that 50% – 80% of small galaxies have such clusters, and that NSCs follow a trend similar to the relation that correlates the masses of SMBHs to the central velocity dispersions of larger galaxies (Ferrarese et al. 2006). NSCs have masses that range from $10^6 - 10^7 M_\odot$ and one dimensional velocity dispersions that extend from $\sigma \sim 13 - 30$ km s^{-1}, with six clusters having $\sigma > 25$ km s^{-1}. The relaxation time of these systems is much less than a Hubble time, so BHs will have had ample time to sink into the cluster centers. As in globular clusters, compact objects in NSCs are likely to swap into binaries that will then have repeated encounters with stars. However, NSCs have much higher escape velocities, $v_{esc} \sim 100 - 200$ kms^{-1}, and will therefore be more likely to retain their BHs in the event of natal or three-body kicks. This makes NSCs prime locations for BH-BH mergers, and due to the multiple exchanges that the binaries will likely undergo, we expect that mergers will involve much more massive BHs than in the isolated

case. Hence, BH-BH mergers in NSCs are a distinct new source for LIGO and other ground-based detectors.

1.5 Larger Galaxies: Sources for LIGO and LISA

Like their smaller counterparts, larger galaxies are promising environments for the production of LIGO sources such as BH-BH mergers, but the presence of SMBHs in their centers introduces the potential for an additional type of gravitational radiation source: extreme mass ratio inspirals.

1.5.1 Extreme Mass Ratio Inspirals

Extreme mass ratio inspirals (EMRIs) are key sources for the future space-based gravitational radiation detector LISA (Danzmann & et al. 1996). EMRIs are events in which a low-mass object such as a white dwarf, neutron star, or BH spirals into a SMBH. Of these compact objects, BHs are the most massive, hence their inspirals are observable to the largest distances. The strain amplitude of an EMRI goes like

$$h \sim m(M_{SMBH})^{2/3} \quad , \tag{1.9}$$

where m is the mass of the smaller object. An EMRI involving a 10 $M_\odot$ BH can be observed at a distance $\sim$10 times greater than an event involving a 1 $M_\odot$ object (Freitag et al. 2006), which increases the volume of detection by 10^3. EMRIs are extremely important because they provide means to directly test general relativity through the comparison of theoretical waveforms to the signals received by LISA. In effect, as the BH spirals in, it acts as a test particle, providing a map of the curved spacetime surrounding the rotating SMBH (Ryan 1995, 1997).

There are several ways in which EMRIs are thought to be produced. The most widely-discussed formation mechanism involves the capture of a single stellar-mass

black hole by a SMBH, as illustrated in Figure 1.6. The two-body capture scenario begins with a BH in a distant orbit around a SMBH. The cumulative effect of distant encounters with much lighter field stars slowly decreases the semimajor axis of the BH orbit and causes its eccentricity to wander away from its initial value. If the pericenter of the BH orbit reaches a value such that a significant amount of energy is dissipated by gravitational radiation, then capture can occur. This required pericenter is quite small, of order 0.1 AU. The two-body capture process typically results in high-eccentricity orbits with apocenters that are very large, frequently exceeding 0.1 pc (Hils & Bender 1995; Hopman & Alexander 2005). Because of these large apocenters, it is likely that passing stars will perturb the orbit of the BH, which will often prevent it from becoming a detectable EMRI. In some cases, the encounter will significantly lower the eccentricity such that the emission of gravitational radiation becomes negligible, halting the inspiral. At the other extreme, a perturbation can send the BH into a direct plunge before the orbit reaches the frequency range required for a detectable LISA signal (Hils & Bender 1995). As many as $80\% - 90\%$ of would-be EMRIs might be lost in this manner (Hopman & Alexander 2005). EMRIs with apocenters that are sufficiently small to avoid perturbation will have considerable eccentricities and random inclinations when they reach the LISA sensitivity band (Freitag 2003).

A second formation scenario invokes an accretion disk around the SMBH. If a BH plunges through the disk, the resultant energy loss can dampen its motion and bring its orbit into the plane of the disk. Subsequent gas drag then simultaneously shrinks and circularizes the BH orbit until it is small enough that gravitational radiation takes over, leading to inspiral and merger. This process creates circular EMRIs with zero inclination.

Binaries provide a means of depositing stellar-mass black holes very close to

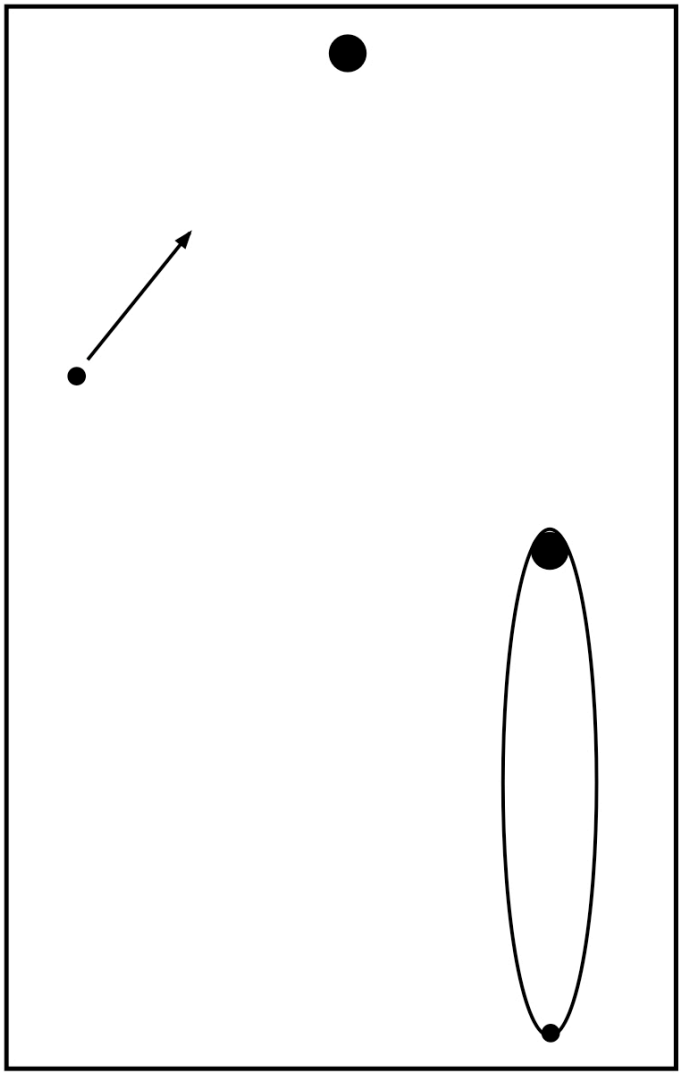

Figure 1.6: Capture of a BH by a SMBH via gravitational radiation emission. The resultant orbit is large and very eccentric, with an apocenter of $\sim 10^4$ AU, which makes the BH susceptible to plunge-inducing perturbations by passing stars. When such objects survive to become EMRIs, they produce eccentric, inclined LISA sources.

the SMBH without requiring energy dissipation (Miller et al. 2005). Like that of its single counterpart, the orbit of a black hole binary is altered by two-body relaxation. As the binary sinks through the field of less massive stars, the semimajor axis of its orbit around the SMBH decreases and its eccentricity wanders. When the BH-BH binary gets close to the SMBH, tidal forces pull the binary apart, causing one of the BHs to be captured into a close orbit, while the other is flung off at a high speed, as

shown in Figure 1.7. The capture radius, at which tidal forces separate the binary,

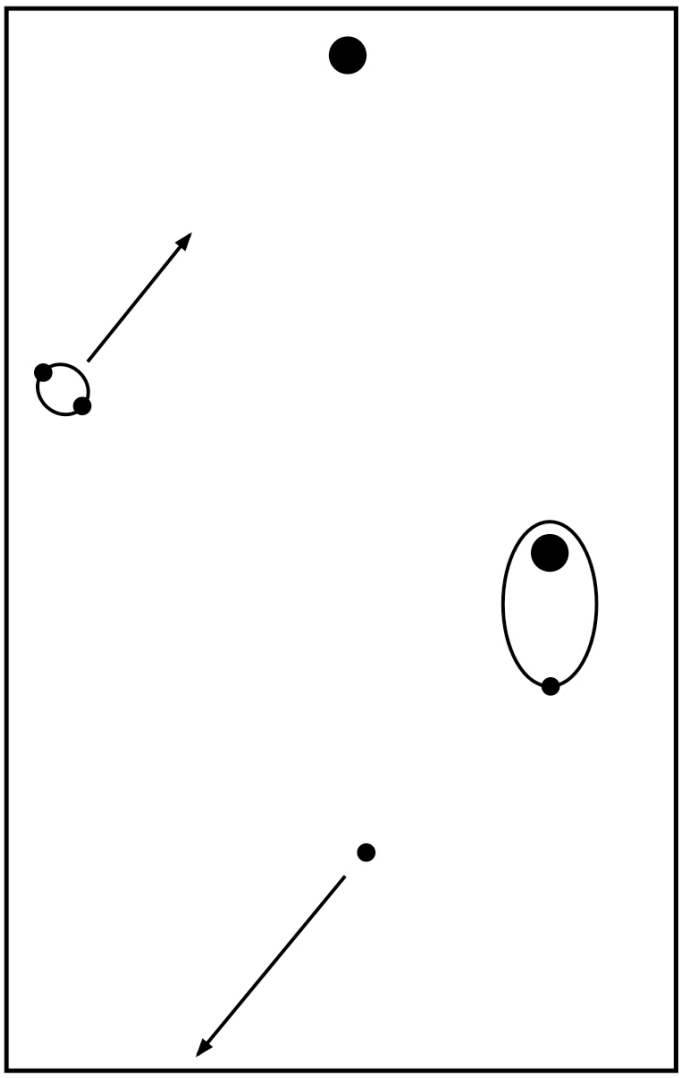

Figure 1.7: Tidal separation of BH-BH binary by a SMBH. One binary member is captured into a small orbit, and the other is ejected. The captured orbit has a larger pericenter (typically ~ 10 AU) and a smaller apocenter ($\sim$ few hundred to 1000 AU) than in the two-body capture case. When the EMRI reaches the LISA band, it will be circular with random inclination.

is given by (Miller et al. 2005)

$$r_{\rm tide} \approx a_{\rm bin}\left(\frac{3M_{\rm SMBH}}{m_{\rm bin}}\right)^{1/3}, \tag{1.10}$$

where $m_{\rm bin}$ and $a_{\rm bin}$ are the total mass and semimajor axis of the binary. For $m_{\rm bin} =$ 10 $M_\odot$, $a = 0.1$ AU, and $M_{\rm SMBH} = 10^6 M_\odot$, $r_{\rm tide} \approx 7$ AU. For comparison, two-body

capture with the same masses requires a pericenter pass $r_p \approx 0.1$ AU. Figure 1.8 shows a three-body simulation that results in the tidal separation of the binary, which demonstrates the capture of a BH into a moderately-sized orbit. The binary separation mechanism allows the BH to be captured at a much greater distance from the SMBH than in the two-body process. Also, the apocenter distance after tidal separation is typically only $\sim$ one hundred times the pericenter distance, or $\sim$ 1000 AU, compared to $\sim$ 0.1 pc for two-body capture. This reduces the threat of orbital perturbation by field stars. The newly-captured orbit of the BH around the SMBH has a larger pericenter than in the two-body capture case. This allows for circularization of the orbit by gravitational wave emission, producing very low-eccentricity events when the EMRI reaches the LISA band. In future observations, the distinction between high- and low-eccentricity, and high- and low-inclination events will not only provide direct insight into these formation mechanisms, but will also yield information about the fraction of BH binaries that exist in galactic nuclei.

1.5.2 Influence of SMBH on Binary Dynamics

As a BH-BH binary sinks through the nucleus, it will have multiple encounters with single stars. While this is reminiscent of the fates of binaries in NSCs, the presence of an SMBH makes the nuclei of larger galaxies less quiescent than those of their smaller relations. Within the central $\sim$ 1 pc of a nucleus, the dynamics are dominated by the SMBH. Whereas in NSCs the stellar velocities are constant throughout, this is not the case in regions that are SMBH-influenced, where velocities increase as one approaches the center. In this region, the velocity dispersion is related to the distance from the SMBH, r, by

$$\sigma(r) \propto r^{-1/2} \tag{1.11}$$

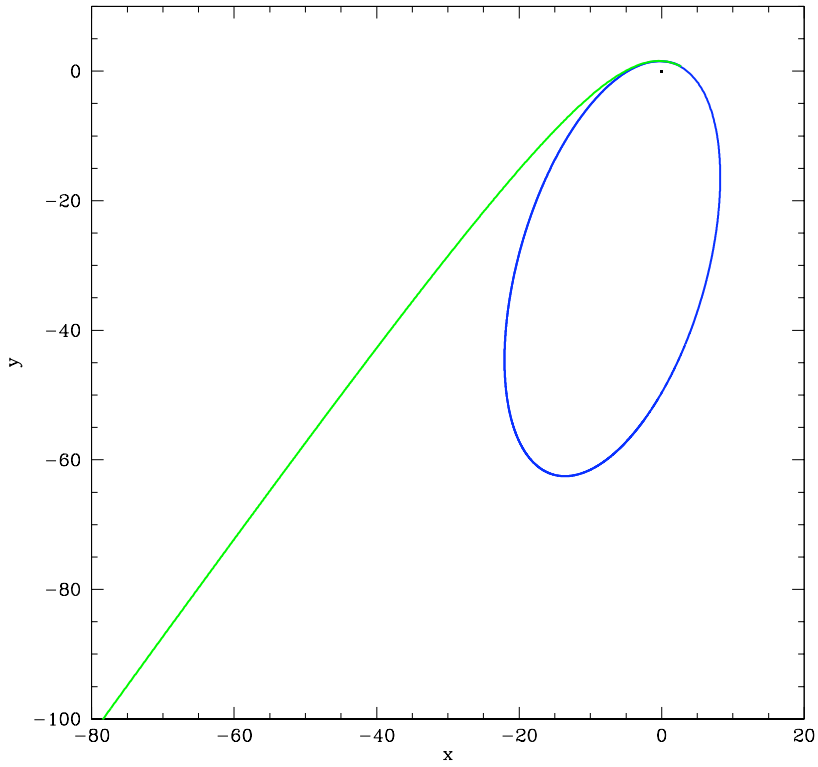

Figure 1.8: Results of a 3-body simulation in which a BH-BH binary is tidally separated by a SMBH. The axes are in AU. The light green curve shows the path of the ejected BH, and the dark blue curve is the captured orbit.

As discussed in Section 1.3, whether a binary is hard or soft determines how frequently it interacts and impacts the outcome of those encounters. Hardness and softness depends on how the binding energy of the binary compares to the kinetic energy of interloping stars, therefore a binary that remains internally unchanged will be softer if it encounters faster stars. This is precisely what happens as a binary sinks towards the center of the galactic nucleus where the velocity dispersion is higher. Because binaries become softer as they sink, subsequent encounters tend to soften them further, which leads to frequent ionizations. Additionally, wider binaries are tidally disrupted at a greater distance from the SMBH, which increases the time required for the BH to spiral in to the region where it will become a detectable

EMRI. Even with this caveat, some BHs will have initial inspiral times $\leq 10^9$ yr, and many others likely will be perturbed by passing stars into orbits that will spiral in. Lastly, we find that those binaries that are not separated by the SMBH often undergo dynamically-induced mergers. Therefore, galactic nuclei are excellent settings for the production of both LIGO and LISA sources.

1.6 Dissertation Overview

Chapters 2 and 3 of this dissertation give more detailed background information about gravitational radiation and nuclear star clusters. We then analyze BH-BH mergers in NSCs in Chapter 4. We investigate the formation of circular EMRIs via the tidal separation of BH-BH binaries in Chapter 5, and in Chapter 6 we present a study of BH-BH dynamics in galaxies containing SMBHs.

Chapter 2

Gravitational Radiation

"It is enjoyable to make things visible which are invisible."

—Eric Cantona

2.1 Introduction

Astronomy, by its nature, is the study of objects at a distance. We can't dissect a star, or form a quasar in a lab, or, with the exception of objects within our solar system, travel to astronomical bodies in order to analyze them. For some of Earth's nearest relatives–comets, asteroids, rocky planets, and satellites–we can directly test some properties, such as the characteristics of rock fracture and ice formation, and we have even directly sampled the surfaces of a select few. However, the vast multitude of celestial objects lie beyond our reach, and we must determine their properties remotely by analyzing their light. Luckily, light contains information about composition, temperature, and a host of attributes from which astronomers have built a taxonomy of the astronomical menagerie. Detection of gravitational radiation will add another dimension to our knowledge set, complimenting electromagnetic observations by allowing us to study the details of black hole mergers, probe the interior

structure of neutron stars, and perhaps examine the first moments after the Big Bang.

2.2 Overview

Gravitational waves communicate the acceleration of an asymmetric distribution of mass, resulting in the squeezing and stretching of spacetime. In an analog to electromagnetism (see Jackson 1998), the gravitational potential can be expressed in terms of moments (following e.g. Misner et al. 1973); for radiation to be produced, there must be a frame-independent variation of a moment with time. In order to determine the lowest order gravitational wave radiation, we begin our electromagnetic analogy with the electric monopole, which is

$$\int \rho_e(\mathbf{r}) d^3r \tag{2.1}$$

where $\rho_e(\mathbf{r})$ is the charge density. This is the total charge of the system, and since the total charge does not vary, there is no electromagnetic monopolar radiation. Similarly, for a mass density $\rho(\mathbf{r})$, the gravitational monopole is

$$\int \rho(\mathbf{r}) d^3r \quad , \tag{2.2}$$

or the total mass-energy of the system, which is constant, thereby excluding the possibility of gravitational monopolar radiation. Next, we have the electric dipole moment

$$\int \rho_e(\mathbf{r}) \mathbf{r} d^3r \quad , \tag{2.3}$$

which is not conserved, therefore electric dipole radiation is possible. The gravitational equivalent is

$$\int \rho(\mathbf{r}) \mathbf{r} d^3r \quad , \tag{2.4}$$

but this is the center of mass-energy, which is constant in the center-of-mass frame and can not radiate. The next possibility is the magnetic dipole, which in electromagnetism is

$$\int \rho_e(\mathbf{r})\mathbf{r} \times \mathbf{v}(\mathbf{r}) d^3r \quad , \tag{2.5}$$

the variation of which leads to magnetic dipole radiation. The gravitational analog is

$$\int \rho(\mathbf{r})\mathbf{r} \times \mathbf{v}(\mathbf{r}) d^3r \quad , \tag{2.6}$$

which is the angular momentum of the system, another conserved quantity, so there is no magnetic dipolar gravitational radiation. The next possibility is the static gravitational quadrupole moment

$$I_{ij} = \int \rho(\mathbf{r}) r_i r_j d^3r \quad . \tag{2.7}$$

This is the first moment for which there is no applicable conservation law, therefore quadrupolar gravitational radiation can exist. Furthermore, the lowest order radiation is generally the strongest, so gravitational radiation is dominated by the quadrupole moment. Therefore, gravitational wave sources are limited to objects with non-axisymmetric configurations.

There are several astrophysical scenarios that break axisymmetry, which leads to a variety of potential gravitational radiation sources. For example, compact object binaries, the asymmetric collapse of stars, non-axisymmetric processes in the early universe, and rotating lumpy neutron stars are all candidates. As we will discuss in §2.2, many of the details of these prospective sources and their associated signal strengths are unknown at present. Binaries, however, are the best understood class due, in large part, to electromagnetic observations of neutron star and white dwarf binaries. While potential sources are widely varied, their asymmetric motions have a similar effect: causing the stretching and squeezing of spacetime. Though

the objects that produce detectable gravitational radiation are very massive, the resulting waves are quite diminutive.

We can estimate the strength of the gravitational wave strain produced by an astrophysical source by using the Newtonian-quadrupole approximation (following Thorne 1996). The relation states that

$$h(t) \sim \frac{G}{c^4\ r}\ddot{\mathbf{Q}} \quad , \tag{2.8}$$

where $\ddot{\mathbf{Q}}$ is the second time derivative of the quadrupole moment of a system a distance r away. A source producing significant gravitational waves will be elongated, so we can assume that

$$\mathbf{Q} \sim ML^2 \quad . \tag{2.9}$$

This has units of

$$\mathbf{Q} \sim (mass) \times (distance)^2 \quad . \tag{2.10}$$

Taking the first derivative gives

$$\dot{\mathbf{Q}} \sim (mass) \times \frac{(distance)^2}{(time)} \quad , \tag{2.11}$$

and from the second we have

$$\begin{aligned} \ddot{\mathbf{Q}} &\sim (mass) \times \frac{(distance)^2}{(time)^2} \\ &\sim (mass) \times (velocity)^2 \\ &\sim E_{\rm kin} \qquad . \end{aligned} \tag{2.12}$$

Combining this and Equation (2.8) produces,

$$h \sim \text{few} \times \left(\frac{G}{c^4\ r}\right) E_{\rm kin} \quad , \tag{2.13}$$

where $E_{\rm kin}$ is the kinetic energy. It is clear from the factor of G/c^4 in Equation (2.13), that h will be extremely small unless the observer is close to a very rapidly-moving source. For instance, consider a binary consisting of two $1.4M_\odot$ neutron

stars with an orbital period, P, at a distance, r, from Earth. The strength of the resulting gravitational radiation is measured by the strain (Schutz 1996)

$$h \approx 10^{-22}\left(\frac{M}{2.8M_{\odot}}\right)^{5/3}\left(\frac{0.01 \text{ sec}}{P}\right)^{2/3}\left(\frac{100 \text{ Mpc}}{r}\right) \quad . \tag{2.14}$$

This shows that a relatively nearby binary, in the Virgo cluster at 18 Mpc, for instance, will only produce a signal amplitude of $h \sim 10^{-21}$. These systems are rare—there are only $\simeq$ a few known double neutron stars in the Milky Way that will merge within a Hubble time (see e.g. Phinney 1991)—so it is clear that a successful detection will require that instruments be sensitive enough to detect sources at great distances. This will come into reach when detectors sensitive to $h \sim 10^{-22}$ and better are operational. In making the painstaking measurements that are required to detect gravitational waves, scientists hope to reap incredible rewards: singular insight into the mysteries of neutron stars and black holes, and, possibly, an unparalleled look back to the first seconds of the universe.

2.3 Sources

Several models for potential gravitational radiation sources have been considered, and they fall into a handful of broad categories: bursts, continuous sources, binaries, and stochastic sources. Of these, binaries are the only sources that are known to emit gravitational waves at detectable amplitudes, but we will briefly discuss other possible sources as well.

2.3.1 Burst Sources

Bursts of gravitational waves are expected to be released immediately prior to a supernova explosion when the core of the progenitor star collapses. This collapse, which will almost certainly be asymmetric (Ott 2009), releases a large amount of energy, possibly ∼15% of the rest mass-energy of the core, but this is largely in the form of neutrinos (Ciufolini et al. 2001). Uncertainties in the theory of neutron star interiors and lack of knowledge of the degree to which the collapse is asymmetric make it very difficult to predict the amount of energy released as gravitational waves. It is possible that only $\sim 10^{-6}$ of the mass-energy becomes gravitational radiation, which would limit our hopes of detection to our own galaxy. Supernovae are rare, only occurring once every ~ 50 years in our galaxy, therefore detections with advanced ground-based detectors will likely be infrequent (Schutz 2003). After the burst of its formation, it is possible that a rapidly spinning neutron star might produce a continuous gravitational wave signal.

2.3.2 Continuous Sources

A rotating neutron star could produce detectable gravitational waves if it is asymmetric. If its spin axis is misaligned with its principal moment of inertia axis, then it will wobble by an angle, θ_w, as it rotates. A typical spinning, non-spherical star will generate waves with a strain amplitude (Thorne 1996)

$$h \sim 6 \times 10^{-25} \left(\frac{f_{\rm rot}}{500\ {\rm Hz}}\right)^2 \left(\frac{1\ {\rm kpc}}{r}\right) \left(\frac{\epsilon_e \text{ or } \theta_w \epsilon_p}{10^{-6}}\right) \quad , \tag{2.15}$$

where the deviation of the star from a sphere is given by its equatorial and poloidal ellipticities, ϵ_e and ϵ_p. While this gravitational wave amplitude is quite small, rotating stars might be detectable over many cycles if the change in frequency with time is known. The frequency of the gravitational radiation, f, is a combination of the

rotation frequency, $f_{\rm rot}$, and the precession frequency that arises due to the wobble, $f_{\rm prec}$

$$f = f_{\rm rot} + f_{\rm prec} \quad . \tag{2.16}$$

If such radiation is detected from a known pulsar, then the analysis of these two frequencies in concert with the timing of the pulses could yield insight into the internal structure of the neutron star. Unfortunately, so little is known about the degree to which a typical neutron star deviates from a sphere, or how much wobble is expected, that it is difficult to predict detection rates. Upper limits on neutron star ellipticity vary from 10^{-4} to 10^{-6}, however these might be far greater than the average (Thorne 1996). The necessary asymmetries for the production of gravitational waves might come in the form of either lumps or waves, and several mechanisms of producing them have been proposed.

In order to generate continuous gravitational radiation, neutron stars must have sustained asymmetry. If a neutron star is spinning extremely rapidly immediately after it forms, there is a chance that it could elongate enough before it hardens to radiate detectable waves. This scenario of dynamically-produced lumps is likely uncommon at best (Thorne 1996). All known neutron stars rotate far too slowly to make this mechanism feasible. It is also possible that magnetic pressure from very strong fields within a neutron star might produce triaxiality, however the signal strength from such a source is difficult to predict without knowledge of the interior properties of the stars. Sustained asymmetric accretion onto a non-spherical star has also been proposed as a means of producing radiation by increasing θ_w and therefore strengthening emission. In each of these scenarios, uncertainties make the prediction of signal strength difficult. If detections are made, then we will learn a great deal about the internal properties of neutron stars, and in the worst case, non-detection will provide a useful upper limit on neutron star ellipticities.

Waves, or deformations that move with respect to the surface of a neutron star, might result from unstable modes, however it is unclear whether such waves are detectable or sustained. Surface waves might be produced on rapidly rotating stars via the CFS instability (Chandrasekhar 1970; Friedman & Schutz 1978). In this scenario, density perturbations move in the direction opposite to the rotation of the star, however as the star spins it drags the waves forward. From the perspective of a distant observer, the propagation of the waves is prograde and gravitational radiation is emitted. From the perspective of an observer on the surface of the star, however, the wave motion is retrograde, and the gravitational radiation appears to carry away negative energy, hence amplifying the waves (Thorne 1996). These waves can reach large amplitudes in perfect fluids, but the expected amplitudes in neutron stars are unknown. It is possible that magnetic fields damp the waves (Rezzolla et al. 2001), and viscosity in the neutron fluid also likely plays a role in decreasing the amplitude of the modes (Schutz 1996). Because the viscosity depends on the interior temperature of the star, the range of viscosity in which the CFS instability will operate corresponds to a limited range in temperature. In fact, it is believed that CFS waves will only be produced in the first few years after a neutron star forms, when the temperature is $10^9\ K \leq T \leq 10^{10}\ K$ (Thorne 1996), and it is possible that detectable gravitational radiation might last as briefly as a few seconds (Schutz 1996).

In any case, coherent signals are easier to detect than bursts of comparable amplitude, and although very little can be predicted at present about signal strengths from rotating neutron stars, it could be that such sources will be detectable even if their signals are weak. Because these signals are periodic, it is possible to increase the effective sensitivity of a detector such as LIGO by integrating over many cycles and matching signals in the data to the patterns predicted from theory (Schutz

2003). The effective signal strength is then increased by the factor $\sqrt{n}$, where (Thorne 1996)

$$\sqrt{n} = \sqrt{f_{\rm rot}\ \hat{\tau}} = 10^5 \Big(\frac{f_{\rm rot}}{1000\ {\rm Hz}}\Big)^{1/2} \Big(\frac{\hat{\tau}}{4\ {\rm months}}\Big)^{1/2} \quad . \tag{2.17}$$

Here $f_{\rm rot}$ is, again, the spin frequency, and $\hat{\tau}$ is the integration time. This technique of using matched filtering to search for signals over an integration time of many months is a computationally demanding form of data analysis, but this effort will make ground-based detectors significantly more sensitive to periodic signals. It is important to note that all known millisecond pulsars are too weak to be detected, even if their spindown is entirely due to gravitational radiation. If wide searches are conducted, they could lead to the discovery of unknown neutron stars, though such searches present even more taxing computational challenges. Any detections would give direct insight into the evolution of massive stars and physics at high densities and in strong magnetic fields, which motivates the continued development of matched filtering techniques.

2.3.3 Stochastic Sources

In addition to carrying the signatures of exotic objects in our galaxy, it could be that gravitational waves also bear the imprint of the Big Bang itself. Gravitational radiation interacts so weakly that the waves generated very soon after the Big Bang make their way to us unaltered. This fact has lead to a great deal of enthusiasm for what could potentially be learned about the early universe if we can harness this radiation. If we consider the wealth of knowledge gained by studying the cosmic microwave background, which hails from $\sim 10^5$ years after the Big Bang, then it is clear that our understanding would be revolutionized if we could analyze gravitational radiation originating from only $\sim 10^{-35}$ seconds after the birth of the universe (Schutz 1996).

While the motivating factors are clear, the detectability of these waves is highly uncertain. The models proposed for the generation of primordial gravitational waves are very speculative, and are rooted in the poorly understood physics of inflation and early universe phase transitions. The standard model of inflation would predict amplitudes well below the sensitivity of any planned detector, and phase transitions can only produce detectable radiation if one takes into account very optimistic parameters (Schutz 2003). While we can be sure that a wealth of information would accompany a background of primordial gravitational waves, we know so little about the epoch in which it was produced that it is difficult to feel confident that we will detect it. In contrast, there are sources that are not nearly as mysterious. In fact, we have observed the effects of gravitational waves within these systems, and with every measure undertaken to increase detector sensitivity we come closer to detecting their radiation directly. They are compact object binaries.

2.3.4 Binary Sources

Merging compact object binaries stand out when compared to bursts, spinning neutron stars, and the primordial background as the most completely understood sources of gravitational radiation. This is due to observations as well as our ability to model the inspiral stage analytically, and, with recent computational advances, to simulate the mergers themselves. We can discuss the effect of gravitational radiation on a binary by first considering the orbital energy

$$E = -\frac{Gm_1m_2}{2a} \quad . \tag{2.18}$$

Because gravitational waves carry energy, the total energy of the orbit must decrease as the radiation leaves the system. The binding energy becomes more negative, hence the semimajor axis of the orbit decreases. We know from Kepler's laws that

the orbital frequency, ω, semimajor axis, and mass of the binary, $M_{\rm tot}$, are related by

$$\omega^2 a^3 = GM_{\rm tot} \quad , \tag{2.19}$$

therefore the orbital frequency increases as the binary shrinks. From Equation (2.14), it follows that the strength of the gravitational radiation increases as the binary orbits more rapidly, which speeds up the energy loss. Thus, this is a runaway process in which the binary members spiral together more and more quickly, and eventually coalesce. The effect of gravitational radiation on a non-circular binary can be understood qualitatively by considering a binary with a large eccentricity. The gravitational radiation of such a binary is considerably stronger at pericenter, where the bodies pass each other closely, therefore the energy loss at close approach dominates. If we imagine this as an impulse, then energy is removed from the orbit, which decreases the semimajor axis while the pericenter distance remains fixed. This means that the apocenter distance must decrease, thereby resulting in a less eccentric orbit. We see, then, that gravitational radiation simultaneously circularizes and shrinks the orbits of binaries. Peters (1964) formulated the loss of energy and angular momentum and showed that the semimajor axis and eccentricity will change with respect to time such that

$$\left\langle \frac{da}{dt} \right\rangle = -\frac{64}{5} \frac{G^3 m_1 m_2 (m_1 + m_2)}{c^5 a^3 (1-e^2)^{7/2}} \left(1 + \frac{73}{24} e^2 + \frac{37}{96} e^4\right) \quad , \tag{2.20}$$

and

$$\left\langle \frac{de}{dt} \right\rangle = -\frac{304}{15} \frac{G^3 m_1 m_2 (m_1 + m_2)}{c^5 a^4 (1-e^2)^{5/2}} \left(e + \frac{121}{304} e^3\right) \quad . \tag{2.21}$$

The first confirmation of this energy loss came with the observations of a binary pulsar by Hulse & Taylor (1974).

The observation of PSR1913+16, taken in 1974 at the Arecibo telescope, would become the first empirical confirmation of gravitational wave theory. The first pe-

culiarity noted about this pulsar was its short orbital period of $\sim$ 8 hr (Hulse & Taylor 1974), which indicates that the pulsar is orbiting at the relativistic speed of $\sim 0.1\%\ c$. With follow-up observations, Taylor determined that each binary member has a mass of $\sim 1.4\ M_\odot$ (Taylor et al. 1976), revealing that the unseen companion of the pulsar is a neutron star as well. Because the semimajor axis of the binary and the masses of its constituents are known to a high accuracy, it is possible to calculate the orbital decay due to gravitational radiation. The measured rate of shrinking is $(2.4349 \pm 0.010) \times 10^{-12}$ seconds per second (Schutz 1996), which agrees within the uncertainties with theoretical predictions. Although PSR1913+16 is too widely separated to be observed by any planned detector, this Nobel Prize winning work is an astounding verification of general relativity in the limit of weak gravity.

As a binary shrinks, the frequency of the gravitational radiation it emits increases. Because of the quadrupolar nature of gravitational waves, the gravitational radiation frequency, $f_{\rm gw}$, of a circular binary is twice the orbital frequency

$$f_{\rm gw} = 2\omega \quad . \tag{2.22}$$

For an eccentric binary, the signal will have the same fundamental frequency, $f_{\rm gw}$, but will also contain harmonics that are dependent on the eccentricity. The amplitude of the gravitational radiation goes like (see, e.g. Schutz 1996)

$$h \propto \frac{f_{\rm gw}^{2/3} M_c^{5/3}}{r} \quad , \tag{2.23}$$

where M_c is the chirp mass of a binary with reduced mass μ (see, e.g. Thorne 1996),

$$M_c \equiv \frac{(m_1 m_2)^{3/5}}{(m_1 + m_2)^{1/5}} = \mu^{3/5} M_{\rm tot}^{2/5} \quad , \tag{2.24}$$

which determines the rate at which the frequency changes (Schutz 1996)

$$\frac{{\rm d}\ \ln f_{\rm gw}}{{\rm d}t} \propto M_c^{5/3} f_{\rm gw} f_{\rm gw}^{8/3} \quad . \tag{2.25}$$

Figure 2.1 demonstrates the effect of frequency changes on the detectability of binary sources. It shows estimated sensitivity curves for first-generation and advanced ground-based gravitational wave detectors overlaid with the paths traced by neutron star and black hole binaries as they sweep to higher frequencies during inspiral. Figure 2.2 is similar, showing the motion of massive black hole sources through the operational frequency range of LISA. Measurement of the frequency sweep, amplitude, and harmonic content of a source will yield its chirp mass, eccentricity, inclination, and distance.

2.3.5 Merging Black Holes

As discussed in the introductory chapter, gravitational waves will provide a direct observational foundation on which to ground our knowledge of black hole binaries, however until they are detected, we rely on our theoretical understanding of the evolution of these binaries from inspiral to merger and ringdown. The inspiral stage can be modeled analytically using Newtonian gravity via the Peters formulae (Equations 2.21 and 2.22), however when the black holes are separated by a ∼few gravitational radii, the quadrupole approximation is no longer sufficient. In this regime, post-Newtonian terms are added to the equations of motion to represent higher moments.

When the black holes enter the plunge phase, analytical approximations are not as accurate as general relativistic simulations in determining the waveforms. Within the past few years, several separate groups of numerical relativists have developed independent methods of simulating the overlapping event horizons of merging black holes and the resulting gravitational waves, and their results are comparable (Miller 2007b). In the wake of the merger process, the resultant black hole will initially have a complicated, lumpy horizon. General relativity dictates, however, that a

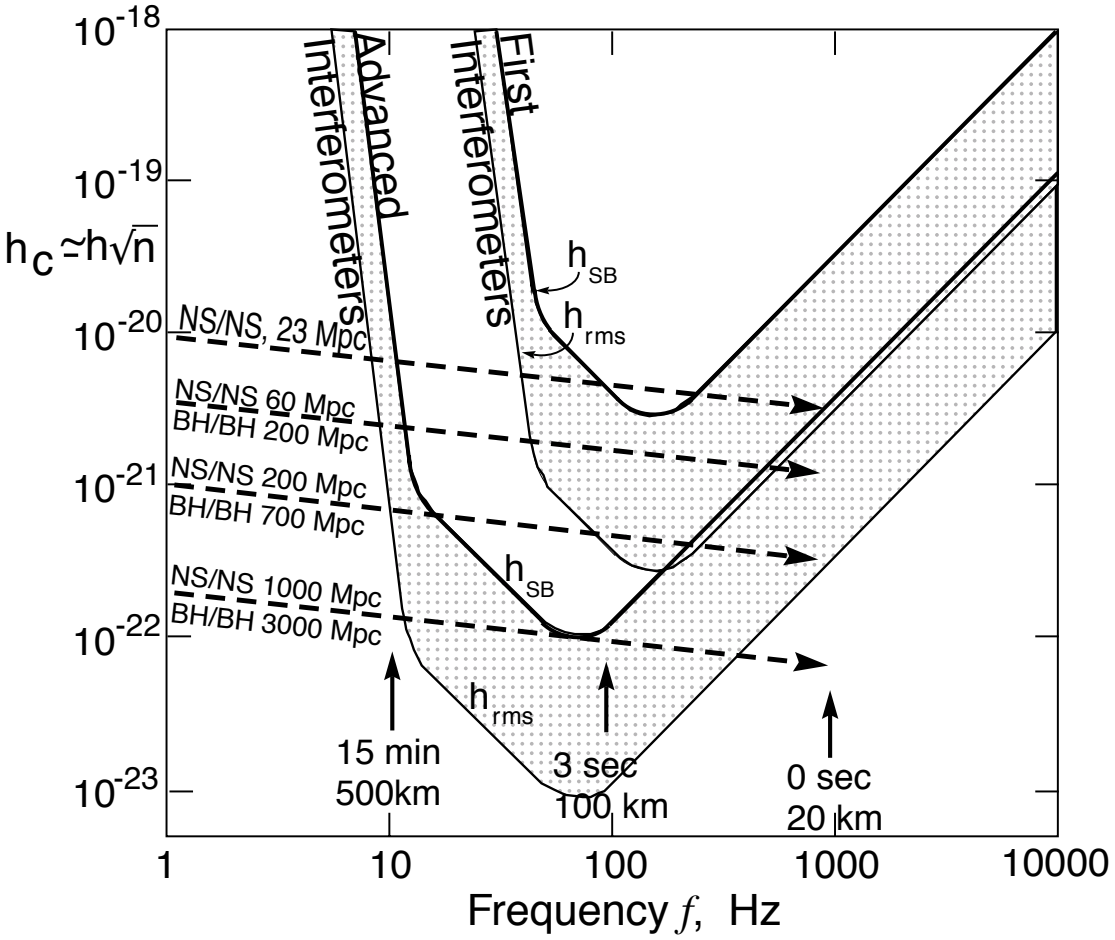

Figure 2.1: (Thorne 1996) Estimated sensitivity curves for both first-generation and advanced ground-based gravitational wave detectors. Dashed arrows show the paths made by neutron star and black hole binaries at various distances as they sweep to higher frequencies during inspiral. The curves labeled $h_{\rm sb}$ represent the sensitivities required for high-confidence detections, while the curves labeled $h_{\rm rms}$ are the optimal, root-mean-square sensitivities.

black hole in isolation is described completely by its mass and spin, and that its geometry is described by the comparatively simple Kerr spacetime metric. This means that the lumpy merger remnant must settle into a smoother state, and it does so by radiating gravitational waves. Like the inspiral phase, the radiation from this ringdown process has been calculated analytically (Teukolsky 1973). With the addition of advances in numerical relativity, we can now paint a much more complete picture of black hole coalescence than was possible even a few years ago.

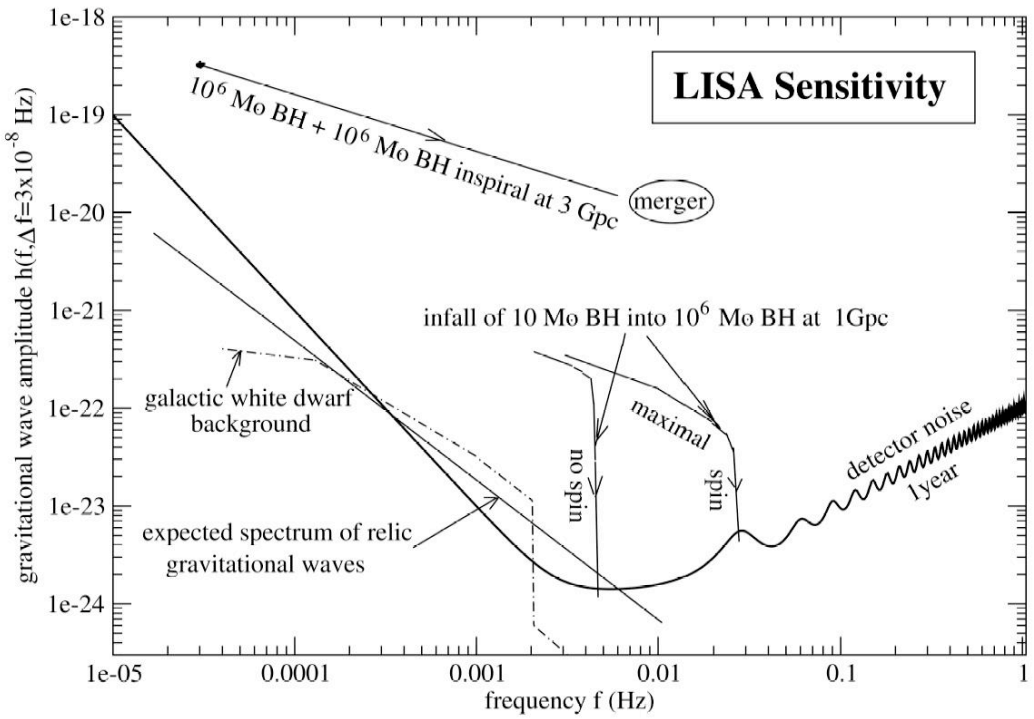

Figure 2.2: (Thorne 1996) Estimated sensitivity curve of LISA, showing the white dwarf population and primordial background as well as the sweeping paths of merging black hole binaries.

2.4 Sources and Detectors

Gravitational wave sources radiate at a wide range of frequencies, hence a variety of detectors have been designed to be sensitive in different frequency bands. Figure 2.3 shows several different classes of sources, their expected frequencies, and the detectors that will operate at those frequencies. Primordial gravitational waves might leave a polarization signature on the cosmic microwave background, known as B-mode CMB polarization. Space-based missions operating at the very low end of the frequency spectrum, such as the Planck satellite or the future Cosmic Inflation Probe, will search for such a signature. Pulsar timing arrays, which operate at frequencies below those of ground- and space-based detectors, might make the first direct measurements of gravitational waves. These arrays are sensitive to super-

massive black hole binaries and stochastic background sources. Moving to slightly higher frequencies, space-based detectors such as LISA will detect nearby neutron star and white dwarf binaries, with the latter being numerous enough to constitute a stochastic noise source. Extragalactic black hole binaries and the inspirals of stellar-mass black holes into massive black holes are important LISA sources. In addition, if gravitational waves from processes in the early universe are sufficiently strong, then LISA will operate in the correct frequency band to detect them. High frequency, ground-based interferometers such as LIGO are also promising candidates to make the first gravitational radiation detection, and they are sensitive to coalescing neutron stars and stellar-mass black holes. If bursts from collapsing stars and rotating galactic neutron stars are detectable, then they will also be in this high-frequency range.

2.5 Summary

We have discussed gravitational radiation, detectors, and sources. Coalescing binaries are the most promising sources, and the detection of gravitational waves will be an important landmark in our understanding of compact object binaries and black holes, in particular. In the next chapter, we will discuss a promising host for black hole mergers: star clusters in the centers of small galaxies.

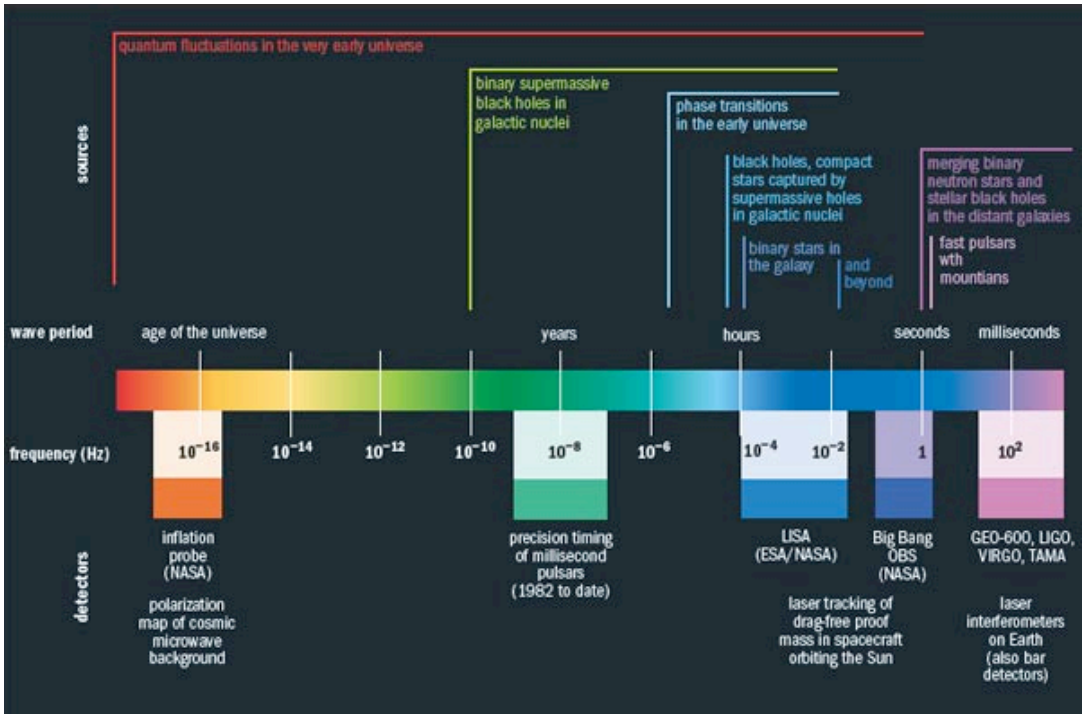

Figure 2.3: (Source: NASA) Diagram showing the frequencies of various gravitational wave sources and the instruments that could detect them. Ground-based detectors operate at the high frequency end, and are sensitive to coalescing neutron stars, black holes, and, possibly, collapsing stars and rotating neutron stars. Space-based detectors operate at lower frequencies where extragalactic stellar-mass and massive black holes radiate. Pulsar timing arrays operate at yet lower frequencies, and are sensitive to supermassive black hole binaries. At the low frequency end, the Planck satellite and the future Cosmic Inflation Probe will look for gravitational wave signatures in the CMB.

Chapter 3

Nuclear Star Clusters

"Many a small thing has been made large by the right kind of advertising."

—Mark Twain

3.1 Introduction

In recent years, the improvement in optical resolution made possible with the *Hubble Space Telescope* (HST), has led to the discovery that very dense clusters of stars are common in the centers of galaxies across a broad range of Hubble types (Böker 2008). While nuclear star clusters (NSCs) were identified in late-type spirals through ground-based observations (Matthews & Gallagher 1997), HST surveys have since discovered NSCs in earlier-type spirals (Carollo et al. 1997) and spheroidal galaxies (Côté et al. 2006). The prevalence of NSCs across galaxy type contributes to the body of evidence that indicates that the formation and evolution of nuclei and their host galaxies are linked.

Nuclear star clusters are very compact (Geha et al. 2002) and luminous (Böker

et al. 2002), and are located at the dynamical centers of their galaxies; though they are similar in size to typical globular clusters, NSCs are significantly more massive. The mass densities of NSCs appear to be related to those of globulars and other compact clusters (Walcher et al. 2005). This has lead to speculation that some globular clusters might be the remains of NSCs that survived the destruction of their original hosts during mergers.

Like globular clusters, NSCs are dense stellar environments that are conducive to the formation of compact object binaries. In such a setting, compact binaries will have close encounters with stars, which could cause the binaries to be ejected before they have the chance to merge. Globular clusters, with their low escape speeds, likely lose most of their black holes due to post-encounter recoil kicks (Portegies Zwart & McMillan 2000; Sigurdsson & Hernquist 1993), or possibly due to large natal kicks delivered to the black hole by its supernova (Mirabel et al. 2002). NSCs, on the other hand, have both high densities and high escape speeds, hence they are promising potential hosts of gravitational radiation sources.

In §3.2 of this chapter, we discuss the properties of NSCs, following with possible formation scenarios in §3.3. §3.4 considers possible links between NSCs, globular clusters, and compact dwarf galaxies, and in §3.5 we discuss possible connections with supermassive black holes.

3.2 Properties of Nuclear Star Clusters

3.2.1 Prevalence

One of the most intriguing properties of NSCs is how common they are. There are confirmed NSC detections in 70% of E and S0 galaxies (Côté et al. 2006), 50% of Sa-Sc spirals (Carollo et al. 1997), and 75% of late-type spirals (Böker et al.

2002). In general, the presence of a NSC is determined by a marked increase in surface brightness at or near the photometric center of the galaxy, which exceeds the inward extrapolation of the underlying bulge/disk profile. Figure 3.1 is a selection of HST images from the Böker et al. (2002) survey of bright central clusters in late-type, low surface brightness spirals. In galaxies with less prominent NSCs, the locations of the clusters are circled. Figure 3.2 shows the corresponding surface brightness profiles (diamond symbols), where the best fits for the inward extrapolation of the disk are plotted as solid lines. Here, the dashed lines represent the level of constant surface brightness measured at the radius at which the disk profile and the surface brightness diverge (Böker et al. 2002). In the interior regions of galaxies with prominent NSCs, the surface brightness profiles are well above the estimated magnitude of the inner disk. For comparison, in galaxies appearing to lack NSCs, the surface brightness profiles match well with their disk profiles, as illustrated in Figure 3.3. It is difficult to pinpoint the centers of many late-type spirals, which are often bulgeless (Walcher et al. 2005), therefore NSCs could be more prevalent than indicated by the percentages above. In addition, many early-type galaxies have surface brightness profiles that are too steep for NSCs to be observable, because there is insufficient contrast between the clusters and their surroundings (Böker 2008).

3.2.2 Size and Luminosity

Regardless of the Hubble types of their host galaxies, NSCs are similar in size to globular clusters, yet they are far more luminous. Late-type spirals have central clusters with half-light radii ranging from 2 to 5 pc (Böker et al. 2004), and a large survey of early-type galaxies yields a comparable median half-light radius of $\sim$4 pc (Côté et al. 2006). In the I-band, NSCs are $\sim$4 magnitudes more luminous than the average globular cluster, with absolute magnitudes of order -14 to -10 (Böker

2008). The luminosities of some bright NSCs can reach as high as ∼2 orders of magnitude greater than the most luminous globulars in the Milky Way. NSCs have larger luminosities because they tend to contain both more mass and younger stars than their globular cluster counterparts.

3.2.3 Mass and Mass Density

While typical globular clusters are less massive, the measured mass densities of NSCs align them more closely with globulars and other compact clusters than with small galactic bulges (Walcher et al. 2005). The first directly-determined NSC mass was calculated using the stellar velocity dispersion and assuming virialization in the central cluster in IC 342, which yields a mass of 6×10^6 $M_\odot$ (Böker et al. 1999). A subsequent HST study of nine NSCs found a range in masses from $10^6 - 10^7$ $M_\odot$, thereby establishing NSCs as considerably more massive than Milky Way globulars, which fall in the $10^4 - 10^6$ $M_\odot$ range (Walcher et al. 2005). The mean surface densities of NSCs are among the highest measured in any type of compact cluster to date, and can reach $\sim 10^5$ $M_\odot$ pc^{-2}. Figure 3.4 (Walcher et al. 2005) shows the mean projected mass density versus the total mass for a variety of systems. NSCs in late-type spirals lie in the same region as Milky Way and extra-galactic globulars, super star clusters, ultra-compact dwarfs, and dwarf elliptical nuclei, however nuclear clusters are clearly distinct from galactic spheroids. In fact, typical dwarf spheroids are ∼4 orders of magnitude less dense than the most massive NSCs (Böker 2008). The fact that NSCs are similar in structure to other compact clusters could indicate that they are evolutionarily linked.

3.2.4 Star Formation History and Age

A number of observations demonstrate that the stars in NSCs are of varying age, which suggests that these clusters undergo recurrent star formation events. Spectroscopic and photometric studies indicate that NSCs tend to contain much younger stars than do globular clusters (Seth et al. 2006). The Walcher et al. (2006) study of nine NSCs found that the most recent bouts of star formation in clusters occurred as recently as 34 Myr ago, and every NSC in this sample contains stars with ages < 100 Myr. A larger survey of 40 galaxies found that 50% of NSCs have stars with ages < 1 Gyr, and that the clusters are best-fit with multiple-age models in all cases (Rossa et al. 2006). This study also discovered that the ages of stellar populations in NSCs differ across Hubble-types, with mean ages of ~ 250 Myr in late-type spirals and ~ 1.6 Gyr in early-type spirals.

While it is possible to rebuild the recent star formation history of NSCs by observing young and moderately-aged stars, establishing the time of cluster formation requires the determination of the ages of the oldest stars. This is a difficult analysis in late-type spirals because the NSC spectra are dominated by bright young stars, which makes the older stars difficult to detect. There are fewer young stars in the comparably gas-deficient early-types, yet the lack of contrast between NSCs and the bright backgrounds of these galaxies make detection and spectral analysis of the clusters difficult (Böker 2008). However, analysis of mass-to-light ratios suggests that large numbers of old stars underly the younger population, contributing the bulk of the mass while producing very little light (Rossa et al. 2006). Additionally, the overall colors of NSCs in dwarf nuclei are congruous with older populations with ages > 1 Gyr (Stiavelli et al. 2001). Because older stars can easily hide, it is likely that any age estimates are lower limits.

3.2.5 Extension of Scaling Relations

A number of scaling relations link the properties of galactic nuclei to those of their host galaxies, which indicates that these regions share a common evolutionary history despite vastly differing scales. Among the most often discussed correlations are those between the mass of the nuclear supermassive black hole, M_{SMBH}, and a variety of bulge characteristics, such as luminosity (Kormendy & Richstone 1995), velocity dispersion (Ferrarese & Merritt 2000; Gebhardt et al. 2000), and mass (Magorrian et al. 1998). As discussed in §3.2.3, NSCs extend the high end of globular cluster trends in both mass and mass density, and recent work has also revealed that, like massive black holes, some properties of NSCs scale with those of their hosts.

Figure 3.5 (Ferrarese et al. 2006) shows that NSCs follow a trend similar to the established $M_{SMBH} - \sigma$ relation, which links supermassive black hole masses to bulge velocity dispersions in luminous spiral and spheroidal galaxies. The similarity in the trends followed by both NSCs and SMBHs have sparked speculation about the possibility that these classes of objects share common formation mechanisms, however it should be noted that the M$-\sigma$ relation followed by NSCs is clearly offset from the M$-\sigma$ trend for black holes.

3.3 NSC Genesis

There are two primary classes of mechanisms that have been proposed to explain the formation of NSCs: gradual build up via the accretion of globular clusters (Böker et al. 2004), and in-situ formation by the infall of gas and ensuing star formation (Milosavljević 2004). There is support for each category, both from simulations and observations.

As globular clusters orbit a galaxy, dynamical friction can cause them to spiral

in and ultimately merge with the galactic nucleus (Tremaine et al. 1975). N-body simulations have demonstrated that globular clusters orbiting an initially triaxial galactic center can sink and form a nuclear cluster in well under a Hubble time, and the resultant NSC has a surface density, mass, and velocity dispersion comparable to observed values (Capuzzo-Dolcetta & Miocchi 2008). It is as yet unclear how dependent the success of this mechanism is on the initial conditions (Böker 2008).

The second class of formation scenarios requires a mechanism to channel gas into the galactic center, which in turn leads to star formation and the eventual growth of a NSC. Several such mechanisms have been proposed. For example, the magneto-rotational instability has been demonstrated to be a viable process by which gas can be transported in sufficient quantities to form NSCs (Milosavljević 2004). Bar instabilities are another possible mechanism, with supporting evidence provided by observations by Schinnerer et al. (2007), which show that a bar has funneled gas into the central 60 pc of NGC 6946, leading to a build-up of mass and increased star formation. It has, therefore, been suggested that a NSC might currently be forming in this galaxy. Young stars were recently discovered in extended structures surrounding NSCs in several galaxies, providing additional evidence that new stars form episodically in gas disks and later assume the spherical structure of the NSC, possibly by dynamical heating (Seth et al. 2006). It also has been suggested that the inflow of gas into the nucleus is simply a by-product of galaxy formation. Emsellem & van de Ven (2008) demonstrated that the tidal field of a shallow potential is compressive on the scales of typical NSCs, which can result in the compression of gas and star formation. This scenario could clarify why NSCs are so prevalent regardless of Hubble type, and could provide a natural explanation for the scaling trends discussed in §3.2.5 that link NSCs to their hosts.

3.4 Forced Retirement as Globulars or Ultra-Compact Dwarfs

After discussing the births of NSCs, perhaps it is natural to consider their twilight years. It is possible that some NSCs are stripped from galactic nuclei and later become globular clusters or ultra-compact dwarfs. As discussed in §3.2.3, the NSCs in late-type spirals share structural similarities with these classes of compact clusters and galaxies. As first suggested by Freeman (1993), some globular clusters might have formed as compact clusters in the nuclei of small galaxies, which then underwent merger events. In this scenario, the nuclear cluster survives the merger, and is left to orbit in the halo of the merged galaxy. This might explain the composite-age populations observed in some Milky Way globulars (Lee et al. 2007). Similarities in structure (Walcher et al. 2005), size, luminosity, and color (Côté et al. 2006) have also lead to the suggestion that some ultra-compact dwarfs are the surviving NSCs of tidally shredded galaxies.

3.5 NSCs and Black Holes

As discussed in §3.2.5, the masses of NSCs are related to the bulge velocity dispersions of their host galaxies in a manner similar to the well-known $M_{SMBH} - \sigma$ relation. This discovery prompted the idea that NSCs and SMBHs together might constitute a class of "Central Massive Objects" (CMOs) that are ubiquitous among galaxies. In this picture, NSCs populate the low-mass end, and are present in low- to intermediate-luminosity galaxies, and SMBHs are found in bright galaxies with masses $> 10^{10}$ $M_{\odot}$ (Ferrarese et al. 2006). This scenario is intriguing because it would indicate that there is a formation mechanism common to both SMBHs and

NSCs, and that the type of CMO that forms in a particular galaxy is determined by the mass of that galaxy. However, it is unclear that this picture can account for the fact that the M-σ relation for NSCs is clearly offset from the M-σ trend for SMBHs.

Observations have shown that many galaxies with NSCs evidently do not host massive black holes, however this is not always the case (see e.g. Graham & Spitler 2009). In a recent large survey of galaxies of varying Hubble types, Seth et al. (2008) find that $\sim 10\%$ of galaxies appear to host both an AGN and a NSC. Further work will be necessary to determine whether the CMO scenario is consistent with observations of coincident NSCs and SMBHs, or with observations of galaxies that do not appear to have either type of central object (Böker 2008).

3.6 Summary

NSCs are massive, luminous, compact clusters that reside in the centers of a large fraction of galaxies $-$ 75% in the case of late-type spirals. They contain multiple stellar populations, which might indicate that they have undergone episodic star formation. NSCs appear to have formed either by multiple mergers of globular clusters or in-situ via star formation resulting from the inflow of gas to the nucleus. In addition, evidence, such as structural similarity, points to NSCs as possible progenitors to some globular clusters and ultra-compact dwarf galaxies. Various properties of NSCs have been found to correlate with those of their galactic hosts, which might indicate that the formation of NSCs is intimately related to that of galaxies as a whole. While it appears that many NSCs do not contain massive black holes, some fraction of galaxies have been observed to host both AGN and NSCs.

The high densities in NSCs are conducive to close encounters between binaries and single stars. With this in mind, we investigate NSCs as potential hosts of

stellar-mass black hole mergers in the following chapter.

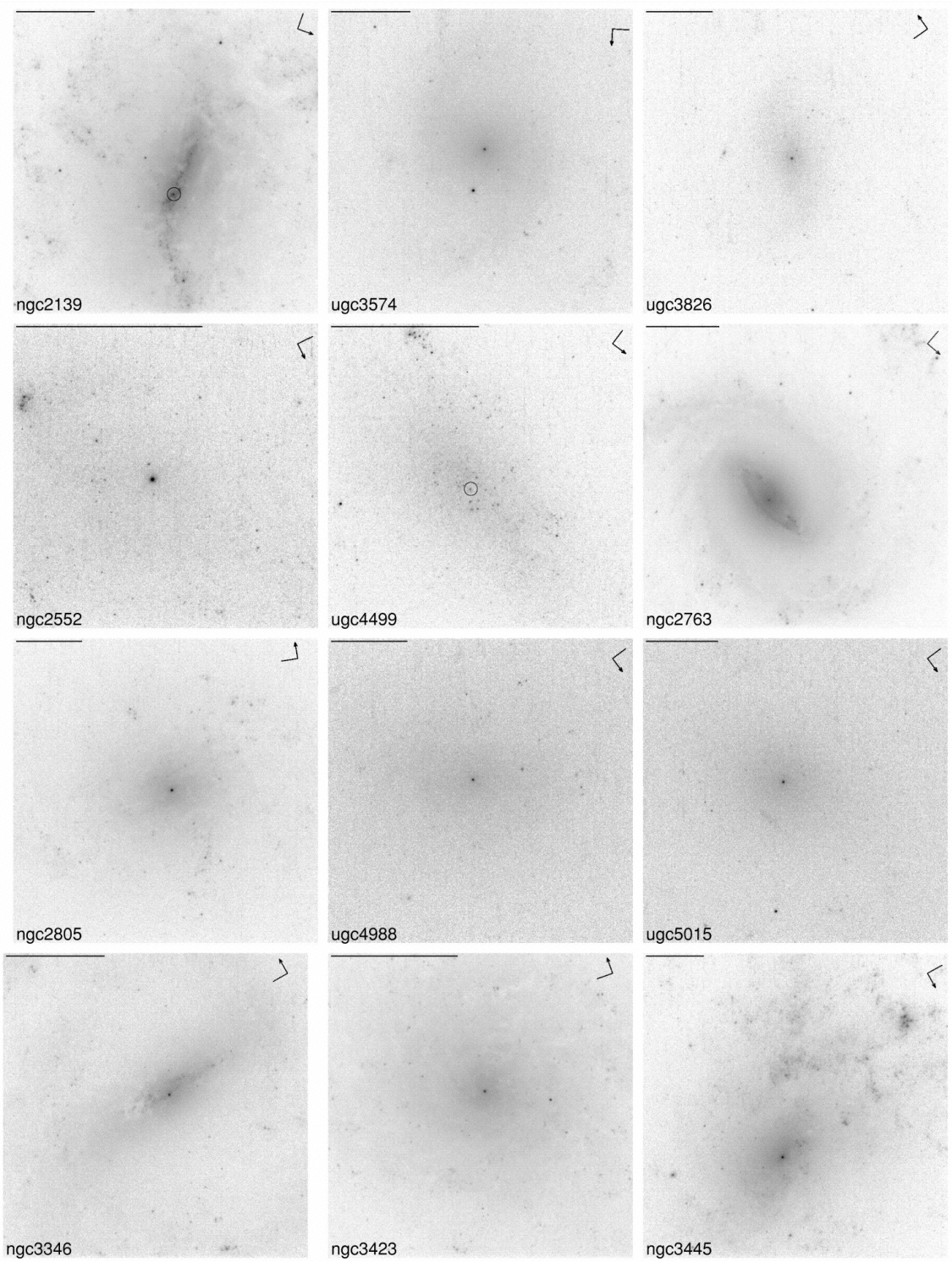

Figure 3.1: (Böker et al. 2002) Selected HST images from a survey of bright central clusters in late-type, low surface brightness spirals. In galaxies with less prominent NSCs, the clusters are circled. The lines in the upper right of each panel indicate north (arrow) and east.

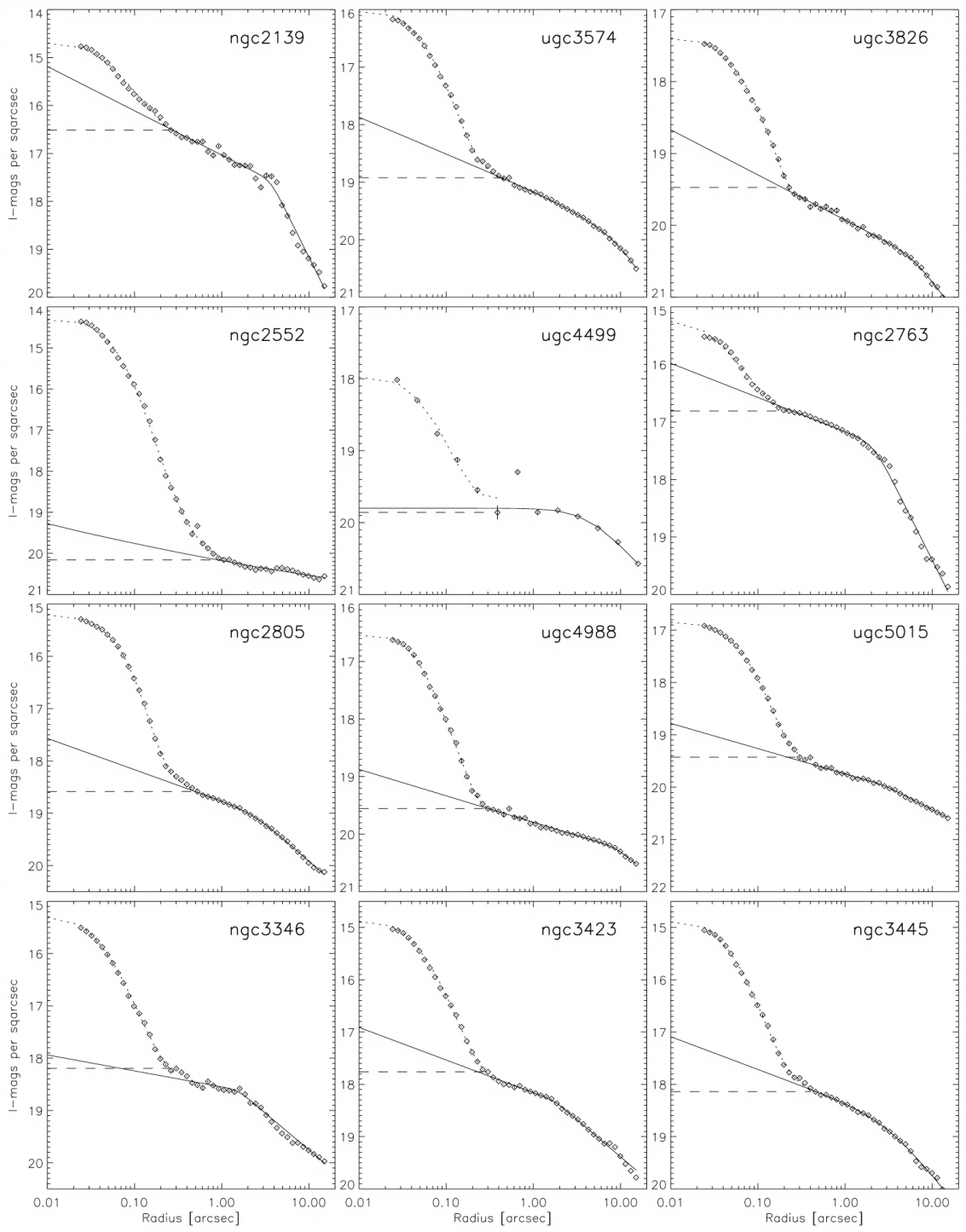

Figure 3.2: (Böker et al. 2002) Surface brightness profiles (diamond symbols) corresponding to the images in Figure 3.1. The solid lines are best fits for the inward extrapolation of the disk, and dashed lines represent the level of constant surface brightness measured at the radius at which the disk profile and the surface brightness diverge. In the interior regions of galaxies with prominent NSCs, the surface brightness profiles are well above the estimated magnitudes of the inner disks.

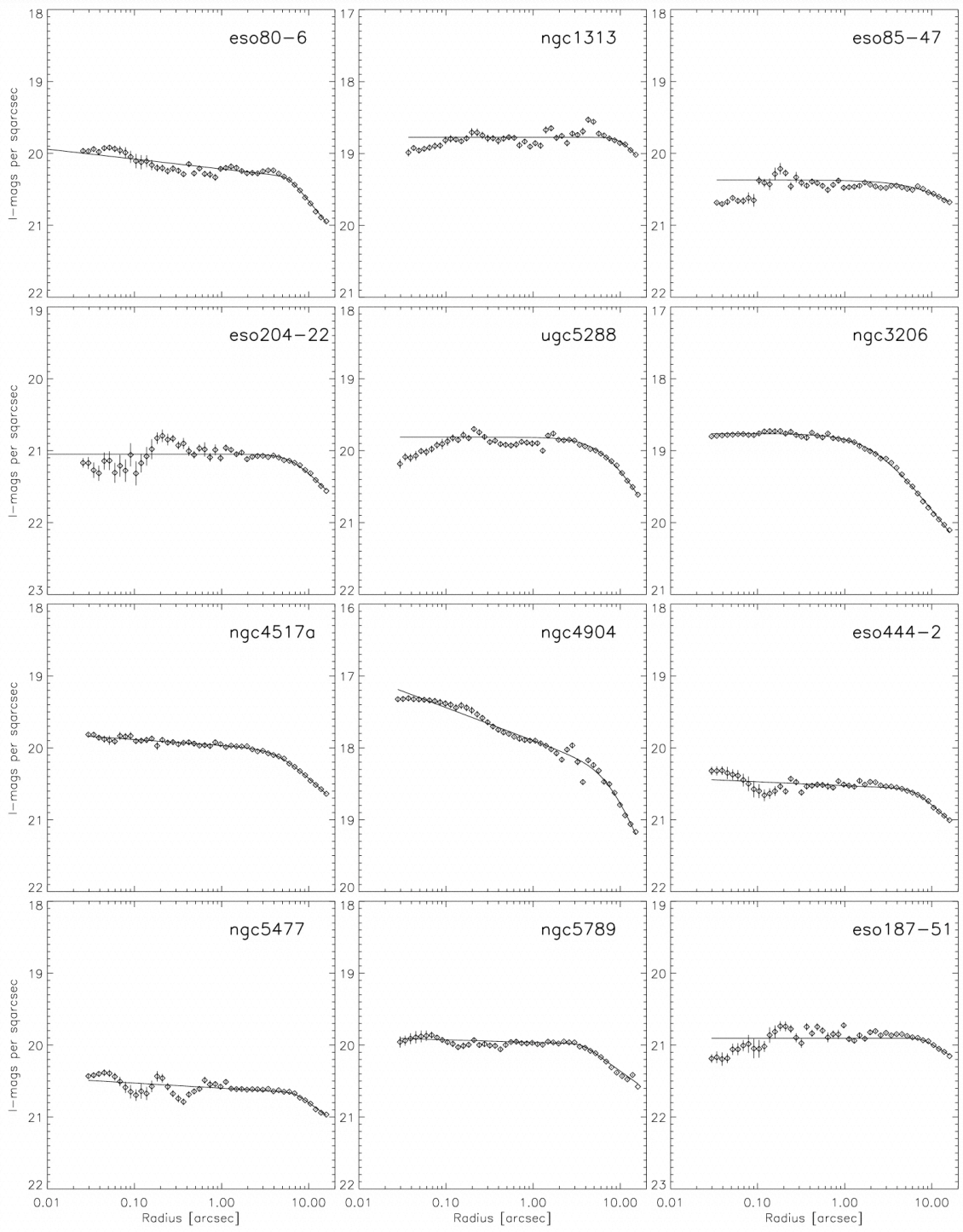

Figure 3.3: (Böker et al. 2002) Galaxies for which the measured surface brightness profiles match well with the estimated disk profiles. These appear to lack NSCs.

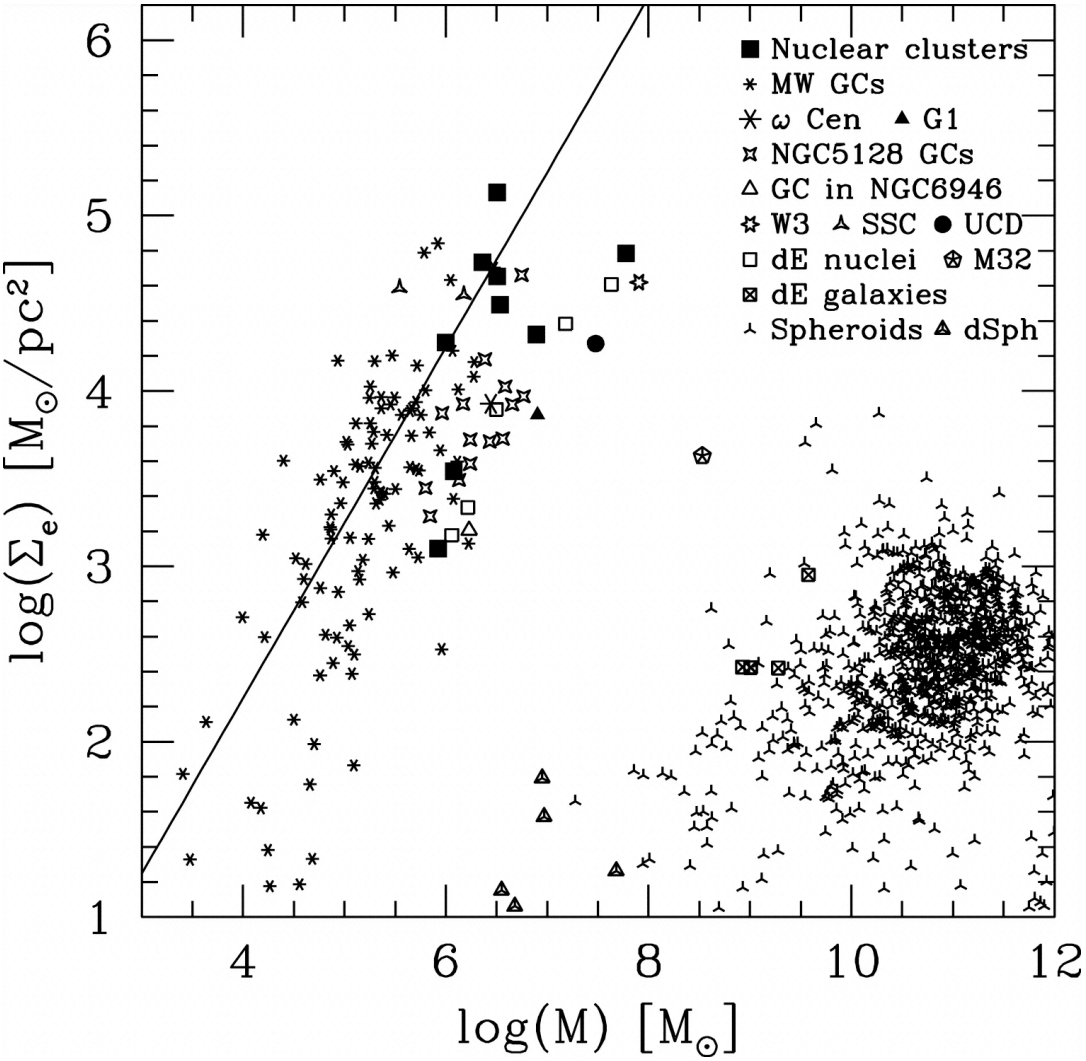

Figure 3.4: (Walcher et al. 2005) Mean projected mass density versus the total mass for a variety of systems. NSCs in late-type spirals lie in the same region as Milky Way and extra-galactic globulars, super star clusters, ultra-compact dwarfs, and dwarf elliptical nuclei. However, NSCs are clearly distinct from galactic spheroids.

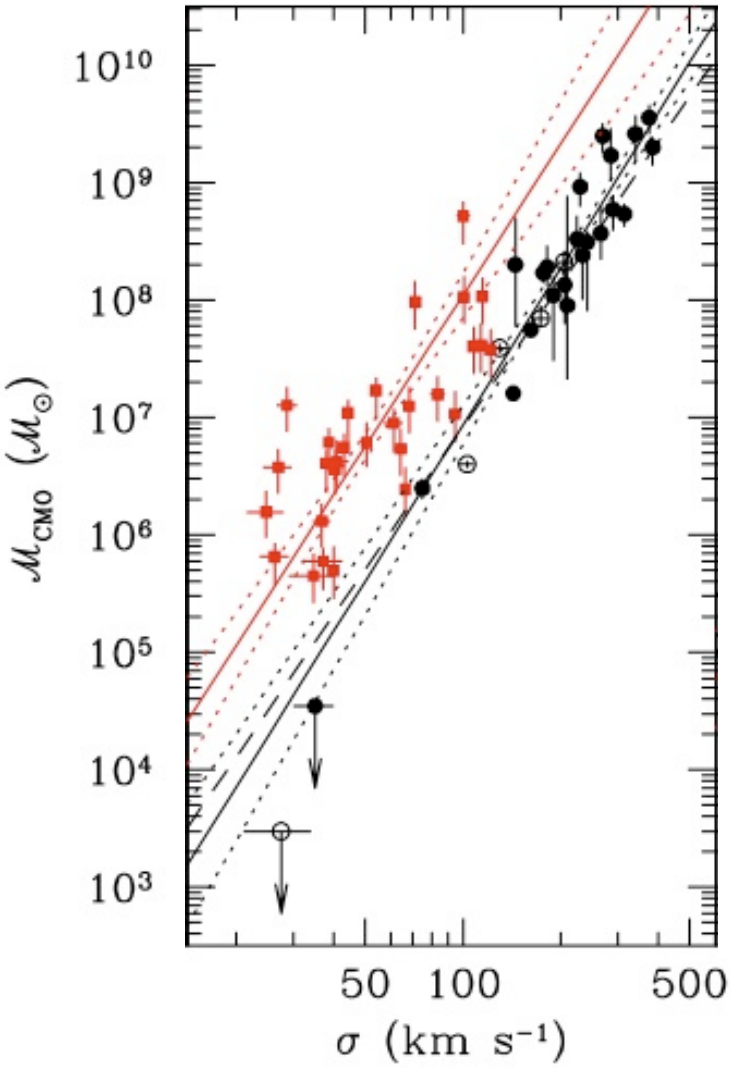

Figure 3.5: (Ferrarese et al. 2006) Mass versus velocity dispersion. Black circles are spiral and spheroidal galaxies containing SMBHs, and red squares are early-type galaxies with NSCs. While the trends are somewhat similar, the M-σ relation for NSCs is clearly offset from the M-σ trend for SMBHs.

Chapter 4

Mergers of Stellar-Mass Black Holes in Nuclear Star Clusters

4.1 Introduction

Ground-based gravitational wave detectors have now achieved their initial sensitivity goals (e.g., Abbott & et al. 2007). In the next few years, these sensitivities are expected to improve by a factor of ~ 10, which will increase the observable volume by a factor of $\sim 10^3$ and will lead to many detections per year (Thorne 1996).

As we discussed in Ch. 1, one of the most intriguing possible sources for such detectors is the coalescence of a double stellar-mass black hole (BH-BH) binary. Such binaries are inherently invisible, meaning that we have no direct observational guide to how common they are or their masses, spin magnitudes, or orientations. Comparison of the observed waveforms (or of waveforms from merging supermassive black holes [SMBHs]) with predictions based on approximate solutions and numerical relativity will be a strong test of the predictions of strong-gravity general relativity.

The fact that we can not detect these sources electromagnetically makes it challenging to estimate rates, because we are left to derive our only observational handles on BH-BH binaries from observations of their possible progenitors. For example, a commonly discussed scenario involves the effectively isolated evolution of a field binary containing two massive stars into a binary with two black holes (BHs) that will eventually merge (e.g., Belczyński & Bulik 1999; Lipunov et al. 1997). There are profound uncertainties involved in calculations of these rates due to the lack of knowledge of the details of the common envelope phase in these systems and the absence of guides to the distribution of supernova kicks delivered to BHs. For example, note that the Advanced LIGO detection rate of BH-BH coalescences is estimated to be anywhere between $\sim 1 - 500$ yr^{-1} by Belczyński et al. (2007), depending on how common envelopes are modeled.

Another promising location for BH-BH mergers is globular clusters, where stellar number densities are high enough to cause multiple encounters and hardening of binaries. Even though binaries are kicked out before they merge (Kulkarni et al. 1993; O'Leary et al. 2006; Portegies Zwart & McMillan 2000; Sigurdsson & Hernquist 1993; Sigurdsson & Phinney 1993, 1995), these clusters can still serve as breeding grounds for gravitational wave sources. Indeed, O'Leary et al. (2007) estimate a rate of 0.5 yr^{-1} for initial LIGO and 500 yr^{-1} for Advanced LIGO via this channel. There is, however, little direct evidence for BHs in most globulars, which could be because they are simply difficult to see or perhaps because globulars do not retain their BH populations. In support of the latter, at least one BH in a low-mass X-ray binary apparently received a $\gtrsim 100$ km s^{-1} kick from its supernova (GRO J1655–40; see Mirabel et al. 2002). This is double the escape speed from the centers of even fairly massive globulars (Webbink 1985), which leads to uncertainties about the initial BH population and current merger rates in these clusters.

Here we propose that mergers occur frequently in the nuclear star clusters that may be in the centers of many low-mass galaxies (Böker et al. 2002; Ferrarese et al. 2006; Wehner & Harris 2006; note that some of these are based on small deviations from smooth surface brightness profiles and are thus still under discussion). It has recently been recognized that in these galaxies, which may not have SMBHs (for a status report on ongoing searches for low-mass central black holes, see Greene & Ho 2007), the nuclear clusters have masses that are correlated with the one-dimensional velocity dispersion $\sigma_{\rm 1D,bulge}$ at one galactic effective radius as $M \approx 10^7\ M_\odot(\sigma_{\rm 1D,bulge}/54\ {\rm km\ s^{-1}})^{4.3}$ (Ferrarese et al. 2006). A black hole with a mass a factor of a few below the M-σ relation would be undetectable dynamically. Note that this velocity dispersion is typically a factor of ~ 2 larger than the measured one-dimensional volume-weighted velocity dispersion $\sigma_{\rm 1D}$ of the nuclear star cluster itself (compare $\sigma_{\rm 1D}$ and M for the clusters in Walcher et al. 2005 with the values predicted with the Ferrarese et al. 2006 relation above). Measurements indicate that $\sigma_{\rm 1D}$ is commonly in the range $24 - 34$ km s^{-1}, as is the case for seven of the ten total nuclear star clusters described in Walcher et al. 2005 and Seth et al. 2008. If the velocity distribution is isotropic, then the three-dimensional velocity dispersion $\sigma_{\rm 3D} = \sqrt{3}\sigma_{\rm 1D}$ is often between $\sigma_{\rm 3D} \sim 40 - 60$ km s^{-1}.

At these three-dimensional velocity dispersions, the half-mass relaxation time is small enough that BHs (which have $\sim 20\times$ the average stellar mass) can sink to the center in much less than a Hubble time. In addition, although systems with equal-mass objects require roughly 15 half-mass relaxation times to undergo core collapse (Binney & Tremaine 1987), studies show that systems with a wide range of stellar masses experience core collapse within $\sim 0.2\times$ the half-mass relaxation time (Gürkan et al. 2004; Portegies Zwart & McMillan 2002). Combined with the Ferrarese et al. (2006) relation between cluster mass and $\sigma_{\rm 1D,bulge}$, we find that

clusters with masses less than $\sim$ few $\times 10^7$ $M_\odot$ and no central SMBH (or a highly undermassive SMBH) will have collapsed by now and hence increased the escape speed from the center, allowing retention of most of their BHs.

As we show in this chapter, nuclear star clusters are therefore excellent candidates for stellar-mass black hole binary mergers because they keep their BHs while also evolving rapidly enough that the BHs can sink to a region of high density. If tens of percent of the BHs in eligible galaxies undergo such mergers, the resulting rate for Advanced LIGO is tens per year. In § 4.2 we quantify these statements and results more precisely and discuss our numerical three-body method. We give our conclusions in § 4.3.

4.2 Method and Results

4.2.1 Characteristic Times and Initial Setup

Our approach is similar to that of O'Leary et al. (2006), who focus on globular clusters with velocity dispersions $\sigma_{\rm 1D} \leq$ 20 km s^{-1}. Here, however, we concentrate on the more massive and tightly bound nuclear star clusters. Our departure point is the relation found by Ferrarese et al. (2006) between the masses and velocity dispersions of such clusters:

$$M_{\rm nuc} = 10^{6.91\pm0.11} \left(\sigma_{\rm 1D,bulge}/54 \text{ km s}^{-1}\right)^{4.27\pm0.61} \ M_\odot \ . \tag{4.1}$$

Assuming that there is no massive central black hole for these low velocity dispersions, the half-mass relaxation time for the system is (see Binney & Tremaine 1987) $t_{\rm rel} \approx \frac{N/2}{8 \ln N} t_{\rm cross}$ where $N \approx M_{\rm nuc}/0.5\ M_\odot$ is the number of stars in the system (assuming an average mass of 0.5 $M_\odot$) and $t_{\rm cross} \approx R/\sigma_{\rm 3D}$ is the crossing time. Here $R = GM_{\rm nuc}/\sigma_{\rm 3D}^2$ is the radius of the cluster. If we assume that $\sigma_{\rm 3D} = \sqrt{3}\sigma_{\rm 1D}$ and

that typically $\sigma_{\rm 1D,bulge} \approx 2\sigma_{\rm 1D} \approx \sigma_{\rm 3D}$, this gives

$$t_{\rm rel} \approx 1.3 \times 10^{10}\ {\rm yr} \left(\sigma_{\rm 3D}/54\ {\rm km\ s^{-1}}\right)^{5.5} \ . \tag{4.2}$$

The relaxation time scales inversely with the mass of an individual star (Binney & Tremaine 1987), so a 10 $M_\odot$ BH binary will settle in roughly 1/20 of this time. Also note that large N-body simulations with broad mass functions evolve to core collapse within roughly 0.2 half-mass relaxation times (Gürkan et al. 2004; Portegies Zwart & McMillan 2002), hence in the current universe clusters with velocity dispersions $\sigma_{\rm 3D} < 60$ km s^{-1} will have had their central potentials deepened significantly.

The amount of deepening of the potential, and thus the escape speed from the center of the cluster, depends on uncertain details such as the initial radial dependence of the density and the binary fraction. Given that the timescale for segregation of the BHs in the center is much less than a Hubble time, we will assume that the escape speed is roughly $5\sigma_{\rm 1D}$, as is the case for relatively rich globular clusters (Webbink 1985). This may well be somewhat conservative, because the higher velocity dispersion here than in globulars suggests that a larger fraction of binaries will be destroyed in nuclear star clusters. This could lead to less efficient central energy production and hence deeper core collapse than is typical in globulars.

With this setup, our task is to follow the interactions of black holes in the central regions of nuclear star clusters, where we will scale by stellar number densities of $n \sim 10^6$ pc^{-3} (a characteristic value near the center of the Milky Way; see Genzel et al. 2003) because of density enhancements caused by relaxation and mass segregation. We expect to find that binary-single interactions will (1) allow BHs to swap into binaries even if they began as single objects, and (2) harden BH binaries to the extent that they can merge while still in the nuclear star cluster. If a BH starts its life with a binary companion then the interaction time is short, because every interaction it has will be a binary-single encounter that has high cross section.

If instead the BH begins as a single object, the binary-single interaction rate is much less because it relies on the BH encountering comparatively rare binaries. This is the case we will consider, because if there is enough time for a BH to capture into a binary and then harden there is certainly enough time for a black hole that is born into a binary to harden.

All binaries in the cluster will be hard, i.e., will have internal energies greater than the average kinetic energy of a field star, because otherwise they will be softened and ionized quickly (e.g., Binney & Tremaine 1987). If, for example, we consider binaries of two 1 $M_\odot$ stars in a system with $\sigma_{3D} = 50$ km s^{-1}, then for the binary to be hard the semimajor axis has to be less than $a_{\max} \sim 1$ AU. Studies of main sequence binaries in globular clusters, which have $\sigma_{1D} \sim 10$ km s^{-1}, suggest that after billions of years roughly 5–20% of them survive, with the rest falling victim to ionization or collisions (Ivanova et al. 2005). The binary fraction will be lower in nuclear star clusters due to their enhanced velocity dispersion, but since when binaries are born they appear to have a constant distribution across the log of the semimajor axis from $\sim 10^{-2} - 10^3$ AU (e.g., Abt 1983; Duquennoy & Mayor 1991) the reduction is not necessarily by a large factor. We will scale by a binary fraction $f_{\rm bin} = 0.01$, which is likely to be somewhat low and thus we will slightly overestimate the time needed for a BH to be captured into a binary.

If a BH with mass $M_{\rm BH}$ gets within a couple of semimajor axes of a main sequence binary, the binary will tidally separate and the BH will acquire a companion. The timescale on which this happens is $t_{\rm bin} = (n\Sigma\sigma_{3D})^{-1}$, where $\Sigma = \pi r_p^2 \left[1 + 2GM_{\rm tot}/({\sigma_{3D}}^2 r_p)\right]$ is the interaction cross section for pericenter distances $\leq r_p$ when gravitational focusing is included. Here $M_{\rm tot}$ is the mass of the BH plus the mass of the binary. If we assume that $M_{\rm BH} = 10\ M_\odot$ (the mean BH mass in the Milky Way, see e.g. Kubota & Makishima 2005), and it interacts with a binary with

two 1 $M_\odot$ members and an $a = 1$ AU semimajor axis, then the typical timescale on which a three-body interaction and capture of one of the stars occurs is

$$t_{3-\mathrm{bod}} = (n\Sigma\sigma_{3\mathrm{D}})^{-1} \approx 3 \times 10^9 \text{ yr} \left(\frac{n}{10^6 \text{ pc}^{-3}}\right)^{-1} \left(\frac{f_{\mathrm{bin}}}{0.01}\right)^{-1} \left(\frac{\sigma_{3\mathrm{D}}}{50 \text{ km s}^{-1}}\right) \left(\frac{a}{1 \text{ AU}}\right)^{-1}. \tag{4.3}$$

With rapid sinking, BHs can form a subcluster in the galaxy core. This will decrease the number density of main sequence stars in the core, and hence of main sequence binaries (although binaries, being heavier than single stars, will be over-represented). The exchange process might thus take somewhat longer. The timescale in equation (4.3) is, however, small enough compared to a Hubble time that we start our simulations by assuming that each BH has exchanged into a hard binary, and follow its evolution from there.

Another important question is whether, after a three-body interaction, a BH binary will shed the kinetic energy of its center of mass via dynamical friction and sink to the center of the cluster before another three-body encounter. If not, the kick speeds will add in a random walk, thus increasing the ejection fraction.

To calculate this we note that the local relaxation time of a binary is

$$t_{\mathrm{rel}} = \frac{0.34}{\ln \Lambda} \frac{{\sigma_{3\mathrm{D}}}^3}{G^2 \langle m \rangle M_{\mathrm{bin}} n} \tag{4.4}$$

(Spitzer 1987) where $\ln \Lambda \sim 10$ is the Coulomb logarithm, $\langle m \rangle$ is the average mass of interloping stars, n is their number density, and M_{bin} is the mass of the binary. The timescale for a three-body interaction is $t_{3-\mathrm{bod}} = (n\Sigma\sigma_{3\mathrm{D}})^{-1}$ as above. Note, however, that for this calculation we assume that the BH has already captured into a binary. Therefore, it can interact with every star instead of just those in binaries, and thus the factor f_{bin} is no longer applicable and the timescale is typically 100 times less than indicated by the numerical factor in equation (4.3). For a gravitationally focused binary, which is of greatest interest because only these could in principle

produce three-body recoil sufficient to eject binaries or singles, $r_p < GM_{\rm bin}/{\sigma_{\rm 3D}}^2$. If we also assume that the total mass $M_{\rm tot}$ of the three-body system is close to $M_{\rm bin}$ because most of the interlopers have much less mass than the BH, then $\Sigma \approx 2\pi r_p GM_{\rm bin}/{\sigma_{\rm 3D}}^2$ and

$$t_{\rm 3-bod} \approx \frac{\sigma_{\rm 3D}}{2\pi n r_p G M_{\rm bin}} \ . \tag{4.5}$$

If we let $r_p = qGM_{\rm bin}/{\sigma_{\rm 3D}}^2$, with $q < 1$, then

$$t_{\rm 3-bod} \approx \frac{{\sigma_{\rm 3D}}^3}{2\pi q G^2 M_{\rm bin}^2 n} \tag{4.6}$$

so that

$$t_{\rm rel}/t_{\rm 3-bod} \approx \frac{2q}{\ln\Lambda}\frac{M_{\rm bin}}{\langle m\rangle} \ . \tag{4.7}$$

The encounters most likely to deliver strong kicks to the binary occur when the binary is very hard, $q \ll 1$, hence this quantity is typically less than unity, meaning that after a three-body encounter a binary has an opportunity to share its excess kinetic energy via two-body encounters and thus settle back to the center of the cluster. We therefore treat the encounters separately rather than adding the kick speeds in a random walk.

In a given encounter, suppose that a binary of total mass $M_{\rm bin} = M_1 + M_2$, a reduced mass $\mu = M_1 M_2/M_{\rm bin}$, and a semimajor axis $a_{\rm init}$ interacts with an interloper of mass $m_{\rm int}$, and that the kinetic energy of the interloper at infinity is much less than the binding energy of the binary (i.e., this is a very hard interaction). If after the interaction the semimajor axis is $a_{\rm fin} < a_{\rm init}$, then energy and momentum conservation mean that the recoil speed of the binary is given by $v_{\rm bin}^2 = G\mu\frac{m_{\rm int}}{M_{\rm bin}+m_{\rm int}}(1/a_{\rm fin} - 1/a_{\rm init})$, and the recoil speed of the interloper is $v_{\rm int} = (M_{\rm bin}/m_{\rm int})v_{\rm bin}$. For example, suppose that $M_1 = M_2 = 10\ M_\odot$, $M_{\rm int} = 1\ M_\odot$, $a_{\rm init} = 0.1$ AU, and $a_{\rm fin} = 0.09$ AU. The binary then recoils at $v_{\rm bin} = 15$ km s^{-1} and stays in the cluster, whereas the interloper recoils at $v_{\rm int} = 300$ km s^{-1} and is

ejected.

We treat all three objects as point masses, but in fact main sequence stars are extended enough that they have a good chance of being tidally disrupted in an encounter with a BH binary. Almost all of the disrupted mass is eventually ejected at speeds comparable to the binary orbital speed, hence we assume that tidal disruptions of main sequence stars have the same effect on the energy of the binary as normal 3-body ejections. Note, however, that in this case the ejected mass will not go in a single direction, therefore it is likely that tidal disruptions will not cause the binary to recoil as much as encounters with point masses. Thus such interactions are likely to result in a somewhat greater retention fraction than we calculate. We also find that close approach distances are large enough during interactions that post-Newtonian corrections are not necessary, and that a small enough fraction of stars are involved in these encounters that the effect on the mass distribution due to mergers and ejections is negligible. In addition, we assume throughout our calculations that nuclear star clusters do not have massive black holes at their centers.

4.2.2 Results

The central regions of the clusters undergo significant mass segregation, and therefore their mass functions will be at least flattened, and possibly inverted. This has been observed for globular clusters (see Table 3 of Sosin 1997 or Table 1 of De Marchi et al. 2007) and is also seen in numerical simulations (e.g., Baumgardt et al. 2008 or Gill et al. 2008). To include this effect we implement two steps when we consider the mass of a BH, its companion, and the interloping third object. First we select a zero age main sequence (ZAMS) mass between 0.2 $M_{\odot}$ and 100 $M_{\odot}$ using a simple power law distribution $dN/dM \propto M^{-\alpha}$. While there is evidence that the

upper limit of the ZAMS might be $> 120 M_\odot$ (Oey & Clarke 2005), we chose the more traditional value of $100 M_\odot$ (Kroupa & Weidner 2003) to be conservative. We allow α to range anywhere from 2.35 (the unmodified Salpeter distribution) to -1.0, where smaller values indicate the effects of mass segregation. Second, we evolve the ZAMS mass to a current mass. Our mapping is that for $M_{\rm ZAMS} < M_{\rm ms,max}$, where $M_{\rm ms,max}$ is 1 $M_\odot$ or 3 $M_\odot$ depending on the model used, the star is still on the main sequence and retains its original mass; for 1 $M_\odot < M_{\rm ZAMS} < 8$ $M_\odot$ the star has evolved to a white dwarf, with mass $M_{\rm WD} = 0.6\ M_\odot + 0.4\ M_\odot (M_{\rm ZAMS}/M_\odot - 0.6)^{1/3}$; for 8 $M_\odot < M_{\rm ZAMS} < 25$ $M_\odot$ the star has evolved to a neutron star, with mass $M_{\rm NS} = 1.5\ M_\odot + 0.5\ M_\odot (M_{\rm ZAMS} - 8\ M_\odot)/17\ M_\odot$; and for $M_{\rm ZAMS} > 25\ M_\odot$ the star has evolved to a BH with mass $M_{\rm BH} = 3\ M_\odot + 17\ M_\odot (M_{\rm ZAMS} - 25\ M_\odot)/75\ M_\odot$. Therefore, we assume that BH masses range from 3 $M_\odot$ to 20 $M_\odot$.

These prescriptions are overly simplified in many ways. We therefore explore different mass function slopes, main sequence cutoffs, and so on, and find that our general picture is robust against specific assumptions. Note that, consistent with O'Leary et al. (2006), we find that there is a strong tendency for the merged black holes to be biased towards high masses. Therefore, if BHs with masses $> 20\ M_\odot$ are common, then these will dominate the merger rates. This is important for data analysis strategies, because the low-frequency cutoff of ground-based gravitational wave detectors implies that higher-mass BHs will have proportionally more of their signal in the late inspiral, merger, and ringdown.

The three-body interactions themselves are assumed to be Newtonian interactions between point masses, and are computed using the hierarchical N-body code HNBody (K. Rauch and D. Hamilton, in preparation), using the driver IABL developed by Kayhan Gültekin (see Gültekin et al. 2004, 2006 for a detailed description). Between interactions, we use the Peters equations (Peters 1964) to follow the grad-

ual inspiral and circularization of the binary via emission of gravitational radiation. This is negligible except near the end of any given evolution.

We begin by selecting the mass of the BH and of its companion (which does not need to be a BH) from the evolved mass function. We also begin with a semimajor axis that is 1/4 of the value needed to ensure that the binary is hard. We do this because soft binaries are likely to be ionized and thus become single stars rather than merge. We also select an eccentricity from a thermal distribution $P(e)de = 2ede$. We then allow the binary to interact with single field stars drawn from the evolved mass function, one at a time, until (1) the binary merges due to gravitational radiation, (2) the binary is split apart and thus ionized (this is exceedingly rare given our initial conditions), or (3) the binary is ejected from the cluster. The entire set of interactions until merger typically takes millions to tens of millions of years, and only rarely more than a hundred million years, so it finishes in much less than a Hubble time. This implies that the total time for an initially single BH to merge with another object is dominated by the few billion years needed to capture into a binary rather than by subsequent interactions. In the course of these interactions there are typically a number of exchanges, which usually swap in more massive for less massive members of the binary. This is the cause of the bias towards high-mass mergers that was also found by O'Leary et al. (2006). As shown in Table 1, for $\alpha < 1$ most BHs acquire a BH companion in the process of exchanges, and for $\alpha \leq 0.5$ virtually all do.

The results in Table 1 are focused on different mass function slopes and escape speeds. As expected, we find that for $V_{\rm esc} > 150$ km s^{-1} the overwhelming majority of BH binaries merge in the nuclear star cluster rather than being ejected (see Figure 4.1, which illustrates the main results). This is the difference from lower-σ globular clusters, where the mergers happen outside the cluster. Note also that

in addition to few binaries being ejected, there are typically only 1–2 single BHs ejected per merger, showing that $> 50\%$ of black holes will merge. In contrast, at the 50 km s^{-1} escape speed typical of globulars, > 20 single BHs are ejected per merger, suggesting an efficiency of $< 10\%$. For well-segregated clusters (with $\alpha \leq 0$), the average mass of BHs that merge, binary ejection fraction, number of singles ejected, and number of BHs that merge with each other instead of other objects are all insensitive to the particular mass function slope. For less segregated clusters with $\alpha > 0$, the retention fraction of BHs rises rapidly to unity because most of the objects that interact with the BHs are less massive stars. For example, in clusters with $\alpha \geq 1.0$ about 10% of BH mergers occur with neutron stars, in contrast to a few percent or less for more segregated clusters. In such clusters there might be a channel by which the mass of a BH increases via accretion of main sequence stars, but we expect $\alpha > 0$ to be rare for nuclear star clusters because of the shortness of the segregation times of BHs. Overall, there appears to be a wide range of realistic parameters in which fewer than 10% of binary BHs are ejected before merging.

4.3 Discussion and Conclusions

We have shown that nuclear star clusters with velocity dispersions around $\sigma_{3D} \sim 40 - 60$ km s^{-1} are promising breeding grounds for stellar-mass BH mergers. At significantly lower velocity dispersions, as found in globulars, the escape speed is low enough that the binaries are ejected before they merge. Significantly higher velocity dispersions appear correlated with the presence of supermassive black holes (Ferrarese & Merritt 2000; Gebhardt et al. 2000). In such an environment there might also be interesting rates of BH mergers (see O'Leary & Loeb 2008 for a recent discussion), but, as we will demonstrate in Ch. 6, the increasing velocity

dispersion close to the central object means that binary fractions are lower and softening, ionization, or tidal separation by the supermassive black hole itself are strong possibilities for stellar-mass binaries (Miller et al. 2005).

To estimate the rate of detections with Advanced LIGO, we note that velocity dispersions in the $\sigma_{3D} \sim 40 - 60$ km s^{-1} range correspond to roughly a factor of $\sim 5 - 10$ in galaxy luminosity (Ferrarese et al. 2006). Galaxy surveys suggest (e.g., Blanton et al. 2003) that for dim galaxies the luminosity function scales as roughly $dN/dL = \phi^*(L/L_*)^\beta$, where $\phi^* = 1.5\times10^{-2}h^3$ Mpc^{-3} $\approx 5\times10^{-3}$ Mpc^{-3} for $h = 0.71$, and $\beta \approx -1$. This implies that there are nearly equal numbers of galaxies in equal logarithmic bins of luminosity. A factor of $5 - 10$ in luminosity is roughly e^2, so the number density of relevant galaxies is approximately 10^{-2} Mpc^{-3}. To get the rate per galaxy, we note that typical initial mass functions and estimates of the mass needed to evolve into a BH combine to suggest that for a cluster of mass $M_{\rm nuc}$, approximately $3\times10^{-3}(M_{\rm nuc}/M_\odot)$ stars evolve into BHs (O'Leary et al. 2007). That implies a few$\times10^4$ BHs per nuclear star cluster. If a few tens of percent of these merge in a Hubble time, and if the rate is slightly lower now because many of the original BHs have already merged (see O'Leary et al. 2006), that suggests a merger rate of $> 0.1 \times$ few $\times\ 10^4/(10^{10}$ yr) per galaxy, or few$\times10^{-9}$ Mpc^{-3} yr^{-1}.

Mergers of the original BHs are not expected to significantly decrease the detection rates, for two basic reasons. First, nuclear star clusters are not isolated. Instead, the cluster itself is surrounded by a stellar distribution. It is, after all, the center of the galaxy; therefore unlike for globular clusters, nuclear star clusters are not surrounded by vacuum. This distribution will include BHs. In time, those holes will sink by dynamical friction into the nuclear star cluster itself. This helps replenish the BHs that are kicked out by three-body processes in the cluster. For example, if the number density scales as $n \propto r^{-2}$ (a reasonable approximation for

many galactic centers) then there are as many stars (and presumably black holes) from some radius R to $2R$ as from 0 to R, and from $2R$ to $3R$ as from R to $2R$. In such a circumstance the relaxation time scales as the square of the radius, so there should be an abundant supply of BHs over any reasonable timescale.

The second reason is that the timescale for BHs to capture into a binary goes up with increasing nuclear star cluster mass, because relaxation times all increase. As a result, if clusters of the particular mass we suggested have been depleted significantly, clusters of higher mass will not have been. This shifts the optimal cluster mass to a larger value. However, as in the previous point, it seems reasonable that clusters will be replenished anyway.

At the average detection distance of $\sim$ 1.15 Gpc at which Advanced LIGO is expected to be able to see mergers of two 10 $M_\odot$ BHs (I. Mandel, personal communication), the available volume is 6.4×10^9 Mpc^3, for a rate of $\gtrsim 30$ per year. Roughly 50–80% of galaxies in the eligible luminosity range appear to have nuclear star clusters (see Ferrarese et al. 2006 for a summary). If the majority of the clusters do not have a supermassive black hole, this suggests a final rate of tens per year for Advanced LIGO. This could be augmented somewhat by small galaxies that originally had supermassive black holes, but had them ejected after a merger and then reformed a central cluster (Volonteri 2007; Volonteri et al. 2008).

For nearby ($z < 0.1$) events of this type it might be possible to identify the host galaxy. However, for more typical $z \sim 0.5 \Rightarrow d \approx 1.15$ Gpc events the number of candidates is too large. We can demonstrate this by adopting extremely optimistic values for angular localization and distance accuracy. Even assuming angular localization of $\Delta\Omega = (1^\circ)^2$ and a distance accuracy of $\Delta d/d = 1\%$, the number of galaxies in the right luminosity range is $N \sim 4\pi(1150 \text{ Mpc})^3(\Delta\Omega/4\pi)(\Delta d/d)(0.01 \text{ Mpc}^{-3}) \approx 45$. Therefore, barring some unforeseen electromagnetic counterpart to the gravita-

tional radiation, the host will usually not be obvious.

We anticipate that tens per year is a somewhat conservative rate. If stellar-mass BHs with masses beyond 20 $M_\odot$ are common, this increases the detection radius and hence the rate. For total masses $\sim 30\ M_\odot$ and at redshifts $z \sim 0.5$, the observer frame gravitational wave frequency at the innermost stable circular orbit is $f_{\rm ISCO} \sim 4400\ {\rm Hz}/[30(1+z)] \sim 100$ Hz. This is close enough to the range where the frequency sensitivity of ground-based gravitational wave detectors declines that detection of many of these events will rely strongly on the signal obtained from the last few orbits plus merger and ringdown. In much of this range, numerical relativity is essential.

As a final point, we note that for the same reason that nuclear star clusters are favorable environments for retention and mergers of stellar-mass BHs, they could also be good birthplaces for more massive black holes. This could be prevented, even for the relatively high escape speeds discussed here, if recoil from gravitational radiation during the coalescence exceeds ~ 200 km s^{-1}. The key uncertainty here is the spin magnitudes of the BHs at birth. Numerous simulations demonstrate that high spins with significant projections in the binary orbital plane can produce kicks of up to several thousand kilometers per second (González et al. 2007). If there is significant processing of gas through accretion disks the spins are aligned in a way that reduces the kick to below 200 km s^{-1} (Bogdanović et al. 2007), but stellar-mass BHs cannot pick up enough mass from the interstellar medium for this to be effective. For example, the Bondi-Hoyle accretion rate is $\dot{M}_{\rm Bondi} \approx 10^{-13}\ M_\odot\ {\rm yr}^{-1}(\sigma_{\rm 3D}/50\ {\rm km\ s}^{-1})^{-3}(n_{\rm gas}/100\ {\rm cm}^{-3})(M/10\ M_\odot)^2$, where $n_{\rm gas}$ is the particle number density in the gas. This means that to accrete the $\sim 1\%$ of the BH mass needed to realign the spin (Bogdanović et al. 2007) would require at least a trillion years. Current estimates of stellar-mass BH spins suggest $a/M > 0.5$ in

many cases (Liu et al. 2008; McClintock et al. 2006; Miller 2007a; Shafee et al. 2006). If the spins are isotropically oriented and uniformly distributed in the range $0 < a/M < 1$, and the mass ratios are in the $m_{\rm small}/m_{\rm big} \sim 0.6 - 0.8$ range typical in our simulations, then use of the Campanelli et al. (2007) or Baker et al. (2008) kick formulae imply that roughly 84% of the recoils exceed 200 km s^{-1} and 78% exceed 250 km s^{-1}. This suggests that multiple mergers are rare unless there is initially an extra-massive black hole as a seed (e.g., Holley-Bockelmann et al. 2008 for a discussion of the effects of gravitational wave recoil), but further study is important.

In conclusion, we show that the compact nuclear star clusters found in the centers of many small galaxies are ideal places to foster mergers between stellar-mass BHs. It is not clear whether multiple rounds of mergers can lead to a runaway, but this is a new potential source for ground-based detectors such as Advanced LIGO, where numerical relativity will play an especially important role.

In the next chapter, we begin our discussion of BH binaries in larger galaxies by examining one consequence of binary-single encounters in the vicinity of a SMBH: tidal separation and the formation of extreme mass ratio inspirals.

Table 4.1. Simulations of Nuclear Star Clusters[a]

$V_{\rm esc}$ (km s^{-1})[b]	$M_{\rm ms,max}$[c]	α[d]	$\langle M_{\rm BH}\rangle(M_\odot)$[e]	$f_{\rm merge}$[f]	$f_{\rm notBH}$[g]	$\langle M_{\rm bin,merge}\rangle(M_\odot)$[h]	$\langle N_{\rm single,eject}\rangle$[i]
50	$1M_\odot$	0	11.7	0.25	0.0	31.2	24.8
62.5	$1M_\odot$	0	11.7	0.33	0.0	31.6	15.3
75	$1M_\odot$	0	11.7	0.42	0.0	30.9	11.5
87.5	$1M_\odot$	0	11.7	0.52	0.0	31.9	7.9
20	$1M_\odot$	0	11.7	0.63	0.02	30.0	6.2
112.5	$1M_\odot$	0	11.7	0.68	0.0	31.4	4.7
125	$1M_\odot$	0	11.7	0.72	0.02	31.8	4.3
137.5	$1M_\odot$	0	11.7	0.76	0.01	32.0	3.0
150	$1M_\odot$	0	11.7	0.80	0.03	32.3	2.8
162.5	$1M_\odot$	0	11.7	0.93	0.03	31.3	2.0
175	$1M_\odot$	0	11.7	0.89	0.02	31.9	2.0
187.5	$1M_\odot$	0	11.7	0.90	0.01	31.3	2.1
200	$1M_\odot$	0	11.7	0.94	0.08	31.1	1.3
212.5	$1M_\odot$	0	11.7	0.89	0.05	30.5	1.0
225	$1M_\odot$	0	11.7	0.98	0.06	31.0	1.2
237.5	$1M_\odot$	0	11.7	0.94	0.06	30.1	1.0
250	$1M_\odot$	0	11.7	0.96	0.06	30.0	0.71
200	$1M_\odot$	-1.0	13.4	0.94	0	32.4	1.3
200	$1M_\odot$	-0.5	12.6	0.95	0.01	32.2	1.5
200	$1M_\odot$	0.5	10.7	0.94	0.1	28.3	0.91
200	$1M_\odot$	1.0	9.7	0.98	0.41	27.3	0.43
200	$1M_\odot$	1.5	8.8	0.99	0.79	23.0	0.04
200	$1M_\odot$	2.0	7.5	1.00	0.99	—	0
200	$1M_\odot$	2.35	7.4	1.00	1.00	—	0
200	$3M_\odot$	-1.0	13.4	0.85	0.03	33.3	1.5
200	$3M_\odot$	-0.5	12.6	0.94	0.01	31.9	1.3
200	$3M_\odot$	0	11.7	0.95	0.05	30.4	1.5
200	$3M_\odot$	0.5	10.7	0.94	0.11	29.2	1.0
200	$3M_\odot$	1.0	9.7	0.99	0.48	25.3	0.38
200	$3M_\odot$	1.5	8.8	0.99	0.85	24.7	0.04
200	$3M_\odot$	2.0	7.5	1.00	1.00	—	0
200	$3M_\odot$	2.35	7.4	1.00	1.00	—	0

[a]All runs had 100 realizations.

[b]Escape speed from cluster.

[c]Maximum mass of main sequence star.

[d]Number distribution of stars on zero age main sequence: $dN/dM \propto M^{-\alpha}$.

[e]Average mass of all black holes given α and our evolutionary assumptions.

[f]Fraction of runs in which holes merged rather than being ejected.

[g]Fraction of runs in which holes merged with something other than another black hole.

[h]Average mass of double BH binaries that merged.

[i]Average number of single black holes ejected per binary that merged.

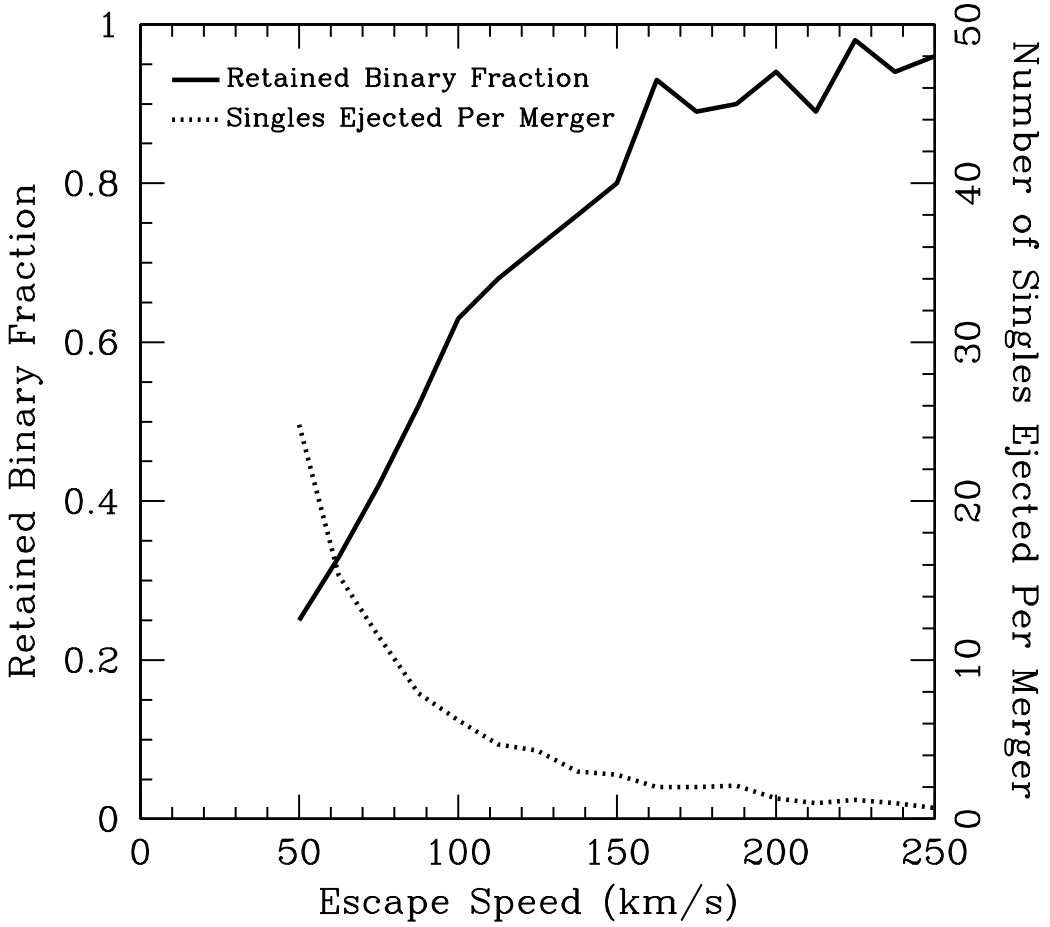

Figure 4.1: Fraction of binaries retained in the nuclear star cluster (solid line) and average number of BHs ejected per BH merger (dotted line) as a function of the cluster escape speed. Here the zero age main sequence distribution of masses is $dN/dM \propto M^0$, to account for mass segregation in the cluster center, where most interactions occur. We also assume a maximum black hole mass of 20 $M_\odot$ and a maximum main sequence mass of 1 $M_\odot$, but most results are robust against variations of these quantities. All runs are done with 100 realizations. We see, as expected, that the retention fraction increases rapidly with escape speed, so that for nuclear star clusters most binaries stay in the cluster until merger. We also see that at $V_{\rm esc} \sim 200$ km s^{-1} and above, tens of percent of BH singles also stay in the cluster. This suggests a high merger efficiency.

Chapter 5

Binary Encounters With Supermassive Black Holes: Zero-Eccentricity LISA Events

5.1 Introduction

Extreme mass ratio inspirals (EMRIs) of stellar-mass compact objects into supermassive black holes are key targets for the Laser Interferometer Space Antenna (LISA). From the fundamental physics standpoint, these events are expected to provide the best available mapping of the spacetime around a rotating black hole (Hughes 2003; Ryan 1995, 1997). Astrophysically, they may well reveal the numbers of supermassive black holes in a mass range ($\sim 10^5 - 10^7\,M_\odot$) that is difficult to probe otherwise (e.g., Greene & Ho 2004).

Recall from Ch. 1 that several studies of EMRI rates and properties (Freitag 2001, 2003; Hils & Bender 1995; Hopman & Alexander 2005; Ivanov 2002; Miralda-Escudé & Gould 2000; Sigurdsson & Rees 1997) have focused exclusively on the

capture of compact objects by emission of gravitational radiation during a close pass. That is, a compact object (for example, a $10\,M_\odot$ black hole) plunges close to the central supermassive black hole (SMBH) and emits gravitational waves that shrink its orbit significantly. The black hole then continues to orbit, and if its motion is not perturbed significantly by interactions with other stars then it eventually spirals into the SMBH. Orbits that allow capture need to have pericenter distances very close to the SMBH (Freitag 2003; Hopman & Alexander 2005). Therefore, even though gravitational radiation circularizes orbits (Glampedakis et al. 2002; Hughes et al. 2005; Peters 1964), by the time the black hole is in the last year of inspiral, when it can be detected with LISA, its orbit still has a significant eccentricity of typically $e \sim 0.5 - 0.9$ (Freitag 2003; Hopman & Alexander 2005, but see Ivanov 2002).

Here we consider a different process, in which a stellar-mass binary containing a compact object comes close enough to the SMBH that the binary is tidally separated, leaving one object bound to the SMBH and the other almost always ejected to infinity at high speed. This process is reminiscent of the hydrodynamical tidal disruption of main-sequence stars first mentioned by Hills (1975). With the exception of the work of Gould & Quillen (2003), the tidal separation of binaries has so far been considered as a way to produce high-velocity stars (Brown et al. 2005; Hills 1988, 1991; Pfahl 2005; Yu & Tremaine 2003). It was also listed by Hils & Bender (1995) and Freitag & Benz (2002) as a mechanism to be examined in the EMRI context, but has not yet been explored quantitatively.

The key point about this process is that, unlike in the two-body capture scenario, no energy needs to be dissipated in order to have a capture. As a result, capture can occur at much larger radii than is possible in the two-body case: for example, a binary with a semimajor axis of tenths of an AU can be captured at pericenter

distances of tens of AU relative to the SMBH, compared with the ~ 0.1 AU that is required for two-body capture. In addition, the semimajor axis of the resulting bound object will be modest, perhaps tens of times the pericenter distance (Hills 1991). EMRIs formed in this way are therefore relatively immune to perturbations of their orbits that could cause them to plunge directly into the SMBH (which lowers rates significantly for EMRIs formed by two-body capture; see Hils & Bender 1995; Hopman & Alexander 2005). Combined with the higher cross section, this suggests that the overall rate of EMRIs could have an important contribution from tidal separation of binaries, even if only a few percent of compact objects are in binaries.

In addition, because the pericenter distance of the bound object after tidal separation is large, the orbital eccentricity at the point when the signal is detectable with LISA (after, typically, shrinkage of the pericenter distance by factors of tens or more) is extremely close to zero. This suggests that the EMRIs detected with LISA will come in two distinct classes of eccentricity, with different histories. As we discuss in this chapter, the relative rates of high-eccentricity and low-eccentricity EMRI events detected by LISA will act as unique probes of stellar evolution and dynamics in the central few parsecs of galaxies.

In § 5.2 we discuss this process in more quantitative detail. In § 5.3 we list some of the questions that will have to be answered to get more specific predictions of relative rates, and to interpret LISA observations when they arrive.

5.2 Tidal Separation and EMRIs

5.2.1 Capture Processes

Let us first discuss the process of two-body capture. Suppose that a point mass of mass m orbiting the SMBH with an orbital speed v_∞ at apocenter (assumed to be

at a large distance) plunges towards a supermassive black hole of mass $M \gg m$. Its orbit will be modified significantly if, during its motion, it releases at least $\frac{1}{2}mv_\infty^2$ of energy in gravitational radiation. As derived by Quinlan & Shapiro (1989), this condition implies

$$\begin{aligned} r_p < r_{p,\mathrm{GW}} &= \left[\frac{85\pi\sqrt{2}G^{7/2}mM(m+M)^{3/2}}{12c^5v_\infty^2}\right]^{2/7} \\ &\approx 0.13\ \mathrm{AU}\left(\frac{m}{10\,M_\odot}\right)^{2/7}\left(\frac{M}{10^6\,M_\odot}\right)^{5/7}\left(\frac{v_\infty}{60\ \mathrm{km\ s^{-1}}}\right)^{-4/7}. \end{aligned} \tag{5.1}$$

We have scaled by 60 km s^{-1} because this is roughly the velocity dispersion inferred for a galaxy with a central black hole mass of $10^6\,M_\odot$ (Barth et al. 2005; Merritt & Ferrarese 2001; Tremaine et al. 2002). The time required to spiral into the SMBH would then be much less than a Hubble time, except that other stars perturb the orbit significantly (see § 5.2.2). The gravitational radius is $r_g \equiv GM/c^2 \approx 0.01\ \mathrm{AU}(M/10^6\,M_\odot)$. Therefore,

$$r_{p,\mathrm{GW}}/r_g \approx 13\left(\frac{m}{10\,M_\odot}\right)^{2/7}\left(\frac{M}{10^6\,M_\odot}\right)^{-2/7}\left(\frac{v_\infty}{60\ \mathrm{km\ s^{-1}}}\right)^{-4/7}. \tag{5.2}$$

For comparison, the radius of the innermost stable circular orbit around a nonrotating SMBH is $6r_g$. As another comparison, detection of an EMRI with LISA will be very difficult if the gravitational wave frequency is less than $f_{GW} \sim 2-3$ mHz, because at lower frequencies there is strong unresolvable foreground noise due to double white dwarf binaries in our galaxy (Bender & Hils 1997; Farmer & Phinney 2003; Nelemans et al. 2001). For a circular orbit, the gravitational wave frequency is double the orbital frequency (Peters & Mathews 1963). At 2 mHz, then, the radius of a circular orbit is

$$r(2\ \mathrm{mHz}) \approx 0.1\ \mathrm{AU}\left(\frac{M}{10^6\,M_\odot}\right)^{1/3} \approx 10\,r_g\left(\frac{M}{10^6\,M_\odot}\right)^{-2/3}. \tag{5.3}$$

Therefore, a stellar-mass compact object needs to go very deep into the potential well of an SMBH to be captured or to be observed with LISA.

Now consider tidal separation. Suppose that a binary with a total mass m and semimajor axis a plunges towards a supermassive black hole of mass M. If the plunge has a pericenter distance less than

$$\begin{aligned} r_{\rm tide} &\approx \left(\frac{3M}{m}\right)^{1/3} a \\ &\approx 7 \text{ AU} \left(\frac{M}{10^6\, M_\odot}\right)^{1/3} \left(\frac{m}{10\, M_\odot}\right)^{-1/3} \left(\frac{a}{0.1 \text{ AU}}\right) , \end{aligned} \tag{5.4}$$

then the binary will be separated by the tidal field of the SMBH. Note that the numerical coefficient in the expression $(3M/m)^{1/3}$ is correct for a prograde binary on a circular orbit around the SMBH, and rises to of order 4 for weakly hyperbolic prograde orbits (Hamilton & Burns 1991, 1992). There is also a strong dependence of the stability of the binary on its inclination. Retrograde orbits are more stable and must plunge to roughly one-half $r_{\rm tide}$ before they can be ripped apart. The cause of this difference is the Coriolis acceleration which tends to stabilize retrograde orbits while destabilizing prograde ones (Hamilton & Burns 1991). Binaries on inclined orbits have effective tidal radii between these two extremes.

Therefore, depending on the semimajor axis of the stellar binary, the required pericenter distance and hence the cross section could be several to thousands of times larger than the pericenter distance needed for two-body capture. If a BH has as a binary companion a much less massive object such as a main sequence star, then some of the interactions will involve capture of the star instead of the BH, reducing rates by a factor of a few. As we discuss in the next section, the enhanced cross section does not translate directly into a rate, but the ultimate result is that the rate per binary is expected to be 1-2 orders of magnitude times the rate per single. Therefore if more than $\sim 1 - 10\%$ of compact objects are in binaries then the overall EMRI rate could be dominated by tidal separation events.

Using HNBody (see section 4.2.2), we have performed exploratory Newtonian point-mass three-body simulations to evaluate the properties of the extreme mass

ratio inspirals produced by tidal separation. For an initially hard circular binary with component masses $10\,M_\odot$ and $10\,M_\odot$ in a hyperbolic pass by a $10^6\,M_\odot$ SMBH, we find that the typical eccentricity is $e \sim 0.98$ after capture, consistent with the results of Hills (1991), who focused on tidal separation of main sequence binaries. For an initial binary separation of $a = 0.1$ AU, the typical pericenter distance after capture is a few AU, and the typical apocenter distance is a few hundred AU. The typical pericenter and apocenter distances are proportional to the semimajor axis of the original binary. We also simulated tidal separation of initially hard circular binaries with component masses $10\,M_\odot$ and $1\,M_\odot$ around a $10^6\,M_\odot$ SMBH, representing for example a binary with a black hole and a white dwarf or a black hole and a neutron star. We find that the $10\,M_\odot$ object is captured in $\sim 40\%$ of the simulations, and that the apocenter distance in such cases is a factor of a few larger than for the $10\,M_\odot - 10\,M_\odot$ simulations (as is expected given the smaller energy transfer from the $1\,M_\odot$ object).

The small apocenter distance after capture (typically a few hundred AU) implies that although compact objects captured in this way may be perturbed by other stars, the changes are small over one orbital period, in contrast to the case for single compact objects captured by gravitational wave emission. The system therefore evolves gradually, and eventually reaches a state in which inspiral via gravitational radiation is shorter than the time to change because of perturbations. At this point the pericenter distance is still much larger than it is for single compact objects. At quadrupolar order, the evolution of the semimajor axis a and eccentricity e of a binary was derived by (Peters 1964). The net result is that orbits with small initial pericenter distances (the case for singles) still have measurable eccentricities in the LISA sensitivity band ($e \sim 0.5 - 0.9$ is typical; see Freitag 2003; Hopman & Alexander 2005). However, for orbits with large initial pericenter distances (the

case for separated binaries), the eccentricities will typically be $e < 0.01$. Therefore, EMRI events from binary separation will be very distinct in eccentricity.

5.2.2 Effects of Nuclear Stellar Dynamics

Even though the cross section for tidal separation is vastly greater than for two-body capture, the motion of a binary must still be close to radial in order to be captured. For example, a binary with semimajor axis $a \sim 1$ AU could be captured if it passed within ~ 100 AU of the SMBH, but this is tiny compared to the distance of a few parsecs from the SMBH where most binaries presumably lie. It is therefore important to map out some of the dynamical processes that will affect the injection into these orbits. These are discussed in detail by many authors (e.g., Frank & Rees 1976; Lightman & Shapiro 1977; Magorrian & Tremaine 1999; Syer & Ulmer 1999), so here we simply quote the results.

A supermassive black hole of mass M will dominate the dynamics out to the radius of influence

$$r_{\rm infl} = \frac{GM}{\sigma_0^2} \approx 1 \text{ pc} \Big(\frac{M}{10^6\, M_\odot} \Big) \Big(\frac{60 \text{ km s}^{-1}}{\sigma_0} \Big)^2 , \tag{5.5}$$

where σ_0 is the velocity dispersion of stars far outside this radius. At radii $r > r_{\rm infl}$, a constant velocity dispersion implies a stellar mass density $\rho \sim r^{-2}$, whereas at $r < r_{\rm infl}$ the density takes a different slope, $\rho \sim r^{-\gamma}$, for example $\gamma = 3/2$ or $\gamma = 7/4$ (e.g., Bahcall & Wolf 1976; Young 1980).

For $r < r_{\rm infl}$ the orbital time is $t_{\rm orb} = 2\pi(r^3/GM)^{1/2}$, whereas for $r > r_{\rm infl}$, $t_{\rm orb} = 2\pi(r/r_{\rm infl})(GM/\sigma_0^3)$. The relaxation time is the time required for the velocity of a star to change by of order itself (in magnitude or direction), by deflections due to two-body encounters. The local relaxation time for a compact object of mass

$m_{\rm CO}$ interacting with stars of average mass $\langle m \rangle$ is (Spitzer 1987)

$$t_{\rm rel}(r) = \frac{0.339}{\ln \Lambda} \frac{\sigma^3(r)}{G^2 \langle m \rangle m_{\rm CO} n(r)} \ . \tag{5.6}$$

Here $\sigma^3(r)$ is the local velocity dispersion (equal to the orbital speed when $r < r_{\rm infl}$), $n(r)$ is the local number density, and $\ln \Lambda \sim 10$ is the Coulomb logarithm obtained by integrating over the two-body encounters.

For an object on a very eccentric orbit, $(1 - e) \ll 1$, the angular momentum is much less than the angular momentum of a circular orbit with the same semimajor axis. Therefore, the angular momentum only needs to change slightly to make an order unity difference in the orbit. This timescale is $t_J(r) \approx (1 - e) t_{\rm rel}(r)$ (e.g., Hopman & Alexander 2005).

In addition to two-body relaxation, a binary can undergo three-body interactions. Only hard binaries, with $G m_{\rm bin}/a \gtrsim \sigma^2(r)$, can survive for a long time in a dense environment because soft binaries are softened and ionized in a relatively short time (see the discussion in Binney & Tremaine 1987). For such binaries, the three-body interaction time is $t_{\rm 3bod} = 1/(n(r) \Sigma v)$, where $v \approx \sigma(r)$ is the relative speed and Σ is the effective cross section of interactions. For hard binaries, gravitational focusing dominates and hence $\Sigma \approx \pi a (2 G m_{\rm CO}/\sigma^2)$. The net result is $t_{\rm rel}/t_{\rm 3bod} \approx (0.68\pi/\ln \Lambda)[\sigma^2(r) a/(G\langle m \rangle)]$, so for binaries in which $G\langle m \rangle/a \gg \sigma^2(r)$ two-body relaxation occurs on a shorter time scale than three-body interactions. However, over several relaxation times, three-body interactions can occur, which might allow initially solitary black holes to exchange into hard primordial binaries. Once a black hole is in a hard binary it is relatively safe from dynamical disruption by stellar-mass objects, but if multiple three-body interactions occur then collisions with main-sequence stars or merger by gravitational radiation with compact objects could reduce the number of binaries. It could also be that plunges through the high-density, high-velocity stellar environment near the SMBH will soften binaries

somewhat. A detailed study of these effects follows in Ch. 6.

For a given position R and speed V, the loss cone is defined as the set of directions of the velocity $\vec{V}$ leading to such small pericenter distances that the object of interest is removed from the system. In the full loss cone regime, for which $t_J < t_{\rm orb}$, objects that enter the loss cone and are removed are immediately replaced, within an orbital time, by objects that are deflected in from other orbits. In this regime, an object that starts down the loss cone is likely to be deflected out of the cone during the orbit. In the empty loss cone regime, for which $t_J > t_{\rm orb}$, replacement of objects through the loss cone has to occur over a relaxation time.

If the number of objects per radius (assuming spherical symmetry) is dN/dr and the angle subtended by the loss cone at radius r is $\theta_{\rm LC}(r)$, then the approximate capture rates in the full and empty loss cone regimes are (see Syer & Ulmer 1999)

$$\begin{aligned} \frac{d\dot{N}_{\rm full}}{dr} &\sim \theta^2_{\rm LC}(r)\frac{(dN/dr)}{t_{\rm orb}} \\ \frac{d\dot{N}_{\rm empty}}{dr} &\sim \frac{(dN/dr)}{\ln(1/\theta^2_{\rm LC}(r))t_{\rm rel}(r)} \ . \end{aligned} \tag{5.7}$$

What are the relevant regimes for the single and binary captures? Suppose that the pericenter distance for a single has to be 0.1 AU, and for a binary has to be 10 AU, for capture to occur. Consider a radius $r \gg r_{\rm infl}$, and consider a density profile that gives a number of objects within radius r of $N(<r) = 10^7(r/5\ {\rm pc})$. This implies a relaxation time of $t_{\rm rel} \sim 10^5(r/5\ {\rm pc})t_{\rm orb}$. Since 1 pc $\approx 2\times10^5$ AU, the eccentricity of the single orbit is given by $(1-e_{\rm single}) \approx 10^{-7}(5\ {\rm pc}/r)$ and the eccentricity of the binary orbit is given by $(1-e_{\rm binary}) \approx 10^{-5}(5\ {\rm pc}/r)$. The angular momentum diffusion times are then

$$\begin{aligned} t_{J,{\rm single}} &\approx (1-e_{\rm single})t_{\rm rel} \sim 10^{-2}t_{\rm orb} \\ t_{J,{\rm binary}} &\approx (1-e_{\rm binary})t_{\rm rel} \sim t_{\rm orb} \ . \end{aligned} \tag{5.8}$$

Therefore, when $r \gg r_{\rm infl}$, the single stars are well within the full loss cone regime, and the binary stars are marginally within the full loss cone regime. This means

that well outside the radius of influence of the SMBH, the binaries have a much higher rate of interaction than the singles because $d\dot{N}/dr \propto \theta^2_{\rm LC}$. Because for gravitationally focused encounters we have $\theta^2_{\rm LC} \propto R_p$, the pericenter distance, this would suggest a ratio of rates of ~ 100.

The overall ratio of rates is not quite that high, however. The increase in number density towards the center, combined with the increased size of the loss cone at smaller radii, turns out to mean that the overall rate is determined by the smallest radius at which the loss cone is full (inside this radius, diffusion into the loss cone is much less efficient). The smaller loss cone for the singles (hence the shorter time required to diffuse across the cone) implies that the loss cone is still full at a smaller radius than it is for binaries. To see this, consider the region $r < r_{\rm infl}$. Within this region the relaxation time is relatively insensitive to radius (in fact, for $n(r) \propto r^{-3/2}$ the relaxation time is constant). Since $t_{\rm orb} \propto r^{3/2}$ and $(1-e) \propto r^{-1}$ (with e defined by the loss cone), this implies $t_J/t_{\rm orb} \propto r^{-5/2}$, so that the full/empty crossover would be at the critical radius $r_{\rm crit} \sim 0.1 r_{\rm infl}$ for our example singles, but $r_{\rm crit} \sim r_{\rm infl}$ for our example binaries. The solid angle of the loss cone $\theta^2_{\rm LC} \propto r^{-1}$, so it is ten times larger at $0.1 r_{\rm infl}$ than at $r_{\rm infl}$. At $r_{\rm infl}$ the rate is still a hundred times greater per binary than per single, so the net rate enhancement is a factor of ten in favor of the binaries.

As pointed out by Hils & Bender (1995) and analyzed by Hopman & Alexander (2005), there is an additional major effect. A single compact object captured by gravitational radiation emission typically has a very large apocenter distance, often on the order of tenths of a parsec or more. As a result, even after it has first been captured, it has a chance to be perturbed in the next orbit. If it is perturbed to a larger pericenter, it will not merge by gravitational radiation, but in equilibrium another orbit will be perturbed to a small pericenter and hence there is no net effect.

However, sometimes a perturbation will cause the orbit to be so close to radial that the object plunges straight into the SMBH. Although this does not affect the merger rate, such objects do not contribute to the LISA event rate, because they plunge before their orbital period has become shorter than $\approx 10^{3-4}$ s. Hopman & Alexander (2005) estimate that ∼80-90% of the potential EMRI events are lost in this fashion (note, however, that mass segregation of black holes into a dense subcluster may reduce the impact of this effect; E. S. Phinney, personal communication).

In contrast, inspirals produced by separation of binaries are not susceptible to this effect. The reason is that, as discussed in § 5.2.1, the apocenter distance is usually only tens of times the pericenter distance. This close to the SMBH, the time necessary to change the pericenter significantly is very large compared to the orbital time. As a result, we expect that any perturbations will be gradual, hence a decrease in the pericenter distance will produce greater gravitational radiation emission and thus circularization rather than a plunge.

Some galactic potentials are found to be triaxial, in which case individual stars still conserve their orbital energy over an orbital time, but their angular momentum can change significantly faster than is possible in standard two-body relaxation (Holley-Bockelmann et al. 2002; Merritt & Poon 2004; Poon & Merritt 2002). This will tend to push the full loss cone regime to smaller radii, which will enhance rates. Note, though, that well inside the radius of influence of the SMBH we expect the potential to be nearly Keplerian and thus insensitive to asymmetries at greater radii. It is therefore likely that the singles (with $r_{\rm crit} \ll r_{\rm infl}$) will be relatively unaffected by global triaxiality, whereas binaries (with $r_{\rm crit} \sim r_{\rm infl}$) could have their rates enhanced moderately.

5.3 Discussion and Conclusions

Our aim in this chapter has been to show that binaries may contribute significantly to EMRI rates, and might even dominate. The net rate of detections with LISA depends on several other factors, so we can parameterize the rate of LISA-detectable compact object EMRIs originating from binaries relative to the rate originating from singles as

$$\frac{\dot{N}_{\rm binary}}{\dot{N}_{\rm single}} = \frac{f_b \mathcal{R}_{\rm binary} \langle f_{\rm binary,LISA} \rangle}{f_s \mathcal{R}_{\rm single} \langle f_{\rm single,LISA} \rangle} \ , \tag{5.9}$$

where f_b is the fraction of compact objects that are in binaries; f_s is the fraction that are single; $\mathcal{R}_{\rm binary}$ is the total rate of tidal separations per binary; $\mathcal{R}_{\rm single}$ is the total rate of gravitational radiation captures per single; $\langle f_{\rm binary,LISA} \rangle$ is the overall fraction of binary sources captured in orbits tight enough to spiral into the LISA band within a Hubble time; and $\langle f_{\rm single,LISA} \rangle$ is the overall fraction of captured singles that end up detectable with LISA (rather than being perturbed into plunge orbits). Our current best guesses are $\mathcal{R}_{\rm binary}/\mathcal{R}_{\rm single} \sim 10$ and $\langle f_{\rm binary,LISA} \rangle / \langle f_{\rm single,LISA} \rangle \sim 1 - 10$.

Therefore, if the binary fraction is $f_b > 0.01 - 0.1$, EMRIs from binaries could dominate the total rates. Evaluation of the importance of the binary separation process will thus depend crucially on both population synthesis models (to get the binary fraction at birth; see Belczyński et al. 2004) and on models of the stellar dynamical interactions of binaries and singles in the dense stellar environments of galactic nuclei, such as exchange interactions that could allow initially solitary black holes to acquire a companion (e.g., Heggie et al. 1996).

As discussed in § 5.2.1, the low eccentricity of tidal separation EMRIs will distinguish them strongly from two-body capture orbits. The rates of such events, as well as the eccentricity distribution of EMRIs from singles as a function of SMBH mass, are sensitive to binary stellar evolution as well as dynamical interactions.

These effects relate to the very innermost regions of galaxies, which are otherwise extremely difficult to observe. LISA observations of EMRIs will therefore provide a unique window into the hearts of galaxies.

In the next chapter, we investigate the details of the fates of binaries in galaxies that contain SMBHs. In particular, we explore the consequence of the ever increasing encounter velocities near the SMBH on the overall fractions of binary mergers, ionizations, and tidal separations.

Chapter 6

Binaries in Galactic Nuclei with SMBHs

6.1 Introduction

Galactic nuclei hold the keys to many phenomena on the scientific frontier, from galaxy formation to gravitational radiation, and SMBHs play an important role. Observations of star and gas kinematics show that SMBHs reside in most galactic centers, and range in mass from 10^6 to 10^9 $M_\odot$ (Barth 2004; Ferrarese & Merritt 2000; Gebhardt et al. 2000). While the formation mechanism of these massive black holes is not well-understood, it is likely coupled to the genesis of dark matter halos and galaxies themselves (Fan et al. 2001). SMBHs are thought to grow from their less massive progenitors through black hole coalescence after galaxy mergers (Begelman et al. 1980) and via gas accretion, which fuels active galactic nuclei (Rees 1984). SMBHs also exist in more docile environments, much like the modest $\sim 3 \times 10^6$ $M_\odot$ SMBH in our own galactic center (Genzel et al. 2003). In the case of AGN, the luminous accretion onto the SMBHs dominates the light we see from nuclei, but

massive black holes also dominate their surroundings in a less conspicuous way by dictating the dynamics of the stars in their host nucleus.

The gravity of a central SMBH governs the orbits of the objects in the innermost region of a galactic nucleus. The region inside of which the stellar dynamics are dominated by the massive black hole is given by a sphere with a radius known as the radius of influence,

$$r_{\rm infl} = \frac{GM_{\rm SMBH}}{{\sigma_0}^2} \quad , \tag{6.1}$$

where σ_0 is the velocity dispersion well outside this area. Within this sphere, orbits are Keplerian, and the local velocity dispersion at a distance r from the SMBH is

$$\sigma(r) = \sqrt{\frac{GM_{\rm SMBH}}{r}} \quad , \tag{6.2}$$

so that velocities increase as objects move closer to the SMBH. Recall from Ch. 1 that a massive object such as a binary will sink toward the center of the nucleus over the course of a relaxation time

$$t_{\rm rel}(r) = \frac{0.339}{\ln\Lambda}\frac{\sigma^3(r)}{{\rm G}^2 m_{\rm bin} m_* n(r)} \quad , \tag{6.3}$$

where m_* is the average mass of field stars, $m_{\rm bin}$ is the binary mass, $n(r)$ is the local number density, and $\ln\Lambda \sim 10$ is the Coulomb logarithm. For compact galactic nuclei containing SMBHs with $M_{\rm SMBH} \approx 10^6 - 10^7$ $\rm M_\odot$, the relaxation time for a binary is (Miller et al. 2005),

$$t_{\rm rel}(r) \simeq 1.8\times 10^8 {\rm yr}\Big(\frac{\sigma}{100{\rm km\ s^{-1}}}\Big)^3\Big(\frac{10{\rm M_\odot}}{m_{\rm bin}}\Big)\Big(\frac{10^6{\rm M_\odot pc^{-3}}}{m_* n}\Big) \quad , \tag{6.4}$$

hence massive binaries, such as those containing BHs, will find themselves in the central region of the nucleus in much less than a Hubble time. In fact, Monte Carlo simulations of such nuclei show that BHs sink to the center in less than 3 Gyr, and come to dominate the mass density in the inner 0.2 pc of the nucleus (Freitag

et al. 2006). This leads to frequent close encounters between BH binaries and single objects near the galactic center.

The consequence of such three-body encounters on a BH binary depends on whether it hardens or softens significantly as it sinks. A hard binary, for which the internal energy is much greater than the kinetic energy of the interloping star, is not likely to harden significantly because its encounter cross section decreases as it tightens. As discussed in the introductory chapter, this is not the case for soft binaries. As a binary softens it is more likely to have additional encounters that tend to soften it further, which often leads to ionization. The presence of a SMBH increases the likelihood of softening, because the encounter speed increases as the binary sinks. Therefore, a binary becomes softer by virtue of approaching the SMBH.

In addition to promoting increased softening, the presence of a SMBH in a galactic nucleus adds another potential fate for binaries that is not possible in nuclear star clusters without massive black holes. While binaries in both types of galactic nuclei can be ionized and undergo induced mergers, it is also possible that a SMBH will tidally separate binaries, effectively capturing one binary member into a more tightly bound orbit while flinging the other off at a high speed. Tidal separations occur when a binary passes within the separation radius given by

$$r_{\rm tide} \approx a_{\rm bin}\left(\frac{3M_{\rm SMBH}}{m_{\rm bin}}\right)^{1/3}, \tag{6.5}$$

where $a_{\rm bin}$ is the semimajor axis of the binary. Tidal separations deposit BHs very close to the SMBH, where they will potentially spiral into the SMBH and become an EMRI, as discussed in Ch. 5.

As we will discuss in this chapter, the results of our simulations show that ionizations, mergers, and tidal separations are all likely consequences of the three-body encounters that binaries experience in galactic nuclei. These outcomes will con-

tribute to the detection rates of ground-based instruments, in the case of mergers, and space-based detectors, in the case of tidal separations.

In §6.2 of this chapter, we describe the methods employed in carrying out these simulations. We follow with results in §6.3, and then discuss the conclusions drawn from this work as well as implications for LIGO detection rates in §6.4.

6.2 Method

6.2.1 Set Up

Our goal is to study the evolution of BH binaries in galactic nuclei containing SMBHs, and we accomplish this by tracking the dynamics on two different scales: the orbit of the center of mass of the binary around the SMBH as the binary moves through the background of field stars; and the internal semimajor axis and eccentricity of the binary, which change as a result of close encounters with single objects.

To track changes in the orbit around the SMBH, we calculate the effects of distant two-body encounters between stars and the center of mass of the binary. For a binary interacting with an interloper of mass m_* with an initial relative speed V_0, we calculate the change in the velocity $\Delta\mathbf{v}$ of the binary, which has components (Binney & Tremaine 1987)

$$|\Delta\mathbf{v}_\perp| = \frac{2m_* b V_0^3}{G(m_{bin}+m_*)^2}\left[1+\frac{b^2V_0^4}{G^2(m_{bin}+m_*)^2}\right]^{-1} , \tag{6.6}$$

and

$$|\Delta\mathbf{v}_\parallel| = \frac{2m_* V_0}{m_{bin}+m_*}\left[1+\frac{b^2V_0^4}{G^2(m_{bin}+m_*)^2}\right]^{-1} , \tag{6.7}$$

where $\mathbf{v}_\perp$ and $\mathbf{v}_\parallel$ are perpendicular and parallel to $\mathbf{V}_0$, respectively. These individual velocity changes are responsible for dynamical friction, which causes the binary to

slow down. This deceleration decreases the semimajor axis of its orbit and increases its eccentricity, bringing the pericenter of the binary's orbit ever closer to the SMBH.

To track the internal evolution of the binary, we first calculate the probability that the binary will meet a single object in a close interaction. In the event of a close encounter, the full three-body calculation is performed using IABL, a binary-single scattering code (Gültekin et al. 2004), in conjunction with HNBody, an N-body code (Rauch & Hamilton, in preparation). To reduce the computation time, IABL uses a two-body approximation routine which replaces the binary with a single object during long orbits. If an encounter leaves the binary intact, or if there is an exchange, then the internal semimajor axis and eccentricity of the binary are updated and it continues on its orbit through the nucleus.

Binaries begin inside the radius of influence, hence all orbits are Keplerian, and orbit through the nucleus until (1) the binary is ionized, and all three objects are unbound; (2) the binary merges by gravitational radiation, which is calculated using the Peters equations between encounters (see Ch. 2); (3) the binary is ejected from the nucleus (recoil velocities are determined as discussed in Ch. 4 § 4.2.1); or (4) the binary is tidally separated by the SMBH.

The technique described above is a method of isolating the effects of two-body relaxation and close three-body encounters on binaries. While direct N-body calculations would provide insight into this scenario, treating the problem of binaries in a nucleus is very computationally demanding. The largest-scale N-body simulations to date require special purpose hardware such as GRAPE (Makino et al. 2003), and are unable to include a significant binary fraction, or the number of particles necessary for a realistic galactic nucleus (e.g., Freitag et al. 2006).

There are additional effects that can change the orbit of a binary around a SMBH. If a nucleus is triaxial, then stellar orbits will no longer be Keplerian, however this

is only effective on scales well outside the radius of influence (Merritt 2006). In addition, at distances of ~ 0.01 pc from the SMBH, resonant relaxation has been shown to dramatically alter stellar eccentricities because the overlapping Keplerian orbits of stars precess very slowly and exert torques on one another. All of our simulations take place well inside the radius of influence, therefore we do not include triaxiality. Also, in §6.3.4, we show that binaries tend to ionize, merge, or tidally separate outside of the region where resonant relaxation operates. For this reason, we do not include resonant relaxation in our simulations.

6.2.2 Simulations

The nuclei in these simulations contain a central black hole with mass $M_{\rm SMBH} = 10^6$ $M_\odot$), and follow a Bahcall & Wolf (1976) density profile:

$$\rho(r) \propto r^{-7/4} \quad . \tag{6.8}$$

The velocity dispersion well outside the radius of influence is assumed to be $\sigma_0 = 60$ km s^{-1}, in accordance with $\sigma_0 = 78$km s^{-1}($M_{\rm SMBH}/3 \times 10^6$ $M_\odot$), as derived from the $M - \sigma$ relation (Tremaine et al. 2002), and the escape velocity is $5\sigma_0 = 300$ km s^{-1}. As in Ch. 4, we choose the zero-age main sequence mass of the BH, its binary companion, and the interloper from a power law distribution $dN/dM \propto M^{-\alpha}$, and proceed to evolve each to a white dwarf, neutron star, or black hole mass if the ZAMS mass is above the main sequence cutoff (See §4.2.2 for the conversions). We can then explore the effects of mass segregation by choosing a range in α, with $\alpha \leq 0$ representing segregated nuclei, which have an overabundance of compact objects in their central regions. We show in §4.2.1 that single BHs exchange into binaries in $\approx$ a few billion years, therefore we begin each simulation here with a binary containing at least one BH. We divide the simulations into binaries that begin with two BHs

(referred to as BH-BH binaries), and those that start with one BH plus a companion of any type−BH, neutron star, white dwarf, or main sequence star (referred to as BH-companion binaries).

We present the results of three sets of simulations here, which are characterized by the following: (1) binaries of two equal-mass objects interacting with interlopers of a single mass−a simplified set to reproduce known trends and compare to published work; (2) BH-BH and BH-companion binaries in nuclei with a range of initial mass functions−to study the effects of mass segregation; (3) BH-BH and BH-companion binaries in a nucleus with a flat mass function (moderately segregated), with a wide range of initial internal energies−to analyze the impact of whether the binary is originally hard or soft. In this third set of simulations we parameterize the degree of binary hard/softness with

$$\epsilon = \frac{|E|}{m_* \sigma^2} \quad , \tag{6.9}$$

such that binaries with $\epsilon \ll 1$ are initially soft and those with $\epsilon \gg 1$ are initially hard. At the outset, we expect to find that the increased velocities near the SMBH will cause increased softening, leading to ionizations and increasing the distance from the SMBH at which binaries are tidally separated. In addition, we anticipate that few binaries will be ejected from the nucleus due to its large escape velocity.

6.3 Results

Figures 6.1 and 6.2 are examples of the evolution of the orbit of a binary as it sinks through the nucleus, and changes in the internal properties of the binary due to three-body encounters, respectively. In Figure 6.1, the semimajor axis decreases while the eccentricity of its orbit increases, and the binary has increasingly close passes with the SMBH at its orbital pericenter, thereby demonstrating the effects

of dynamical friction. Figure 6.2 demonstrates the aftermath of multiple encounters for one particular binary. This binary's eccentricity rises and drops in value, and its semimajor axis decreases slightly and then ultimately widens before it is tidally disrupted by the SMBH. While these plots provide a sense of the types of journeys experienced by individual binaries, we must look at the cumulative results of many simulations to find general trends.

6.3.1 Equal-Mass Binaries

Simulations involving binaries and interlopers of equal mass have revealed well-studied rules of three-body dynamics. Among these is Heggie's Law, which states that close interactions tend to cause hard binaries to harden and soft binaries to soften (Heggie 1975). Because hard binaries transfer some of their binding energy to single stars with each encounter that results in hardening, they have also been researched as the likely energy source responsible for halting core collapse in globular clusters. While binaries have been studied extensively in the context of clusters, binary-star dynamics in galactic nuclei have also been examined.

The Fokker-Planck approximation was used in a recent paper to study the dynamics of a single-mass population including binaries near a SMBH (Hopman 2009, hereafter H09). These simulations track the evolution of the energies and angular momenta of the binaries with respect to the SMBH. Additionally, results from previous three-body simulations are used to calculate the probability of a change in internal energy for each binary given the densities and speeds of nearby stars, thereby making it possible to track the evolution of the semimajor axes of the binaries. The main findings of H09 are that a large number of binaries are ionized due to three-body encounters close to the SMBH, hard binaries do not harden appreciably as they sink, binaries typically ionize before they undergo an exchange, and tidal

separations occur largely when the binary is on a very eccentric orbit around the SMBH. The lack of a mass spectrum within the population of binaries and single stars is a serious limitation as described by the author, because multi-mass three-body encounters have many more possible outcomes than do the comparatively simple equal-mass interactions.

With our method, we are able to include a mass spectrum, however we first present equal-mass results to compare with those in H09. In Table 1 we show results from three sets of simulations with equal-mass binaries and single mass populations of interlopers. In the first set, the masses of the binary members and interlopers are $m_{\rm bin,1} = m_{\rm bin,2} = m_* = 1$ M$_\odot$; in the second, $m_{\rm bin,1} = m_{\rm bin,2} = 5$ M$_\odot$, and $m_* = 0.5$ M$_\odot$; and in the third $m_{\rm bin,1} = m_{\rm bin,2} = 10$ M$_\odot$, and $m_* = 0.5$ M$_\odot$. The first set corresponds to the simulations in H09, and we find large ionization fractions for soft binaries with $\epsilon \leq 1$ that are consistent with the results of that work. For binaries with $\epsilon = 0.1$, H09 report ionization fractions of $\sim 90\%$, and our simulations give a similar fraction of $f_i = 0.87$. We also agree with H09 with regard to the small numbers of exchanges−for all cases at most a few percent of interactions result in an exchange. While H09 simulate regular stars, our focus is compact objects, and we therefore track mergers by gravitational radiation. Table 2 details the merger results. As binaries increase in hardness−decreasing in semimajor axis−the eccentricity required for merger decreases. This is expected because the inspiral time due to gravitational radiation is $\propto a^4(1-e^2)^{7/2}$. When binaries are significantly more massive than the interlopers (in high-α populations), they undergo far more encounters before they merge because each encounter has less of an effect on the binary. Tidal separations are examined in Table 3, which shows that softening increases the distances at which the binaries are separated. Tidal separations tend to occur when the binary is on an eccentric orbit, though binaries that are initially

Table 6.1. Simulations of Equal-Mass Binaries and Single Mass Interlopers in Nuclei with SMBH [a]

$M_1 : M_2 : M_{\rm int}$ [b]	ϵ [c]	$f_{\rm m}$ [d]	$f_{\rm i}$ [e]	$f_{\rm ts}$ [f]	$f_{\rm ej}$ [g]	$\langle a_{\rm enc}\rangle$ [h]	$\langle N_{\rm ex}\rangle$ [i]	$\langle N_{\rm int}\rangle$ [j]	$\langle N_{\rm ex/int}\rangle$ [k]
1:1:1	0.1	0.01	0.87	0.12	0	0.5006	0.98	76.93	0.0127
1:1:1	0.3	0.04	0.67	0.29	0	0.47	1.77	53.54	0.0331
1:1:1	1.0	0.25	0.29	0.46	0	0.4525	1.62	40.58	0.0399
1:1:1	10.0	0.71	0	0.29	0	0.2281	0.37	5.575	0.0664
5:5:0.5	0.3	0.08	0.16	0.76	0	0.4999	0.01	1929	5.184e-06
5:5:0.5	1.0	0.5	0.06	0.44	0	0.4993	0.04	1229	3.255e-05
5:5:0.5	10.0	0.77	0	0.23	0	0.4855	0.02	123.4	0.0002
10:10:0.5	0.3	0	0.02	0.98	0	0.4985	0	3374	0
10:10:0.5	1.0	0.13	0.01	0.86	0	0.5001	0	2562	0
10:10:0.5	10.0	0.89	0	0.11	0	0.4937	0	352.7	0

[a] All runs had 100 realizations, $\rm M_{SMBH} = 10^6 M_\odot$.

[b] Mass of binary member: Mass of binary member: Mass of single stars ($\rm M_\odot$).

[c] Hardness of initial binary at $\rm r_{infl}$: $\epsilon = |E|/m_{\rm avg}\sigma^2$.

[d] Fraction of runs in which binary members merged.

[e] Fraction of runs in which binary was ionized.

[f] Fraction of runs in which binary was tidally separated.

[g] Fraction of runs in which binary was ejected.

[h] Average orbital semimajor axis where first encounter occurred (pc).

[i] Average number of exchanges.

[j] Average number of interactions.

[k] Average number of exchanges per interaction.

soft can be separated at larger pericenter distances and therefore lower eccentricities.

Table 6.2. Simulations of Equal-Mass Binaries and Single Mass Interlopers in Nuclei with SMBH (Mergers)[a]

$M_1 : M_2 : M_{\rm int}$[b]	ϵ[c]	$f_{\rm notBH}$[d]	$f_{\rm NS}$[3]	$\langle e_{\rm bin,m}\rangle$[f]	$\langle a_{\rm m}\rangle$[g]	$\langle M_{\rm bin,m}\rangle$[h]	$\langle N_{\rm single,ej}\rangle$[i]	$\langle t_{\rm m}\rangle$[j]	$\langle N_{\rm int}\rangle$[k]
1:1:1	0.1	1	—	0.9759	0.0184	—	—	3.914e+09	37
1:1:1	0.3	1	—	0.9972	0.2192	—	—	3.723e+08	10
1:1:1	1.0	1	—	0.9322	0.1745	—	—	1.308e+09	8.44
1:1:1	10.0	1	—	0.6128	0.1668	—	—	6.945e+08	2.042
5:5:0.5	0.3	0	—	0.9448	0.1745	10	—	9.131e+08	843.5
5:5:0.5	1.0	0.04	—	0.8744	0.1019	10	—	2.05e+09	517.4
5:5:0.5	10.0	0.026	—	0.7307	0.0640	10	—	1.977e+09	101.5
10:10:0.5	0.3	—	—	—	—	—	—	—	—
10:10:0.5	1.0	0	—	0.6783	0.0550	20	—	2.227e+09	1296
10:10:0.5	10.0	0	—	0.641	0.0506	20	—	1.742e+09	323.7

[a]All runs had 100 realizations, $\rm M_{SMBH} = 10^6 M_\odot$.

[b]Mass of binary member: Mass of binary member: Mass of single stars ($\rm M_\odot$).

[c]Hardness of initial binary at $\rm r_{infl}$: $\epsilon = |E|/m_{\rm avg}\sigma^2$.

[d]Fraction of runs in which black hole merged with something other than another black hole.

[e]Fraction of runs in which black hole merged with neutron star.

[f]Average binary eccentricity prior to merger.

[g]Average semimajor axis of orbit around SMBH where merger occurred (pc).

[h]Average mass of binaries that merged ($\rm M_\odot$).

[i]Average number of single black holes ejected per binary that merged.

[j]Average time between first encounter and merger (years).

[k]Average number of interactions before merger.

Table 6.3. Simulations of Equal-Mass Binaries and Single Mass Interlopers in Nuclei with SMBH (Tidal Separations)[a]

$M_1 : M_2 : M_{\rm int}$[b]	ϵ[c]	$\langle e_{\rm orb,ts}\rangle$[d]	$f_{\rm notBH}$[e]	$\langle M_{\rm bhbh,ts}\rangle$[f]	$\langle M_{\rm ts}\rangle$[g]	$\langle a_{\rm bhbh,ts}\rangle$[h]	$\langle a_{\rm bin,ts}\rangle$[i]	$\langle r_{\rm ts}\rangle$[j]	$\langle t_{\rm max,insp}\rangle$[k]	$\langle t_{\rm ts}\rangle$[l]	$\langle N_{\rm int}\rangle$[m]
1:1:1	0.1	0.8057	1	—	2	—	116	—	—	—	122.1
1:1:1	0.3	0.9274	1	—	2	—	40.34	—	—	—	98.24
1:1:1	1.0	0.9646	1	—	2	—	9.959	—	—	—	36.72
1:1:1	10.0	0.9796	1	—	2	—	0.2692	—	—	—	10.38
5:5:0.5	0.3	0.7807	0.0131	10	9.941	101.1	101	6768	5.036e+15	1.852e+08	2123
5:5:0.5	1.0	0.8742	0.0227	10	9.898	42.49	41.52	2844	1.57e+14	1.355e+09	2058
5:5:0.5	10.0	0.9992	0	10	10	0.2464	0.2464	16.49	1.775e+05	2.641e+09	196.7
10:10:0.5	0.3	0.6946	0	20	20	141.2	141.2	7502	7.602e+15	8.215e+07	3276
10:10:0.5	1.0	0.8161	0	20	20	43.86	43.86	2330	7.074e+13	2.129e+08	2718
10:10:0.5	10.0	0.999	0	20	20	0.6477	0.6477	34.41	3.365e+06	1.941e+09	587.5

Note. — (a) All runs had 100 realizations, $\rm M_{SMBH} = 10^6 M_\odot$. (b) Mass of binary member($\rm M_\odot$): Mass of binary member($\rm M_\odot$): Mass of single stars ($\rm M_\odot$). (c) Hardness of initial binary at $\rm r_{infl}$: $\epsilon = |E|/m_{\rm avg}\sigma^2$. (d) Average orbital eccentricity around SMBH prior to tidal separation. (e) Fraction of runs in which tidally separated binary included something other than another black hole. (f) Average mass of BH-BH binaries that tidally separated ($\rm M_\odot$). (g) Average mass of BH-companion binaries that tidally separated ($\rm M_\odot$). (h) Average BH-BH binary semimajor axis prior to tidal separation (AU). (i) Average BH-companion binary semimajor axis prior to tidal separation (AU). (j) Average tidal separation radius (for average BH-BH binary) (AU). (k) Maximum gravitational radiation inspiral time for a captured BH at tidal separation radius (years). (l) Average time between first encounter and tidal separation (years). (m) number of interactions before tidal separation.

6.3.2 Variation of Initial Mass Function

In Tables 4 through 9, we show the results of simulations with different mass populations, ranging from low-α, in which an overabundance of massive objects represents a very mass-segregated nucleus, to the Salpeter value of $\alpha = 2.35$ that characterizes the stellar population in the solar neighborhood. The binaries in these simulations are very mildly hard, with $\epsilon = 4.0$. Again, we find that binaries in high-α nuclei have many more interactions and do not experience significant softening due to the small increments of energy they exchange with the low mass interlopers they encounter. This results in fewer ionizations and produces tidal separations closer to the SMBH. These binaries generally end with mergers or tidal separation; mergers occur if the internal eccentricity reaches a high value after an encounter, and tidal separations happen if a high orbital eccentricity results in a close pericenter pass with the SMBH.

Energetic encounters with massive interlopers in mass-segregated, low-α nuclei result in significant softening that causes a large fraction of binaries to ionize (76% when $\alpha = -1.0$). Tidal separation of these softened binaries take place at increasingly large distances from the SMBH as α decreases, and these binaries survive for less time, regardless of whether they end with a merger, ionization, or tidal separation. Independent of the mass function, exchanges tend to swap more massive objects into the binaries, which means that mergers and tidal separations tend to involve BHs of above average mass. The fractions of ionizations, mergers, and tidal separations do not vary significantly when binaries begin as BH-companion rather than BH-BH. Galactic nuclei will be mass-segregated to some degree because of the inverse relationship between mass and relaxation time, hence we choose a flat mass profile to examine the impact of a range in initial hardness on the fates of binaries.

Table 6.4. Simulations of BH-companion Binaries in Nuclei with SMBH[a]

α[b]	ϵ[c]	$\langle M_{\rm BH}\rangle$[d]	$f_{\rm m}$[e]	$f_{\rm i}$[f]	$f_{\rm ts}$[g]	$f_{\rm ej}$[h]	$\langle a_{\rm enc}\rangle$[i]	$\langle N_{\rm ex}\rangle$[j]	$\langle N_{\rm int}\rangle$[k]	$\langle N_{\rm ex/int}\rangle$[l]
-1.0	4.0	13.4	0.156	0.756	0.086	0.002	0.494	2.912	50.61	0.0575
-0.5	4.0	12.6	0.182	0.720	0.094	0.004	0.4904	2.976	58.2	0.0511
0.0	4.0	11.7	0.232	0.634	0.132	0.002	0.4837	3.19	74.42	0.0429
0.5	4.0	10.7	0.27	0.544	0.182	0.004	0.4714	3.16	85.96	0.0368
1.0	4.0	9.7	0.296	0.404	0.3	0	0.4345	2.152	152.4	0.0141
1.5	4.0	8.8	0.38	0.232	0.386	0.002	0.3816	1.128	216.2	0.0052
2.0	4.0	7.5	0.438	0.092	0.47	0	0.3506	0.658	203	0.0032
2.35	4.0	7.4	0.482	0.064	0.454	0	0.3282	0.496	137.2	0.0036

[a]All runs had 500 realizations, $\rm M_{SMBH} = 10^6 M_\odot$.

[b]Number distribution of stars on zero age main sequence: $dN/dM \propto M^{-\alpha}$.

[c]Hardness of initial binary at $\rm r_{infl}$: $\epsilon = |E|/m_{\rm avg}\sigma^2$.

[d]Average mass of all black holes given α and our evolutionary assumptions ($M_\odot$).

[e]Fraction of runs in which binary members merged.

[f]Fraction of runs in which binary was ionized.

[g]Fraction of runs in which binary was tidally separated.

[h]Fraction of runs in which binary was ejected.

[i]Average orbital semimajor axis where first encounter occurred (pc).

[j]Average number of exchanges.

[k]Average number of interactions.

[l]Average number of exchanges per interaction.

Table 6.5. Simulations of BH-BH Binaries in Nuclei with SMBH[a]

α[b]	ϵ[c]	$\langle M_{\rm BH}\rangle$[d]	$f_{\rm m}$[e]	$f_{\rm i}$[f]	$f_{\rm ts}$[g]	$f_{\rm ej}$[h]	$\langle a_{\rm enc}\rangle$[i]	$\langle N_{\rm ex}\rangle$[j]	$\langle N_{\rm int}\rangle$[k]	$\langle N_{\rm ex/int}\rangle$[l]
-1.0	4.0	13.4	0.15	0.764	0.084	0.002	0.4973	2.764	57.65	0.0479
-0.5	4.0	12.6	0.164	0.744	0.092	0	0.4959	2.936	65.22	0.0450
0.0	4.0	11.7	0.198	0.662	0.14	0	0.493	2.944	69.54	0.0423
0.5	4.0	10.7	0.202	0.644	0.154	0	0.4919	2.892	110	0.0263
1.0	4.0	9.7	0.286	0.470	0.244	0	0.4873	2.274	200.8	0.0113
1.5	4.0	8.8	0.404	0.258	0.338	0	0.4863	1.12	408.3	0.0027
2.0	4.0	7.5	0.45	0.078	0.472	0	0.4777	0.216	588.8	0.0004
2.35	4.0	7.4	0.518	0.018	0.464	0	0.4769	0.082	602.2	0.0001

[a]All runs had 500 realizations, $\rm M_{SMBH} = 10^6 M_\odot$.

[b]Number distribution of stars on zero age main sequence: $dN/dM \propto M^{-\alpha}$.

[c]Hardness of initial binary at $\rm r_{infl}$: $\epsilon = |E|/m_{\rm avg}\sigma^2$.

[d]Average mass of all black holes given α and our evolutionary assumptions ($M_\odot$).

[e]Fraction of runs in which binary members merged.

[f]Fraction of runs in which binary was ionized.

[g]Fraction of runs in which binary was tidally separated.

[h]Fraction of runs in which binary was ejected.

[i]Average orbital semimajor axis where first encounter occurred (pc).

[j]Average number of exchanges.

[k]Average number of interactions.

[l]Average number of exchanges per interaction.

Table 6.6. Simulations of BH-companion Binaries in Nuclei with SMBH (Mergers)[a]

α[b]	ϵ[c]	$\langle M_{\rm BH}\rangle$[d]	$f_{\rm notBH}$[e]	$f_{\rm NS}$[f]	$\langle e_{\rm bin,m}\rangle$[g]	$\langle a_{\rm m}\rangle$[h]	$\langle M_{\rm bin,m}\rangle$[i]	$\langle N_{\rm single,ej}\rangle$[j]	$\langle t_{\rm m}\rangle$[k]	$\langle N_{\rm int}\rangle$[l]
-1.0	4.0	13.4	0	0	0.916	0.1672	33.14	0.3333	1.818e+07	41.37
-0.5	4.0	12.6	0	0	0.8876	0.17	31.73	0.3956	2.232e+07	41.11
0.0	4.0	11.7	0.0259	0.0086	0.921	0.1619	31.16	0.3097	3.109e+07	44.84
0.5	4.0	10.7	0.0222	0	0.8884	0.1321	31.16	0.4015	6.643e+07	52.94
1.0	4.0	9.7	0.2838	0.0608	0.9209	0.1488	27.34	0.1698	1.968e+08	64.17
1.5	4.0	8.8	0.6842	0.0842	0.8955	0.0973	21.73	0.05	1.028e+09	79.82
2.0	4.0	7.5	0.9315	0.0502	0.8363	0.0635	16.94	0	2.372e+09	67.11
2.35	4.0	7.4	0.9876	0.0124	0.8027	0.0583	15.7	0	3.948e+09	70.24

[a]All runs had 500 realizations, $\rm M_{SMBH} = 10^6 M_\odot$.

[b]Number distribution of stars on zero age main sequence: $dN/dM \propto M^{-\alpha}$.

[c]Hardness of initial binary at $\rm r_{infl}$: $\epsilon = |E|/m_{\rm avg}\sigma^2$.

[d]Average mass of all black holes given α and our evolutionary assumptions ($\rm M_\odot$).

[e]Fraction of runs in which black hole merged with something other than another black hole.

[f]Fraction of runs in which black hole merged with neutron star.

[g]Average binary eccentricity prior to merger.

[h]Average semimajor axis of orbit around SMBH where merger occurred (pc).

[i]Average mass of BH-BH binaries that merged ($\rm M_\odot$).

[j]Average number of single black holes ejected per binary that merged.

[k]Average time between first encounter and merger (years).

[l]Average number of interactions before merger.

Table 6.7. Simulations of BH-BH Binaries in Nuclei with SMBH (Mergers)[a]

α[b]	ϵ[c]	$\langle M_{\rm BH}\rangle$[d]	$f_{\rm notBH}$[e]	$f_{\rm NS}$[f]	$\langle e_{\rm bin,m}\rangle$[g]	$\langle a_{\rm m}\rangle$[h]	$\langle M_{\rm bin,m}\rangle$[i]	$\langle N_{\rm single,ej}\rangle$[j]	$\langle t_{\rm m}\rangle$[k]	$\langle N_{\rm int}\rangle$[l]
-1.0	4.0	13.4	0	0	0.8802	0.1602	32.89	0.5333	1.871e+07	40.89
-0.5	4.0	12.6	0	0	0.8991	0.1862	31.65	0.4146	1.986e+07	38.09
0.0	4.0	11.7	0	0	0.9147	0.1742	31.89	0.2626	2.904e+07	46.28
0.5	4.0	10.7	0.0099	0.0099	0.9292	0.1437	30.31	0.26	5.142e+07	57.42
1.0	4.0	9.7	0.0140	0.0070	0.8891	0.118	27.19	0.2057	1.631e+08	99.74
1.5	4.0	8.8	0.0594	0.0198	0.8605	0.0900	21.3	0.0316	6.212e+08	188
2.0	4.0	7.5	0.0356	0.0089	0.8212	0.0565	16.67	0.0046	1.904e+09	368.5
2.35	4.0	7.4	0.0425	0.0039	0.7637	0.0433	14.44	0	3.199e+09	360.2

[a]All runs had 500 realizations, $\rm M_{SMBH} = 10^6 M_\odot$.

[b]Number distribution of stars on zero age main sequence: $dN/dM \propto M^{-\alpha}$.

[c]Hardness of initial binary at $\rm r_{infl}$: $\epsilon = |E|/m_{\rm avg}\sigma^2$.

[d]Average mass of all black holes given α and our evolutionary assumptions ($\rm M_\odot$).

[e]Fraction of runs in which black hole merged with something other than another black hole.

[f]Fraction of runs in which black hole merged with neutron star.

[g]Average binary eccentricity prior to merger.

[h]Average semimajor axis of orbit around SMBH where merger occurred (pc).

[i]Average mass of BH-BH binaries that merged ($\rm M_\odot$).

[j]Average number of single black holes ejected per binary that merged.

[k]Average time between first encounter and merger (years).

[l]Average number of interactions before merger.

Table 6.8. Simulations of BH-companion Binaries in Nuclei with SMBH (Tidal Separations)[a]

α[b]	ϵ[c]	$\langle M_{\rm BH}\rangle$[d]	$\langle e_{\rm orb,ts}\rangle$[e]	$f_{\rm notBH}$[f]	$\langle M_{\rm bhbh,ts}\rangle$[g]	$\langle M_{\rm ts}\rangle$[h]	$\langle a_{\rm bhbh,ts}\rangle$[i]	$\langle a_{\rm bin,ts}\rangle$[j]	$\langle r_{\rm ts}\rangle$[k]	$\langle t_{\rm max,insp}\rangle$[l]	$\langle t_{\rm ts}\rangle$[m]	$\langle N_{\rm int}\rangle$[n]
-1.0	4.0	13.4	0.8803	0.0233	32.18	31.79	251.7	245.9	1.141e+04	4.068e+16	1.519e+06	72.88
-0.5	4.0	12.6	0.8523	0.0213	31.38	31.09	215.9	211.4	9872	2.279e+16	2.39e+06	104.8
0.0	4.0	11.7	0.8581	0.0606	30.16	29.55	193.1	192.6	8947	1.538e+16	7.892e+06	133.1
0.5	4.0	10.7	0.8303	0.0440	29.44	28.57	176.7	174.1	8253	1.113e+16	2.409e+07	160.3
1.0	4.0	9.7	0.8419	0.2267	26.84	22.9	113.9	92.77	5487	2.175e+15	1.889e+08	265.9
1.5	4.0	8.8	0.9337	0.6062	23.57	15.6	23.07	12.26	1160	4.346e+12	8.384e+08	351.5
2.0	4.0	7.5	0.9811	0.9362	19.91	8.985	8.219	1.526	437.4	8.785e+10	2.419e+09	279.9
2.35	4.0	7.4	0.9823	0.9780	9.712	7.988	2.907	0.7164	196.5	3.578e+09	3.677e+09	199.7

Note. — (a) All runs had 500 realizations, $\rm M_{SMBH} = 10^6 M_\odot$. (b) Number distribution of stars on zero age main sequence: $dN/dM \propto M^{-\alpha}$. (c) Hardness of initial binary at $\rm r_{infl}$: $\epsilon = |E|/m_{\rm avg}\sigma^2$. (d) Average mass of all black holes given α and our evolutionary assumptions ($\rm M_\odot$). (e) Average orbital eccentricity around SMBH prior to tidal separation. (f) Fraction of runs in which tidally separated binary included something other than another black hole. (g) Average mass of BH-BH binaries that tidally separated ($\rm M_\odot$). (h) Average mass of BH-companion binaries that tidally separated ($\rm M_\odot$). (i) Average BH-BH binary semimajor axis prior to tidal separation (AU). (j) Average BH-companion binary semimajor axis prior to tidal separation (AU). (k) Average tidal separation radius (for average BH-BH binary) (AU). (l) Maximum gravitational radiation inspiral time for a captured BH at tidal separation radius (years). (m) Average time between first encounter and tidal separation (years). (n) Average number of interactions before tidal separation.

Table 6.9. Simulations of BH-BH Binaries in Nuclei with SMBH (Tidal Separations)[a]

α^b	ϵ^c	$\langle M_{\rm BH}\rangle^d$	$\langle e_{\rm orb,ts}\rangle^e$	$f_{\rm notBH}{}^f$	$\langle M_{\rm bhbh,ts}\rangle^g$	$\langle M_{\rm ts}\rangle^h$	$\langle a_{\rm bhbh,ts}\rangle^i$	$\langle a_{\rm bin,ts}\rangle^j$	$\langle r_{\rm ts}\rangle^k$	$\langle t_{\rm max,insp}\rangle^l$	$\langle t_{\rm ts}\rangle^m$	$\langle N_{\rm int}\rangle^n$
-1.0	4.0	13.4	0.8805	0	32.34	32.34	234.2	234.2	1.06e+04	3.03e+16	1.566e+06	82.43
-0.5	4.0	12.6	0.8713	0	30.92	30.92	216.8	216.8	9962	2.364e+16	2.645e+06	103
0.0	4.0	11.7	0.8625	0	30.16	30.16	190.7	190.7	8836	1.463e+16	4.218e+06	118.7
0.5	4.0	10.7	0.8352	0	29.39	29.39	196.7	196.7	9193	1.714e+16	1.18e+07	185.1
1.0	4.0	9.7	0.8121	0	25.36	25.36	124	124	6087	3.295e+15	6.43e+07	374.8
1.5	4.0	8.8	0.8765	0.041	22.85	22.28	33.69	35.05	1712	2.062e+13	4.908e+08	749.2
2.0	4.0	7.5	0.9538	0.047	16.49	16.15	5.093	4.909	288.6	1.665e+10	1.796e+09	803.6
2.35	4.0	7.4	0.9681	0.026	15.52	15.46	1.926	1.915	111.4	3.696e+08	3.29e+09	874.6

Note. — (a) All runs had 500 realizations, $\rm M_{SMBH} = 10^6 M_\odot r_{infl}$. (b) Number distribution of stars on zero age main sequence: $dN/dM \propto M^{-\alpha}$. (c) Hardness of initial binary at $\rm r_{infl}$: $\epsilon = |E|/m_{\rm avg}\sigma^2$. (d) Average mass of all black holes given α and our evolutionary assumptions ($\rm M_\odot$). (e) Average orbital eccentricity around SMBH prior to tidal separation. (f) Fraction of runs in which tidally separated binary included something other than another black hole. (g) Average mass of BH-BH binaries that tidally separated ($\rm M_\odot$). (h) Average mass of BH-companion binaries that tidally separated ($\rm M_\odot M_{SMBH} = 10^6 M_\odot$). (i) Average BH-BH binary semimajor axis prior to tidal separation (AU). (j) Average BH-companion binary semimajor axis prior to tidal separation (AU). (k) Average tidal separation radius (for average BH-BH binary) (AU). (l) Maximum gravitational radiation inspiral time for a captured BH at tidal separation radius (years). (m) Average time between first encounter and tidal separation (years). (n) Average number of interactions before tidal separation.

6.3.3 Variation of Initial Binary Hardness

In the simulations in Tables 10 through 15 we use a moderately segregated value of $\alpha = 0.0$, and began with binaries ranging from very soft to very hard. As expected, binaries that are initially hard have a higher merger fraction and they merge with lower eccentricities, while soft binaries typically ionize. Moderately soft and borderline ($\epsilon \approx 1$) binaries have the largest tidal separation fractions, because they widen enough to make it possible for the SMBH to pull them apart without requiring an extremely eccentric orbit, but they are not so soft that they undergo rapid runaway softening and ionization. Tidal separations of hard binaries are less frequent, and only occur when their orbits around the SMBH exceed $e \sim 0.9$. The small cross sections of hard binaries ensure that they encounter fewer interlopers than soft binaries, however the interactions that they have are more likely to result in an exchange or an ejection. Exchanges typically occur when the interloper is temporarily bound to the binary and the three objects have a complicated series of close passes. This generally happens when the speed of the interloper is smaller than the orbital speed of the binary members, which is the case when the binary is hard. Thus we find that the number of exchanges per interaction increases with increasing hardness. Ejections take place when a binary hardens and transfers enough of its binding energy to kinetic energy to result in a velocity kick in excess of the escape velocity of the nucleus. For hard binaries, the rate of hardening is independent of the hardness, meaning that the fraction of binding energy released by hardening is the same for any binary regardless of its initial internal energy (see e.g. Binney & Tremaine 1987). If, for instance the binding energy decreases by increments of 20% with each hardening encounter, then very hard binaries with large $|E|$ lose more energy than less hard binaries with smaller $|E|$. Therefore, the relatively

infrequent encounters that a very hard binary experiences are more likely to result in the ejection of the interloper and/or the binary. As in the previous section, exchanges produce massive binaries, and the resultant mergers and tidal separations occur with BHs that are on the high end of the mass spectrum. Again, there is no significant change in the ionization, merger, and tidal separation fractions when varying between binaries that begin as BH-companion or BH-BH. However, the details of the mergers and tidal separations are slightly different; binaries that begin as BH-companion and do not have multiple exchanges to swap in more massive BHs typically meet their end with a smaller total mass. For binaries with mid-range ϵ in Table 15, the increase in binary mass and decrease in the fraction that tidally separate with a non-BH binary member are both due to the comparatively large number of exchanges that those binaries undergo.

Table 6.10. Simulations of BH-companion Binaries in Nuclei with SMBH[a]

α[b]	ϵ[c]	$\langle M_{\rm BH}\rangle$[d]	$f_{\rm m}$[e]	$f_{\rm i}$[f]	$f_{\rm ts}$[g]	$f_{\rm ej}$[h]	$\langle a_{\rm enc}\rangle$[i]	$\langle N_{\rm ex}\rangle$[j]	$\langle N_{\rm int}\rangle$[k]	$\langle N_{\rm ex/int}\rangle$[l]
0.0	0.01	11.7	0	0.914	0.086	0	0.499	0.016	38.65	0.0004
0.0	0.02	11.7	0	0.888	0.112	0	0.499	0.026	48.64	0.0005
0.0	0.05	11.7	0	0.886	0.114	0	0.498	0.072	57.35	0.0013
0.0	0.1	11.7	0	0.896	0.104	0	0.498	0.126	56.02	0.0022
0.0	0.2	11.7	0.002	0.866	0.132	0	0.498	0.242	52.19	0.0046
0.0	0.5	11.7	0.002	0.886	0.112	0	0.4965	0.596	49.1	0.0121
0.0	1.0	11.7	0.02	0.862	0.118	0	0.496	1.058	54.69	0.0194
0.0	2.0	11.7	0.096	0.802	0.1	0.002	0.490	2.064	62.79	0.0329
0.0	5.0	11.7	0.304	0.566	0.126	0.004	0.476	3.614	68.12	0.0531
0.0	10.0	11.7	0.532	0.342	0.122	0.004	0.467	4.45	56.33	0.079
0.0	20.0	11.7	0.78	0.130	0.088	0.002	0.438	3.828	36.49	0.1049
0.0	50.0	11.7	0.882	0.05	0.054	0.014	0.388	2.762	16.96	0.1629
0.0	100.0	11.7	0.918	0.032	0.042	0.008	0.330	1.62	9.701	0.167
0.0	200.0	11.7	0.938	0.006	0.048	0.008	0.274	0.99	5.615	0.1763
0.0	500.0	11.7	0.946	0.002	0.044	0.008	0.208	0.46	1.942	0.2369
0.0	1000.0	11.7	0.936	0	0.064	0	0.153	0.306	1.196	0.2559

[a]All runs had 500 realizations, $\rm M_{SMBH} = 10^6 M_\odot$.

[b]Number distribution of stars on zero age main sequence: $dN/dM \propto M^{-\alpha}$.

[c]Hardness of initial binary at $\rm r_{infl}$: $\epsilon = |E|/m_{\rm avg}\sigma^2$.

[d]Average mass of all black holes given α and our evolutionary assumptions ($M_\odot$).

[e]Fraction of runs in which binary members merged.

[f]Fraction of runs in which binary was ionized.

[g]Fraction of runs in which binary was tidally separated.

[h]Fraction of runs in which binary was ejected.

[i]Average orbital semimajor axis where first encounter occurred (pc).

[j]Average number of exchanges.

[k]Average number of interactions.

[l]Average number of exchanges per interaction.

Table 6.11. Simulations of BH-BH Binaries in Nuclei with SMBH[a]

α[b]	ϵ[c]	$\langle M_{\rm BH}\rangle$[d]	$f_{\rm m}$[e]	$f_{\rm i}$[f]	$f_{\rm ts}$[g]	$f_{\rm ej}$[h]	$\langle a_{\rm enc}\rangle$[i]	$\langle N_{\rm ex}\rangle$[j]	$\langle N_{\rm int}\rangle$[k]	$\langle N_{\rm ex/int}\rangle$[l]
0.0	0.01	11.7	0	0.964	0.036	0	0.499	0.004	45.71	0.00009
0.0	0.02	11.7	0	0.930	0.07	0	0.499	0.01	58.74	0.0002
0.0	0.05	11.7	0	0.828	0.172	0	0.499	0.054	61.08	0.0009
0.0	0.1	11.7	0	0.868	0.132	0	0.498	0.102	68.76	0.0015
0.0	0.2	11.7	0	0.844	0.156	0	0.497	0.186	67.23	0.0028
0.0	0.5	11.7	0	0.87	0.13	0	0.497	0.326	59.41	0.0055
0.0	1.0	11.7	0.016	0.874	0.11	0	0.497	0.818	58.83	0.0139
0.0	2.0	11.7	0.06	0.82	0.12	0	0.497	1.666	66.64	0.025
0.0	5.0	11.7	0.282	0.612	0.102	0.004	0.493	3.452	71.28	0.0484
0.0	10.0	11.7	0.562	0.348	0.084	0.006	0.483	4.458	54.87	0.0813
0.0	20.0	11.7	0.804	0.110	0.074	0.012	0.469	4.28	35.65	0.1201
0.0	50.0	11.7	0.91	0.046	0.036	0.008	0.436	2.962	19.47	0.1521
0.0	100.0	11.7	0.932	0.022	0.034	0.012	0.401	1.978	13.08	0.1512
0.0	200.0	11.7	0.956	0.008	0.026	0.01	0.350	1.222	6.685	0.1828
0.0	500.0	11.7	0.96	0.002	0.032	0.006	0.270	0.528	2.797	0.1888
0.0	1000.0	11.7	0.96	0	0.034	0.006	0.208	0.282	1.337	0.2109

[a]All runs had 500 realizations, $\rm M_{SMBH} = 10^6 M_\odot$.

[b]Number distribution of stars on zero age main sequence: $dN/dM \propto M^{-\alpha}$.

[c]Hardness of initial binary at $\rm r_{infl}$: $\epsilon = |E|/m_{\rm avg}\sigma^2$.

[d]Average mass of all black holes given α and our evolutionary assumptions ($M_\odot$).

[e]Fraction of runs in which binary members merged.

[f]Fraction of runs in which binary was ionized.

[g]Fraction of runs in which binary was tidally separated.

[h]Fraction of runs in which binary was ejected.

[i]Average orbital semimajor axis where first encounter occurred (pc).

[j]Average number of exchanges.

[k]Average number of interactions.

[l]Average number of exchanges per interaction.

Table 6.12. Simulations of BH-companion Binaries in Nuclei with SMBH (Mergers)[a]

α[b]	ϵ[c]	$\langle M_{\rm BH}\rangle$[d]	$f_{\rm notBH}$[e]	$f_{\rm NS}$[f]	$\langle e_{\rm bin,m}\rangle$[g]	$\langle a_{\rm m}\rangle$[h]	$\langle M_{\rm bin,m}\rangle$[i]	$\langle N_{\rm single,ej}\rangle$[j]	$\langle t_{\rm m}\rangle$[k]	$\langle N_{\rm int}\rangle$[l]
0.0	0.01	11.7	—	—	—	—	—	—	—	—
0.0	0.02	11.7	—	—	—	—	—	—	—	—
0.0	0.05	11.7	—	—	—	—	—	—	—	—
0.0	0.1	11.7	—	—	—	—	—	—	—	—
0.0	0.2	11.7	0	0	0.9945	0.3549	30.25	0	3.91e+06	26
0.0	0.5	11.7	0	0	0.9439	0.0947	38.45	0	2.858e+07	106
0.0	1.0	11.7	0	0	0.8691	0.1743	31.52	0.2	2.641e+07	46.4
0.0	2.0	11.7	0.0208	0.0208	0.9261	0.1927	32.28	0.4894	2.699e+07	46.96
0.0	5.0	11.7	0.0132	0.0132	0.8774	0.1489	31.94	0.3133	3.223e+07	43.36
0.0	10.0	11.7	0.0150	0.0075	0.8868	0.1484	31.27	0.3588	3.794e+07	36.94
0.0	20.0	11.7	0.0333	0.0231	0.9065	0.1536	30.66	0.3634	3.494e+07	24.23
0.0	50.0	11.7	0.0658	0.0499	0.8872	0.1475	30.06	0.449	3.722e+07	14.84
0.0	100.0	11.7	0.150	0.1002	0.8174	0.1507	27.99	0.3846	2.86e+07	8.174
0.0	200.0	11.7	0.2004	0.1364	0.7211	0.15	26.36	0.3893	2.126e+07	4.936
0.0	500.0	11.7	0.2156	0.1522	0.563	0.1526	25.37	0.248	7.475e+06	1.945
0.0	1000.0	11.7	0.2137	0.1538	0.4467	0.1368	24.35	0.0978	1.123e+06	1.19

[a]All runs had 500 realizations, $\rm M_{SMBH} = 10^6 M_\odot$.

[b]Number distribution of stars on zero age main sequence: $dN/dM \propto M^{-\alpha}$.

[c]Hardness of initial binary at $\rm r_{infl}$: $\epsilon = |E|/m_{\rm avg}\sigma^2$.

[d]Average mass of all black holes given α and our evolutionary assumptions ($\rm M_\odot$).

[e]Fraction of runs in which black hole merged with something other than another black hole.

[f]Fraction of runs in which black hole merged with neutron star.

[g]Average binary eccentricity prior to merger.

[h]Average semimajor axis of orbit around SMBH where merger occurred (pc).

[i]Average mass of BH-BH binaries that merged ($\rm M_\odot$).

[j]Average number of single black holes ejected per binary that merged.

[k]Average time between first encounter and merger (years).

[l]Average number of interactions before merger.

Table 6.13. Simulations of BH-BH Binaries in Nuclei with SMBH (Mergers)[a]

α[b]	ϵ[c]	$\langle M_{\rm BH}\rangle$[d]	$f_{\rm notBH}$[e]	$f_{\rm NS}$[f]	$\langle e_{\rm bin,m}\rangle$[g]	$\langle a_{\rm m}\rangle$[h]	$\langle M_{\rm bin,m}\rangle$[i]	$\langle N_{\rm single,ej}\rangle$[j]	$\langle t_{\rm m}\rangle$[k]	$\langle N_{\rm int}\rangle$[l]
0.0	0.01	11.7	—	—	—	—	—	—	—	—
0.0	0.02	11.7	—	—	—	—	—	—	—	—
0.0	0.05	11.7	—	—	—	—	—	—	—	—
0.0	0.1	11.7	—	—	—	—	—	—	—	—
0.0	0.2	11.7	—	—	—	—	—	—	—	—
0.0	0.5	11.7	—	—	—	—	—	—	—	—
0.0	1.0	11.7	0	0	0.9258	0.1432	31.08	0	2.145e+07	62.5
0.0	2.0	11.7	0	0	0.863	0.1493	31.32	0.3333	3.9e+07	54.77
0.0	5.0	11.7	0	0	0.8802	0.1569	31.57	0.4894	3.315e+07	43.62
0.0	10.0	11.7	0	0	0.9127	0.1623	31.46	0.3167	2.951e+07	34.95
0.0	20.0	11.7	0	0	0.8977	0.1612	31.53	0.3682	2.937e+07	27.42
0.0	50.0	11.7	0.002	0.002	0.9019	0.1547	30.28	0.4097	3.107e+07	16.76
0.0	100.0	11.7	0	0	0.8763	0.1554	28.62	0.4163	3.27e+07	10.7
0.0	200.0	11.7	0.002	0.002	0.7925	0.162	27.7	0.4696	2.431e+07	6.37
0.0	500.0	11.7	0	0	0.6014	0.1723	25.25	0.2708	1.2e+07	2.688
0.0	1000.0	11.7	0	0	0.4248	0.1812	24.21	0.1146	2.028e+06	1.335

[a]All runs had 500 realizations, $\rm M_{SMBH} = 10^6 M_\odot$.

[b]Number distribution of stars on zero age main sequence: $dN/dM \propto M^{-\alpha}$.

[c]Hardness of initial binary at $\rm r_{infl}$: $\epsilon = |E|/m_{\rm avg}\sigma^2$.

[d]Average mass of all black holes given α and our evolutionary assumptions ($\rm M_\odot$).

[e]Fraction of runs in which black hole merged with something other than another black hole.

[f]Fraction of runs in which black hole merged with neutron star.

[g]Average binary eccentricity prior to merger.

[h]Average semimajor axis of orbit around SMBH where merger occurred (pc).

[i]Average mass of BH-BH binaries that merged ($\rm M_\odot$).

[j]Average number of single black holes ejected per binary that merged.

[k]Average time between first encounter and merger (years).

[l]Average number of interactions before merger.

Table 6.14. Simulations of BH-companion Binaries in Nuclei with SMBH (Tidal Separations)[a]

α[b]	ϵ[c]	$\langle M_{\rm BH}\rangle$[d]	$\langle e_{\rm orb,ts}\rangle$[e]	$f_{\rm notBH}$[f]	$\langle M_{\rm bhbh,ts}\rangle$[g]	$\langle M_{\rm ts}\rangle$[h]	$\langle a_{\rm bhbh,ts}\rangle$[i]	$\langle a_{\rm bin,ts}\rangle$[j]	$\langle r_{\rm ts}\rangle$[k]	$\langle t_{\rm max,insp}\rangle$[l]	$\langle t_{\rm ts}\rangle$[m]	$\langle N_{\rm int}\rangle$[n]
0.0	0.01	11.7	0.8928	0.8837	10.36	13.1	310.7	272.7	2.056e+04	4.288e+17	1.098e+05	7.14
0.0	0.02	11.7	0.8858	0.4643	15.44	14.38	355.6	279	2.06e+04	4.322e+17	2.217e+05	15.98
0.0	0.05	11.7	0.899	0.3333	21.66	18.78	313.8	262.7	1.624e+04	1.669e+17	4.092e+05	17.16
0.0	0.1	11.7	0.8812	0.2115	25.58	23.42	306.3	284.7	1.499e+04	1.212e+17	5.478e+05	40.87
0.0	0.2	11.7	0.8795	0.2727	24.27	21.42	217	213.4	1.081e+04	3.277e+16	7.039e+05	45.59
0.0	0.5	11.7	0.8863	0.1429	26.01	24.85	199.6	202.5	9716	2.139e+16	9.813e+05	81.95
0.0	1.0	11.7	0.8944	0.1525	25.93	24.5	192.6	193	9385	1.862e+16	2.081e+06	71.63
0.0	2.0	11.7	0.8639	0.06	29.49	28.59	212.7	204.7	9929	2.333e+16	3.976e+06	103.6
0.0	5.0	11.7	0.8646	0.0635	30.72	29.52	199.1	195.3	9169	1.696e+16	6.704e+06	112.3
0.0	10.0	11.7	0.8777	0.0984	31.25	29.09	170.7	154	7816	8.957e+15	1.05e+07	95.59
0.0	20.0	11.7	0.8971	0.0909	31.19	29.05	111.9	101.7	5127	1.658e+15	5.429e+07	105.2
0.0	50.0	11.7	0.9875	0.2962	26.75	22.98	28.15	19.82	1358	8.162e+12	6.861e+07	38.04
0.0	100.0	11.7	0.9914	0.4762	23.24	18.05	34.2	17.92	1728	2.14e+13	3.351e+07	11.14
0.0	200.0	11.7	0.9904	0.5	26.35	17.81	3.142	1.574	152.3	1.291e+09	2.128e+07	12.5
0.0	500.0	11.7	1	0.6364	20.69	14.42	0.0214	0.0096	1.122	3.803	3.055e+05	0.1364
0.0	1000.0	11.7	1	0.7813	22.04	12.68	0.0148	0.0045	0.7587	0.7952	1.476e+06	0.1562

Note. — (a) All runs had 500 realizations, $\rm M_{SMBH} = 10^6 M_\odot$. (b) Number distribution of stars on zero age main sequence: $dN/dM \propto M^{-\alpha}$. (c) Hardness of initial binary at $\rm r_{infl}$: $\epsilon = |E|/m_{\rm avg}\sigma^2$. (d) Average mass of all black holes given α and our evolutionary assumptions ($\rm M_\odot$). (e) Average orbital eccentricity around SMBH prior to tidal separation. (f) Fraction of runs in which tidally separated binary included something other than another black hole. (g) Average mass of BH-BH binaries that tidally separated ($\rm M_\odot$). (h) Average mass of BH-companion binaries that tidally separated ($\rm M_\odot$). (i) Average BH-BH binary semimajor axis prior to tidal separation (AU). (j) Average BH-companion binary semimajor axis prior to tidal separation (AU). (k) Average tidal separation radius (for average BH-BH binary) (AU). (l) Maximum gravitational radiation inspiral time for a captured BH at tidal separation radius (years). (m) Average time between first encounter and tidal separation (years). (n) Average number of interactions before tidal separation.

Table 6.15. Simulations of BH-BH Binaries in Nuclei with SMBH (Tidal Separations)[a]

α[b]	ϵ[c]	$\langle M_{\rm BH}\rangle$[d]	$\langle e_{\rm orb,ts}\rangle$[e]	$f_{\rm notBH}$[f]	$\langle M_{\rm bhbh,ts}\rangle$[g]	$\langle M_{\rm ts}\rangle$[h]	$\langle a_{\rm bhbh,ts}\rangle$[i]	$\langle a_{\rm bin,ts}\rangle$[j]	$\langle r_{\rm ts}\rangle$[k]	$\langle t_{\rm max,insp}\rangle$[l]	$\langle t_{\rm ts}\rangle$[m]	$\langle N_{\rm int}\rangle$[n]
0.0	0.01	11.7	0.8939	0	11.31	11.31	382.1	382.1	2.455e+04	8.718e+17	9.313e+04	1.278
0.0	0.02	11.7	0.8782	0	16.81	16.81	366.1	366.1	2.061e+04	4.33e+17	2.265e+05	8.257
0.0	0.05	11.7	0.8884	0	21.12	21.12	315.1	315.1	1.644e+04	1.753e+17	3.073e+05	13.94
0.0	0.1	11.7	0.9108	0	24.93	24.93	270.2	270.2	1.334e+04	7.6e+16	4.279e+05	22.86
0.0	0.2	11.7	0.9061	0	24.76	24.76	205.3	205.3	1.016e+04	2.557e+16	5.164e+05	52.81
0.0	0.5	11.7	0.8835	0	26.43	26.43	217.3	217.3	1.052e+04	2.94e+16	7.48e+05	79.82
0.0	1.0	11.7	0.9016	0	27.86	27.86	204.9	204.9	9748	2.167e+16	1.277e+06	85.38
0.0	2.0	11.7	0.8817	0	29.3	29.3	201.6	201.6	9431	1.899e+16	2.043e+06	93.25
0.0	5.0	11.7	0.8539	0	28.59	28.59	199.7	199.7	9419	1.889e+16	3.831e+06	116
0.0	10.0	11.7	0.8753	0	29.19	29.19	132.3	132.3	6197	3.539e+15	9.518e+06	115.3
0.0	20.0	11.7	0.8866	0	28.86	28.86	102.2	102.2	4805	1.279e+15	2.62e+07	92.78
0.0	50.0	11.7	0.9901	0	28.14	28.14	6.266	6.266	297.1	1.87e+10	2.725e+07	44
0.0	100.0	11.7	0.9836	0	28.7	28.7	6.892	6.892	324.7	2.668e+10	4.023e+07	56.18
0.0	200.0	11.7	0.995	0	20.86	20.86	3.657	3.657	191.6	3.234e+09	5.711e+07	15.38
0.0	500.0	11.7	1	0	20.6	20.6	0.0201	0.0201	1.056	2.984	8.371e+06	0.9375
0.0	1000.0	11.7	1	0	18.63	18.63	0.0100	0.0100	0.542	0.2071	1.56e+06	0.3529

Note. — (a) All runs had 500 realizations, $\rm M_{SMBH} = 10^6 M_\odot r_{infl}$. (b) Number distribution of stars on zero age main sequence: $dN/dM \propto M^{-\alpha}$. (c) Hardness of initial binary at $\rm r_{infl}$: $\epsilon = |E|/m_{\rm avg}\sigma^2$. (d) Average mass of all black holes given α and our evolutionary assumptions ($\rm M_\odot$). (e) Average orbital eccentricity around SMBH prior to tidal separation. (f) Fraction of runs in which tidally separated binary included something other than another black hole. (g) Average mass of BH-BH binaries that tidally separated ($\rm M_\odot$). (h) Average mass of BH-companion binaries that tidally separated ($\rm M_\odot M_{SMBH} = 10^6 M_\odot$). (i) Average BH-BH binary semimajor axis prior to tidal separation (AU). (j) Average BH-companion binary semimajor axis prior to tidal separation (AU). (k) Average tidal separation radius (for average BH-BH binary) (AU). (l) Maximum gravitational radiation inspiral time for a captured BH at tidal separation radius (years). (m) Average time between first encounter and tidal separation (years). (n) Average number of interactions before tidal separation.

6.3.4 Details of Binary End States

Figure 6.3 is a histogram that shows the distance from the SMBH at which binaries with borderline values of initial hardness ($\epsilon = 4$) meet their end. Those that soften significantly are usually ionized (shown in blue) at a few tenths of a pc, while those that are not softened tend to merge closer to the SMBH at a peak distance of ~ 0.1 pc. Tidal separations (in red) do not peak strongly at any radius. We see two distinct paths here: borderline binaries that merge tend to have fewer encounters and soften less than those that ionize, which allows them to sink further in the nucleus. Mergers then typically occur when an encounter drives up the eccentricity to a large value. In contrast, borderline binaries that soften have increasingly frequent encounters, and therefore do not travel very far in the nucleus before they ionize. For comparison, Figure 6.4 is a similar histogram, showing where hard binaries ($\epsilon = 50$) reach their end states. Most of these hard binaries merge at $\sim$0.1 pc, but those that do ionize (open, blue) or tidally separate (filled, red) generally do so at smaller radii than in the case of borderline binaries. We see from these plots that binaries tend to ionize, merge, or tidally separate well outside of the region ($r \sim 0.01$ pc) where resonant relaxation is important, therefore we feel that it is unlikely that the addition of resonant relaxation effects would greatly change our results.

We show in Figure 6.5 that mergers are strongly associated with very high binary eccentricities. While successive hardening could lead to mergers, the gravitational radiation inspiral time depends on the pericenter distance of the binary rather than its semimajor axis. Therefore an encounter that causes a jump to a high eccentricity will induce a merger.

Tidal separations occur predominantly at high eccentricities, as demonstrated in Figure 6.6, which extends the results of H09 to unequal masses. A high orbital

eccentricity is likely the factor that delineates binaries that are tidally separated from those that ionize. Binaries that succumb to these two outcomes have similar journeys. In both cases, the binaries tend to undergo multiple encounters which cause them to soften. Those that wander to a high eccentricity without ionizing have a close pericenter pass with the SMBH and are easily pulled apart, ending as tidal separations. The lack of dependence of mergers on orbital eccentricity is not surprising, since mergers are driven by large internal binary eccentricities.

Figure 6.7 is a scatter plot of the final hardness vs the initial hardness for binaries that range in initial ϵ. Each horizontal strip represents BH-BH binaries of differing initial hardness (as in e.g. Table 10), with very soft binaries at the bottom of the plot, and those that are initially hard at the top. The green circles are binaries that merged, red triangles are those that were tidally separated, and the blue squares are ionized binaries. We see that the initial hardness of a binary determines its range of possible end states. Those that are very hard to begin with merge, while those that are soft typically ionize. A borderline binary has the widest array of possible fates−merging or tidally separating if its internal or orbital eccentricity reaches a high value, and ionizing if it experiences runaway softening.

Additionally, the degree to which the binding energy deviates from its initial value is dependent on its initial hardness. Note that the hardness of very hard binaries does not stray far from the initial value, and the same is true for initially soft binaries. Very soft binaries are not around long before they are ionized, and hard binaries simply do not interact enough to harden significantly. We can illustrate the latter with a quick calculation. Recall that the interaction time is

$$t_{\rm int} = \frac{1}{n\Sigma\sigma} \quad , \tag{6.10}$$

where $\Sigma = \pi {r_{\rm p}}^2 + 2\pi r_{\rm p}(Gm_{\rm bin}/\sigma^2)$ is the encounter cross section for an interaction with close approach $r_{\rm p}$ and encounter speed σ. For a gravitationally focused

encounter,

$$\Sigma \approx 2\pi r_{\rm p}(\mathrm{G}m_{\rm bin}/\sigma^2) \quad , \tag{6.11}$$

and substituting $n = \rho/m_*$ gives an interaction time of

$$t_{\rm int} = \frac{m_*\sigma}{2\pi G m_{\rm bin}\rho\ r_{\rm p}} \quad . \tag{6.12}$$

The time that it takes for a hard binary to harden significantly is the time required for it to interact with approximately its own mass in stars. For these binaries, $r_{\rm p} = 2Gm_{\rm bin}/\sigma^2$, and the hardening timescale is

$$t_{\rm harden} = \left(\frac{m_{\rm bin}}{m_*}\right) t_{\rm int} = \frac{\sigma^3}{4\pi G^2 m_{\rm bin}\rho} \quad . \tag{6.13}$$

If we compare this to the time it takes for the binary to sink, or the relaxation time

$$t_{\rm rel} = \frac{1}{3\ln\Lambda}\frac{\sigma^3}{\mathrm{G}^2 m_{\rm bin}\rho} \tag{6.14}$$

then we find that

$$\frac{t_{\rm rel}}{t_{\rm harden}} = \frac{4\pi}{3\ln\Lambda} \approx 0.4 \quad . \tag{6.15}$$

A hard binary only interacts with $\sim 40\%$ of its mass in interlopers before it sinks to the center of the nucleus, which explains why our simulations show that very hard binaries do not harden significantly. Figure 6.8 further illustrates this point with a histogram of the ratio of initial to final binding energies for merging binaries with three different values of initial hardness. The energies of very hard binaries (shown in green) are largely unchanged, while the softer binaries (in red and blue) wander farther away from their initial values.

6.4 Discussion and Conclusions

6.4.1 The Fates of Binaries

If black hole binaries vary in initial hardness with equal numbers in equal $\log a$, as is the case for main-sequence binaries, then binaries in galactic nuclei have a variety of possible end states. Hard binaries tend to merge when they reach high eccentricities, while soft binaries are typically ionized. Tidal separations generally occur when the orbit around the SMBH is highly eccentric, although the softening that results from increasing encounter velocities near the SMBH makes it possible for binaries to be pulled apart at lower eccentricities. Encounters with hard binaries are more likely to lead to ejections, however ejections are rare due to the high escape velocities of galactic nuclei. Exchanges tend to produce binaries of above average mass, and, consequently, mergers and tidal separations involve BHs on the high end of the mass spectrum. As a rule, the overall fractions of mergers, ionizations, and tidal separations are very similar regardless of whether binaries begin with two BHs or a BH and a less massive companion. Additionally, binaries typically meet their fates within tens to hundreds of millions of years.

Binaries are tidally separated at distances of $\sim 10^3 - 10^4$ AU from the SMBH, depending on whether they are initially hard or soft. A newly-captured BH on a circular orbit with semimajor axis $a = 10^3$ AU will spiral in to the SMBH in $\sim 2 \times 10^{12}$ years, which is clearly too long for such BHs to produce detectable EMRIs. However, this close to the SMBH, interactions with passing stars will cause the eccentricity of the BH orbit to wander, and some percentage of these BHs will be perturbed into orbits that will inspiral and produce the circular EMRIs discussed in Ch. 5. We therefore view tidal separation of binaries as an important means of

depositing BHs near the SMBH, which will contribute to the overall rate of EMRI detections for LISA.

6.4.2 LIGO Detection Rates

Mergers of black hole binaries in galactic nuclei will produce sources for LIGO and other ground-based instruments. The fraction of binaries that merge in moderately segregated nuclei varies from zero for soft binaries to $\sim 96\%$ for very hard binaries. To be conservative in our estimate of LIGO detection rates, we will assume that 10% of BHs will merge in a Hubble time. If there is $\sim 10^6 M_\odot$ in stars within the radius of influence, and 3×10^{-3}(mass in stars/$M_\odot$)$= 3 \times 10^3$ BHs per nucleus, then there will be $\frac{3\times10^3\times0.1}{1.37\times10^{10}} = 2.2 \times 10^{-8}$ mergers per year per galaxy. With a number density of Milky Way equivalent galaxies of 10^{-2} Mpc^{-3}, and if the merger of a 20 $M_\odot$ binary is observable to a volume of 6.4×10^9 Mpc^3, we expect a rate of $(2.2 \times 10^{-8})(10^{-2})(6.4\times10^9) \approx 1.4$ mergers per year to be detectable with Advanced LIGO. This is a conservative estimate because the merger fraction could be significantly higher due to the contribution from hard binaries, and because we have restricted this calculation to within the radius of influence. The total number of BHs is likely higher because massive objects will sink to the center from outside the radius of influence in less than a Hubble time. Also, the observable volume of Advanced LIGO assumes a binary mass of $20M_\odot$, however we find that merging binaries tend to be more massive and could therefore be observed at greater distances. Given these considerations, rates of tens per year with Advanced LIGO are easily within reach.

6.4.3 Summary

In summary, black hole binaries in moderate-sized galactic nuclei containing SMBHs will contribute to the detection rates of LIGO and LISA. Binaries are often ionized due to high velocities at the galactic center, however significant fractions will merge or be tidally separated. Mergers in galactic nuclei will contribute $\sim$ tens of detections per year with Advanced LIGO. In general, hard binaries do not harden significantly as they sink, which means that they will not simply tighten continuously until they are close enough to the SMBH to be tidally separated. The hardening rate is simply not fast enough, and binaries ionize or merge before this scenario can play out. Rather, binaries that are tidally separated typically have at distances of $\sim$ few thousand AU, with eccentric orbits in excess of 0.85. The exception is very hard binaries that essentially plunge directly into the SMBH on radial orbits and hence do not contribute to the EMRI rate. The majority of tidal separations deposit BHs very near the SMBH, which will provide a supply of BHs that could be scattered into orbits that will spiral in and produce circular EMRI signals to be detected with LISA. Therefore, galactic nuclei are a unique environment that will produce gravitational wave sources in the sensitivity bands of both space- and ground-based gravitational wave detectors.

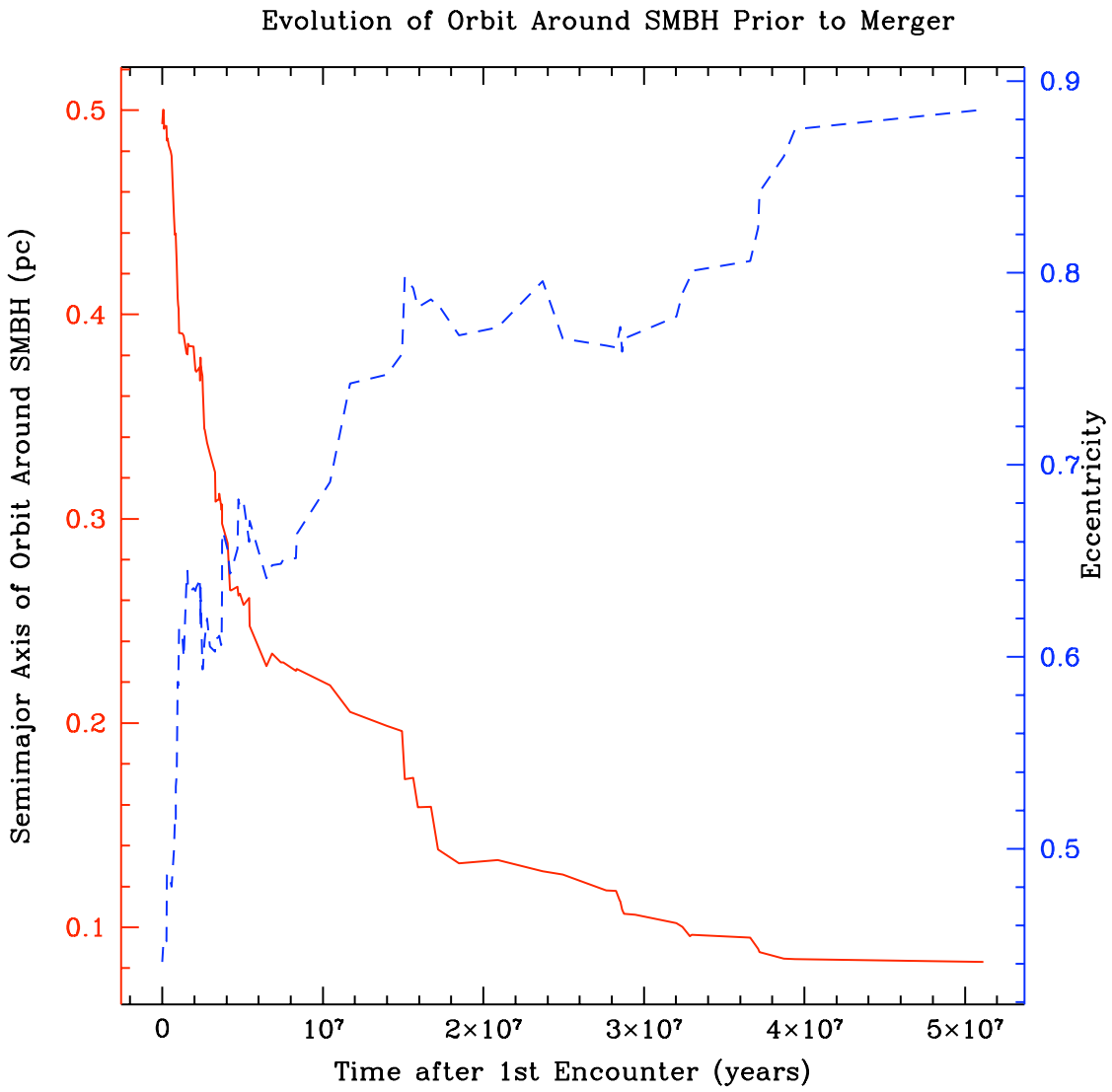

Figure 6.1: As the binary orbits the SMBH, its semimajor axis decreases (solid red curve and left vertical axis) and its eccentricity increases (dashed blue curve and right vertical axis) due to dynamical friction. This particular binary ends with a merger.

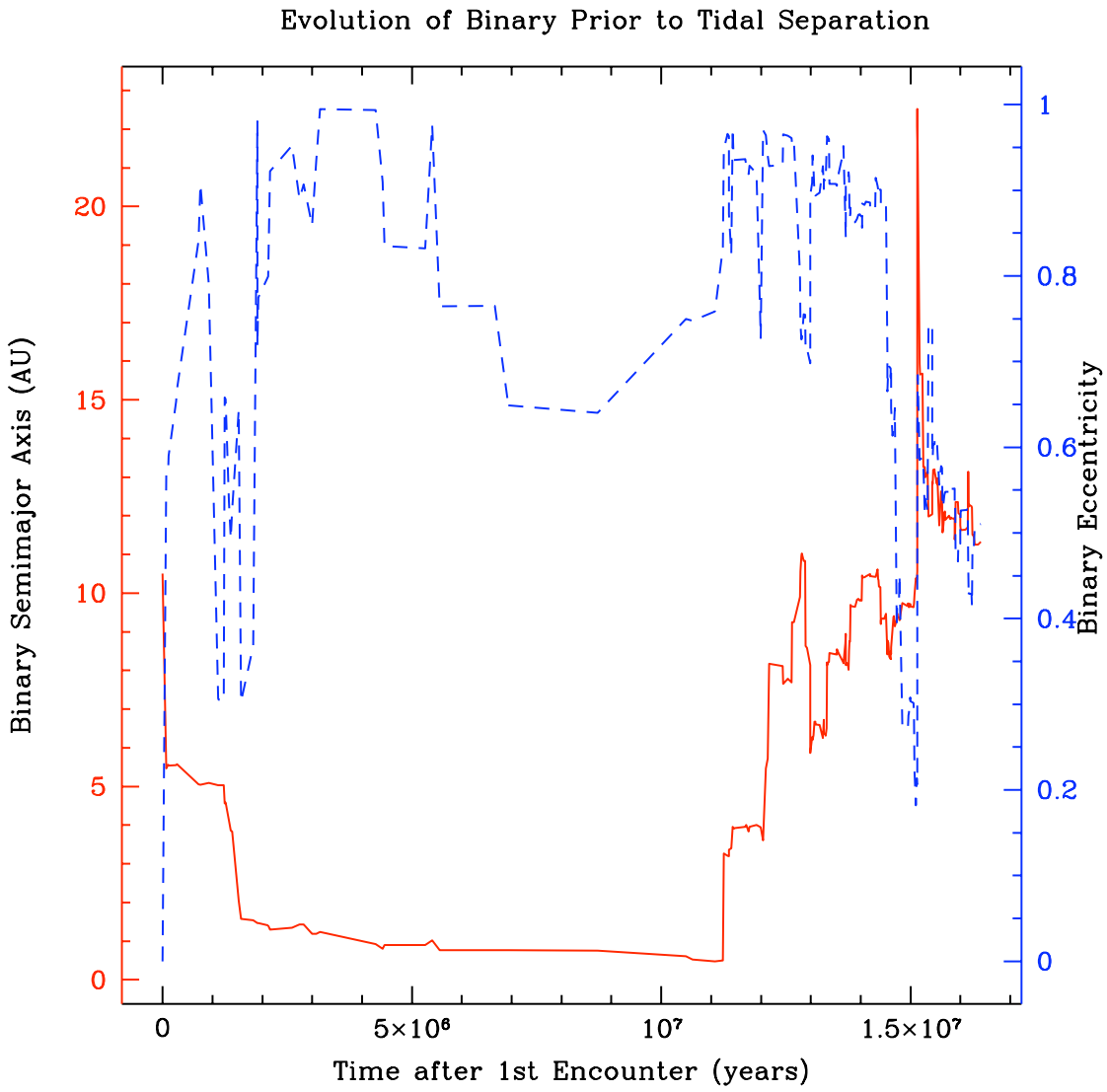

Figure 6.2: Multiple encounters cause the eccentricity (dashed blue curve and right vertical axis) of the binary to vary. In this instance, the semimajor axis (solid red curve and left vertical axis) of the binary decreases and subsequently increases prior to tidal separation.

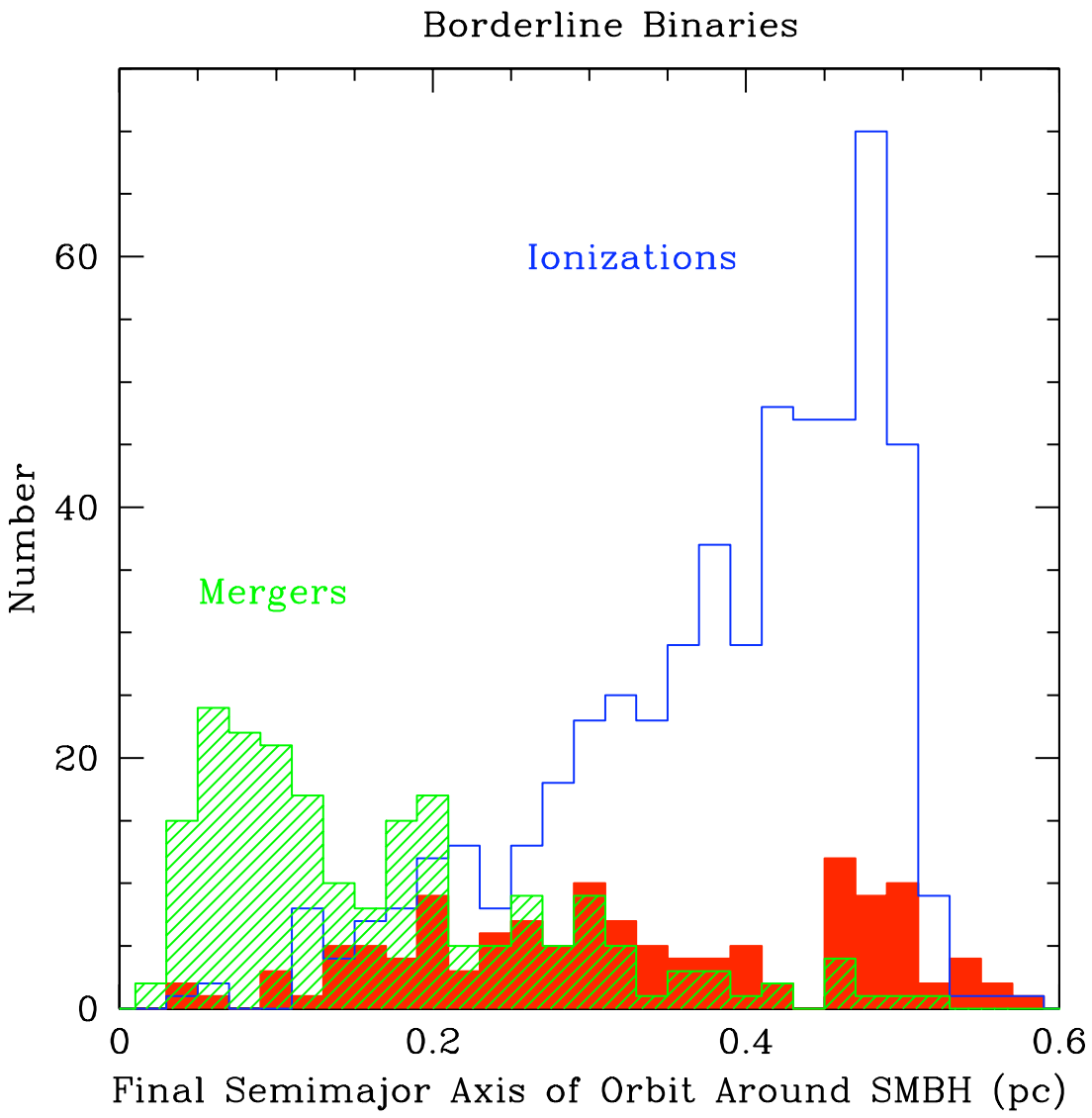

Figure 6.3: Histogram of the final distance from the SMBH reached by borderline ($\epsilon = 4$) binaries. Ionizations (blue, open) occur at a few tenths of a pc, while mergers (green, hatched) peak at ~ 0.1 pc. Tidal separations (red, filled) do not peak strongly at any radius. Borderline binaries that merge tend to have fewer encounters and soften less than those that ionize, which allows them to sink further in the nucleus. Mergers then typically occur when an encounter drives up the eccentricity to a large value. Borderline binaries that soften have increasingly frequent encounters, and therefore do not travel very far in the nucleus before they ionize.

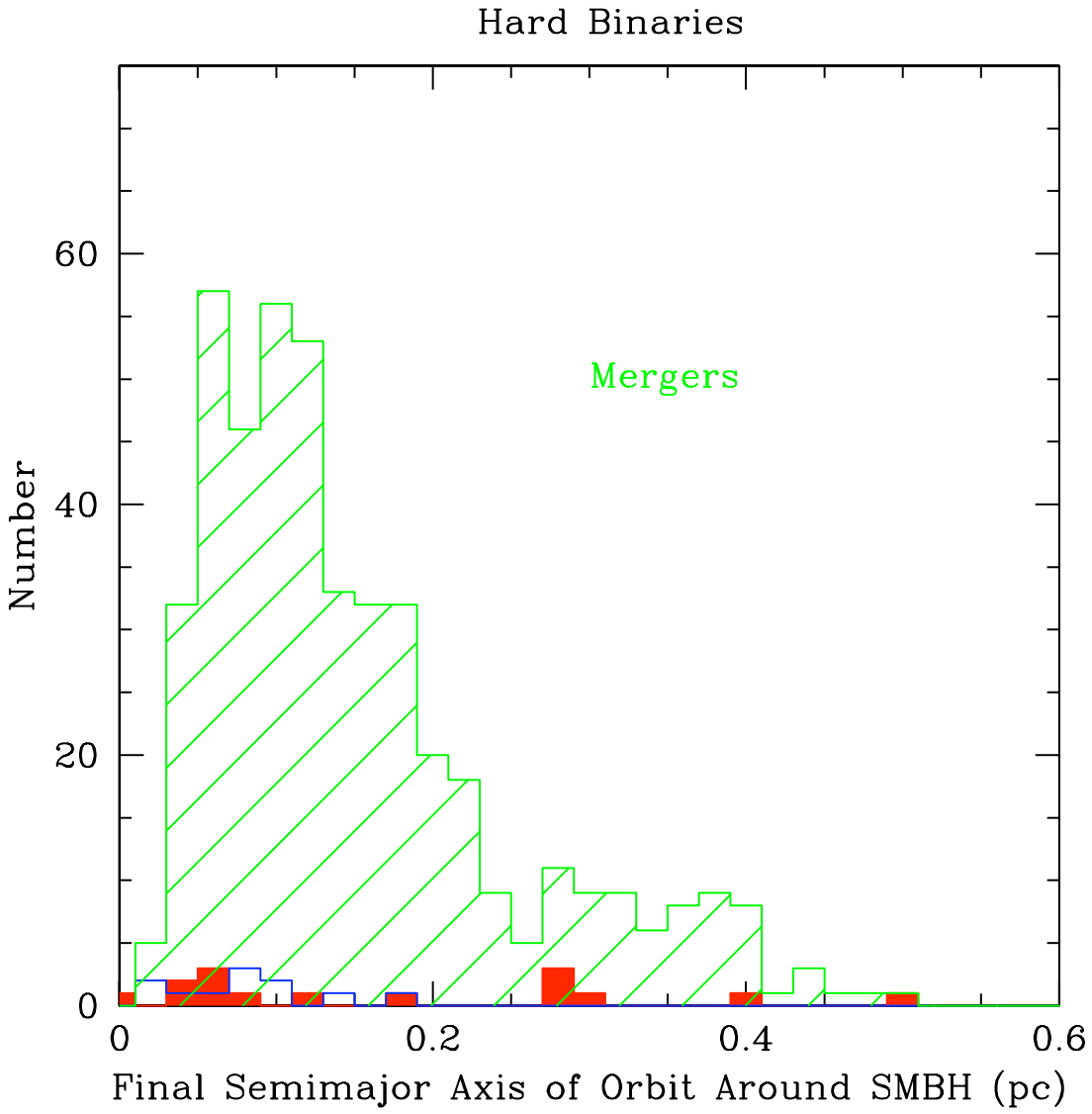

Figure 6.4: This is a similar histogram to Fig 6.3, but for harder binaries. Here we show the final distance from the SMBH reached by hard ($\epsilon = 50$) binaries. Most of these hard binaries merge at ∼0.1 pc, but those that do ionize (open, blue) or tidally separate (filled, red) generally do so at smaller radii than in the case of borderline binaries. This figure and Figure 6.3 demonstrate that binaries are destroyed outside of the region where resonant relaxation is effective (r ∼ 0.01 pc from the SMBH).

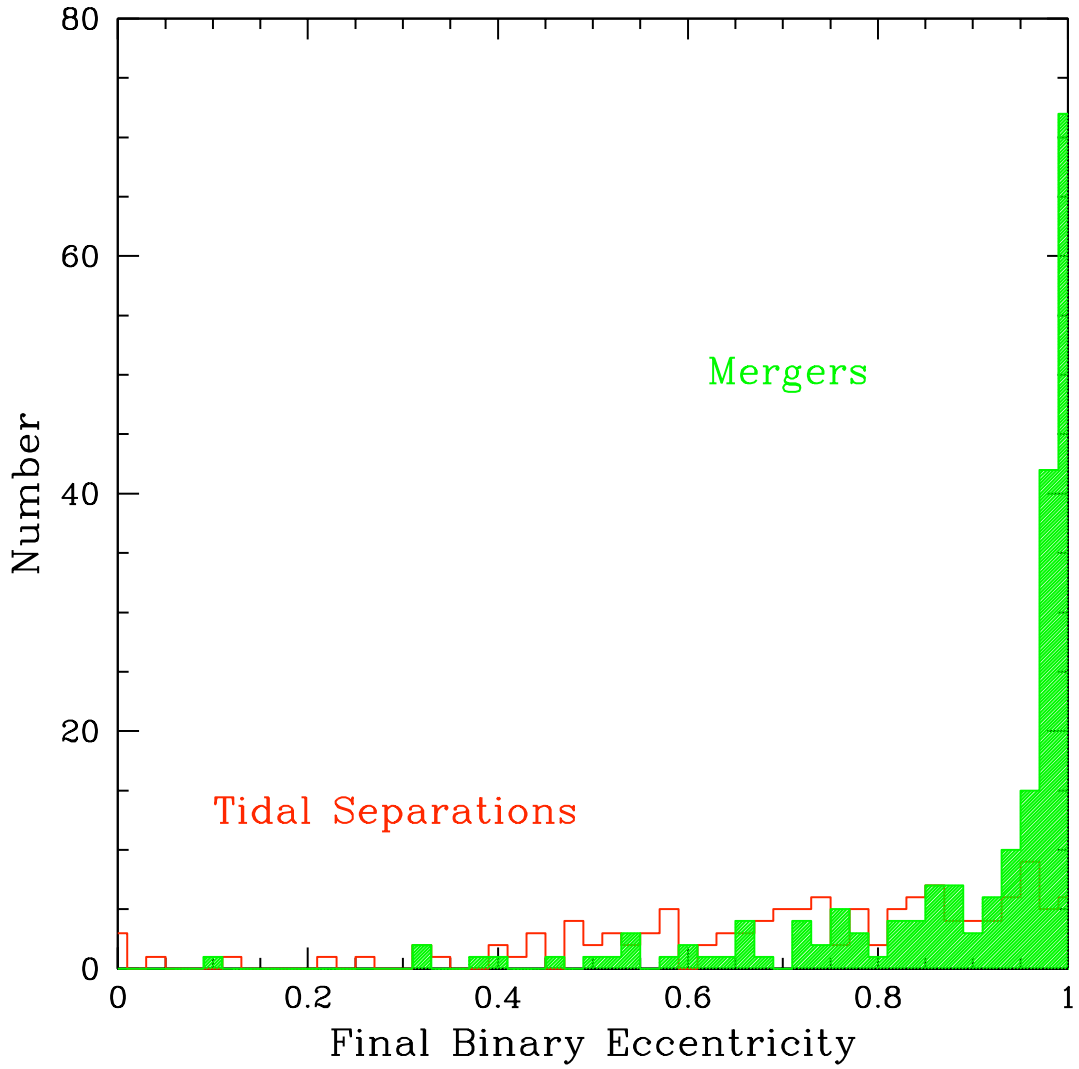

Figure 6.5: Mergers (filled, green) tend to occur when the binary has a high eccentricity. There is not a strong correlation for tidal separations (open, red).

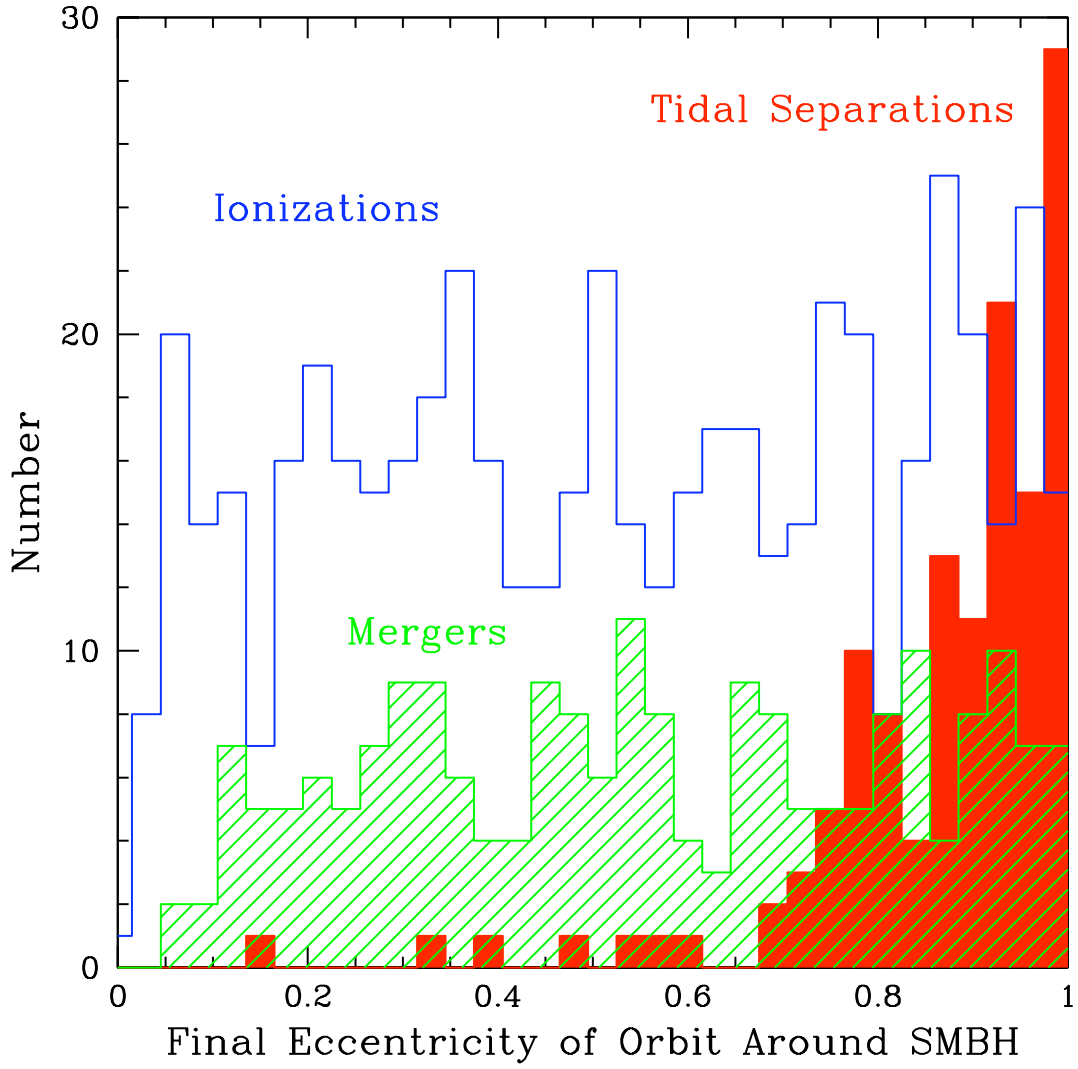

Figure 6.6: Binaries that wander to a high eccentricity without ionizing have a close pericenter pass with the SMBH and are easily pulled apart, ending as tidal separations (filled, red). The lack of dependence of mergers (in green, lightly hatched) on orbital eccentricity is not surprising, since mergers are driven by large internal eccentricities in binaries. Whether a binary is ionized depends on its softness, therefore ionizations (blue, open) can occur at any orbital eccentricity.

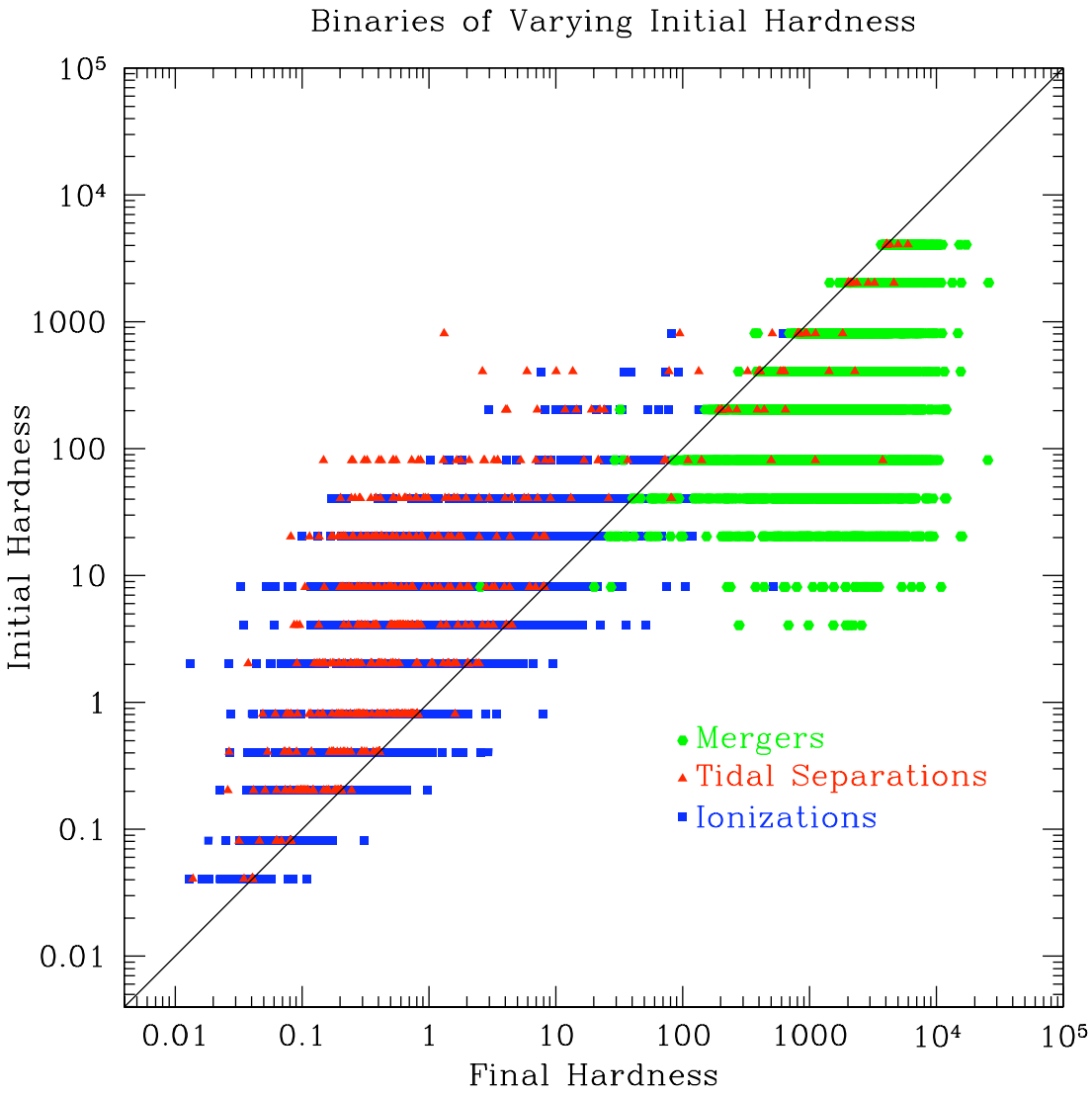

Figure 6.7: Scatter plot of the final hardness vs the initial hardness for binaries that range in initial hardness. Each horizontal strip represents BH-BH binaries of differing initial hardness with binaries that begin soft at the bottom of the plot, and those that are initially hard at the top. The green circles are binaries that merged, red triangles are those that were tidally separated, and the blue squares are ionized binaries. The initial hardness of a binary determines its range of possible end states. Those that are very hard to begin with merge, while those that are soft typically ionize. A borderline binary has the widest array of possible fates−merging or tidally separating if its internal or orbital eccentricity reaches a high value, and ionizing if it experiences runaway softening.

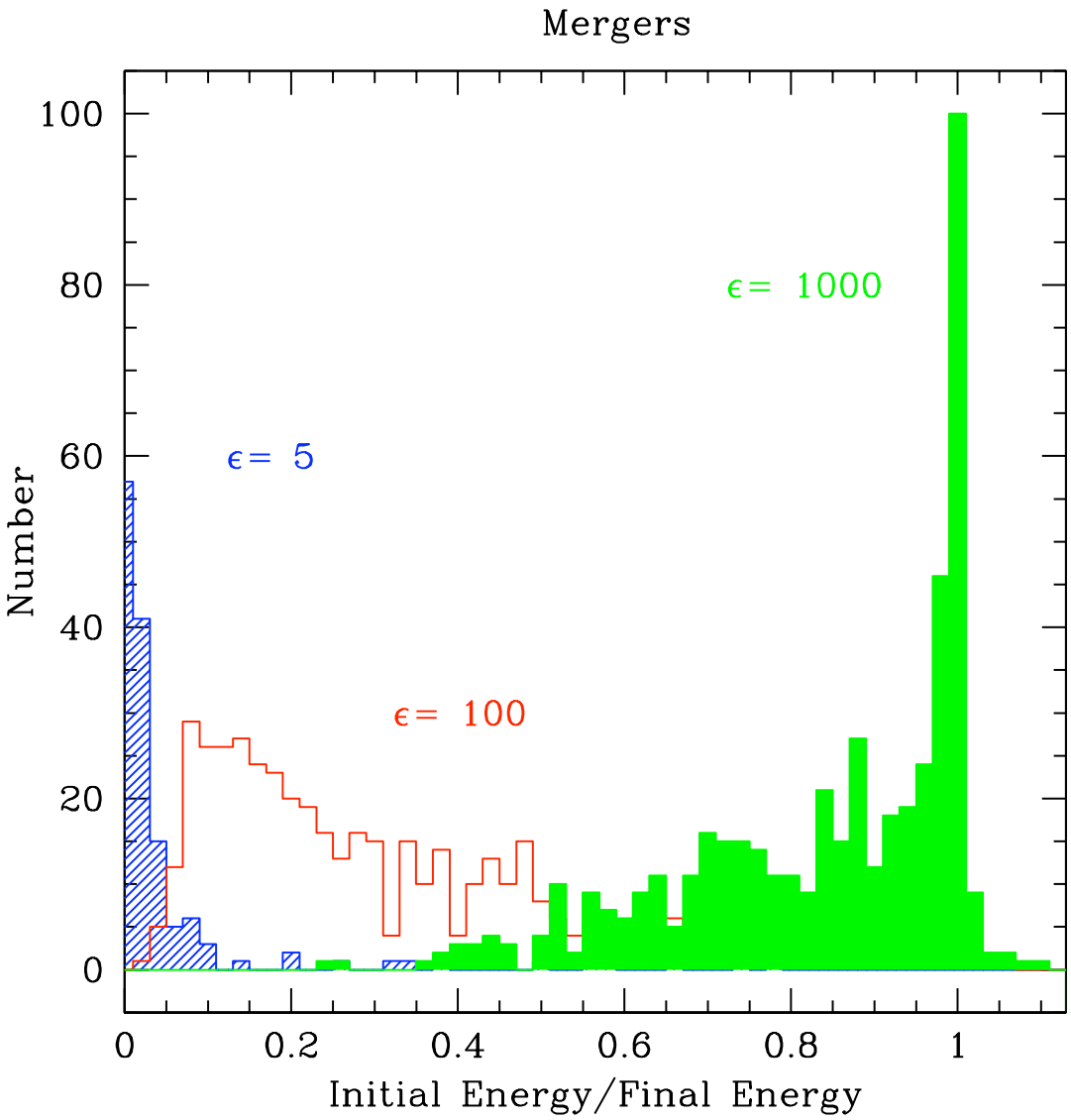

Figure 6.8: Histogram of the ratio of initial to final binding energies for merging binaries with three different values of initial hardness. The energies of very hard binaries (shown in solid green) are largely unchanged, while the softer binaries (in open red and hatched blue) wander farther away from their initial values.

Chapter 7

Conclusions

> "If you haven't found something strange during the day, it hasn't been much of a day."
>
> —John A. Wheeler

In this dissertation we have investigated binaries as a means of producing gravitational wave sources on two galactic scales: small galaxies with central nuclear star clusters but without massive black holes, and larger galaxies with supermassive black holes at their centers. We have shown that both of these environments are promising gravitational radiation hosts.

Our simulations show that binaries merge very efficiently in nuclear star clusters. In clusters with $V_{\rm esc} > 150$ km s^{-1} the overwhelming majority of BH binaries merge in the nuclear star cluster rather than being ejected, which is in contrast with globular clusters. Because globulars have comparatively low escape speeds, BH binaries that form within clusters generally merge after being ejected. Not only do nuclear star clusters tend to retain their BH binaries, but typically there are only 1–2 single BHs ejected per merger, which means that $> 50\%$ of BHs will merge. In contrast, at the 50 km s^{-1} escape speed typical of globulars, > 20 single BHs are

ejected per merger, which gives an efficiency of $< 10\%$. In nuclear star clusters that have undergone significant mass segregation, the average mass of BHs that merge, binary ejection fraction, number of singles ejected per merger, and number of BHs that merge with other BHs rather than another type of object are all robust against variation in the slope of the mass function. For less segregated clusters, the fraction of binaries retained rises quickly to unity because most of the objects that interact with the BHs are less massive stars. On the whole, we find that there is a large range of realistic parameters for which fewer than 10% of binary BHs are ejected before merging, which distinguishes nuclear star clusters as very effective producers of BH mergers. As such, we expect BH mergers in nuclear star clusters in small galaxies to contribute $\sim$tens of events per year to Advanced LIGO rates.

When we leave behind the realm of nuclear star clusters and explore larger galaxies that host supermassive black holes, a new type of gravitational radiation source becomes possible: extreme-mass ratio inspirals. If a BH binary sinks through the nucleus of such a galaxy, then we show that the SMBH can tidally separate the binary and capture one of the BHs onto an orbit that will spiral in and merge within a Hubble time. The resulting tidal separation EMRIs have larger pericenters and smaller apocenters than EMRIs formed by two-body capture. This will produce distinct classes of EMRI signals as detected by LISA: circular EMRIs resulting from binary separation, and eccentric EMRIs resulting from two-body capture. In addition, if $\sim$10% of BHs are in binaries, we find that tidal separation EMRIs could dominate the overall rates. Therefore, the detected signals will not only provide insight into the total number of BHs in nuclei, but also the fraction of those BHs that are in binaries. The binary fraction depends in large part on how well binaries are able to withstand multiple encounters in dense galactic centers.

A binary will have increasingly fast encounters as it sinks through a galactic nucleus toward the SMBH, which can lead to runaway softening and ionization. Because BHs sink more rapidly than less massive stars, we expect that nuclei will have undergone some degree of mass segregation. Hence, the factor that determines the fates of binaries is their initial hardness. We find that if black hole binaries have a range in initial internal energies, then ionizations, mergers, and tidal separations are all likely outcomes of encounters in galactic nuclei. Hard binaries interact less frequently and tend to merge when they reach high internal eccentricities, while soft binaries have more encounters and are typically ionized. Tidal separations generally occur when the orbit around the SMBH is highly eccentric, although the softening that results from the increase in encounter velocities near the SMBH makes it possible for some binaries to be pulled apart at lower eccentricities. Tidal separations that occur at distances of ∼thousand AU are close enough to the SMBH that passing stars can gradually perturb the BHs into orbits that will produce circular EMRIs and thereby contribute to the LISA rate. We find that encounters with hard binaries are more likely to cause ejections, however ejections are rare due to the high escape velocities of galactic nuclei and the infrequency with which very hard binaries interact. Massive BHs tend to swap into binaries, therefore mergers and tidal separations involve BHs on the high end of the mass spectrum. Our conservative estimate of the Advanced LIGO rate from dynamically-induced BH mergers in galactic nuclei is ∼tens per year.

In closing, we have demonstrated that mergers of BH binaries in nuclear star clusters in small galaxies, as well as mergers and tidal separations in larger galaxies with SMBHs are important sources of gravitational waves for both ground-based and space-based detectors.

Bibliography

Abbott, B., & et al. 2007, arXiv:0711.3041

Abt, H. A. 1983, ARA&A, 21, 343

Albrow, M. D., Gilliland, R. L., Brown, T. M., Edmonds, P. D., Guhathakurta, P., & Sarajedini, A. 2001, ApJ, 559, 1060

Ashby, N. 2003, Living Reviews in Relativity, 6, 1

Bahcall, J. N., & Wolf, R. A. 1976, ApJ, 209, 214

Baker, J. G., Boggs, W. D., Centrella, J., Kelly, B. J., McWilliams, S. T., Miller, M. C., & van Meter, J. R. 2008, ApJ, 682, L29

Barth, A. J. 2004, in IAU Symposium, Vol. 222, The Interplay Among Black Holes, Stars and ISM in Galactic Nuclei, ed. T. Storchi-Bergmann, L. C. Ho, & H. R. Schmitt, 3–8

Barth, A. J., Greene, J. E., & Ho, L. C. 2005, ApJ, 619, L151

Baumgardt, H., De Marchi, G., & Kroupa, P. 2008, ApJ, 685, 247

Begelman, M. C., Blandford, R. D., & Rees, M. J. 1980, Nature, 287, 307

Belczyński, K., & Bulik, T. 1999, A&A, 346, 91

Belczyński, K., Sadowski, A., & Rasio, F. A. 2004, ApJ, 611, 1068

Belczyński, K., Taam, R. E., Kalogera, V., Rasio, F. A., & Bulik, T. 2007, ApJ, 662, 504

Bender, P. L., & Hils, D. 1997, Classical and Quantum Gravity, 14, 1439

Binney, J., & Tremaine, S. 1987, Galactic Dynamics, ed. P. U. Press

Blanton, M. R., Hogg, D. W., Bahcall, N. A., Brinkmann, J., Britton, M., Connolly, A. J., Csabai, I., Fukugita, M., Loveday, J., Meiksin, A., Munn, J. A., Nichol, R. C., Okamura, S., Quinn, T., Schneider, D. P., Shimasaku, K., Strauss, M. A., Tegmark, M., Vogeley, M. S., & Weinberg, D. H. 2003, ApJ, 592, 819

Bogdanović, T., Reynolds, C. S., & Miller, M. C. 2007, ApJ, 661, L147

Böker, T. 2008, Journal of Physics Conference Series, 131, 012043

Böker, T., Laine, S., van der Marel, R. P., Sarzi, M., Rix, H.-W., Ho, L. C., & Shields, J. C. 2002, AJ, 123, 1389

Böker, T., Sarzi, M., McLaughlin, D. E., van der Marel, R. P., Rix, H.-W., Ho, L. C., & Shields, J. C. 2004, AJ, 127, 105

Böker, T., van der Marel, R. P., & Vacca, W. D. 1999, AJ, 118, 831

Brown, W. R., Geller, M. J., Kenyon, S. J., & Kurtz, M. J. 2005, ApJ, 622, L33

Campanelli, M., Lousto, C. O., Zlochower, Y., & Merritt, D. 2007, Physical Review Letters, 98, 231102

Capuzzo-Dolcetta, R., & Miocchi, P. 2008, ApJ, 681, 1136

Carollo, C. M., Stiavelli, M., de Zeeuw, P. T., & Mack, J. 1997, AJ, 114, 2366

Chandrasekhar, S. 1970, Physical Review Letters, 24, 611

Ciufolini, I., Gorini, V., Moschella, U., & Fré, P., eds. 2001, Gravitational Waves

Côté, P., Piatek, S., Ferrarese, L., Jordán, A., Merritt, D., Peng, E. W., Haşegan, M., Blakeslee, J. P., Mei, S., West, M. J., Milosavljević, M., & Tonry, J. L. 2006, ApJS, 165, 57

Danzmann, K., & et al. 1996, Classical and Quantum Gravity, 13, 247

De Marchi, G., Paresce, F., & Pulone, L. 2007, ApJ, 656, L65

Duquennoy, A., & Mayor, M. 1991, A&A, 248, 485

Emsellem, E., & van de Ven, G. 2008, ApJ, 674, 653

Fan, X., Narayanan, V. K., Lupton, R. H., Strauss, M. A., Knapp, G. R., Becker, R. H., White, R. L., Pentericci, L., Leggett, S. K., Haiman, Z., Gunn, J. E., Ivezić, Ž., Schneider, D. P., Anderson, S. F., Brinkmann, J., Bahcall, N. A., Connolly, A. J., Csabai, I., Doi, M., Fukugita, M., Geballe, T., Grebel, E. K., Harbeck, D., Hennessy, G., Lamb, D. Q., Miknaitis, G., Munn, J. A., Nichol, R., Okamura, S., Pier, J. R., Prada, F., Richards, G. T., Szalay, A., & York, D. G. 2001, AJ, 122, 2833

Farmer, A. J., & Phinney, E. S. 2003, MNRAS, 346, 1197

Ferrarese, L., Côté, P., Dalla Bontà, E., Peng, E. W., Merritt, D., Jordán, A., Blakeslee, J. P., Haşegan, M., Mei, S., Piatek, S., Tonry, J. L., & West, M. J. 2006, ApJ, 644, L21

Ferrarese, L., & Merritt, D. 2000, ApJ, 539, L9

Frank, J., & Rees, M. J. 1976, MNRAS, 176, 633

Freeman, K. C. 1993, in Astronomical Society of the Pacific Conference Series, Vol. 48, The Globular Cluster-Galaxy Connection, ed. G. H. Smith & J. P. Brodie, 608–+

Freitag, M. 2001, Classical and Quantum Gravity, 18, 4033

—. 2003, ApJ, 583, L21

Freitag, M., Amaro-Seoane, P., & Kalogera, V. 2006, ApJ, 649, 91

Freitag, M., & Benz, W. 2002, A&A, 394, 345

Friedman, J. L., & Schutz, B. F. 1978, ApJ, 222, 281

Gebhardt, K., Bender, R., Bower, G., Dressler, A., Faber, S. M., Filippenko, A. V., Green, R., Grillmair, C., Ho, L. C., Kormendy, J., Lauer, T. R., Magorrian, J., Pinkney, J., Richstone, D., & Tremaine, S. 2000, ApJ, 539, L13

Geha, M., Guhathakurta, P., & van der Marel, R. P. 2002, AJ, 124, 3073

Genzel, R., Schödel, R., Ott, T., Eisenhauer, F., Hofmann, R., Lehnert, M., Eckart,

A., Alexander, T., Sternberg, A., Lenzen, R., Clénet, Y., Lacombe, F., Rouan, D., Renzini, A., & Tacconi-Garman, L. E. 2003, ApJ, 594, 812

Gill, M., Trenti, M., Miller, M. C., van der Marel, R., Hamilton, D., & Stiavelli, M. 2008, ApJ, 686, 303

Glampedakis, K., Hughes, S. A., & Kennefick, D. 2002, Phys. Rev. D, 66, 064005

González, J. A., Hannam, M., Sperhake, U., Brügmann, B., & Husa, S. 2007, Physical Review Letters, 98, 231101

Gould, A., & Quillen, A. C. 2003, ApJ, 592, 935

Graham, A. W., & Spitler, L. 2009, ArXiv e-prints

Greene, J. E., & Ho, L. C. 2004, ApJ, 610, 722

—. 2007, ApJ, 667, 131

Gültekin, K., Miller, M. C., & Hamilton, D. P. 2004, ApJ, 616, 221

—. 2006, ApJ, 640, 156

Gürkan, M. A., Freitag, M., & Rasio, F. A. 2004, ApJ, 604, 632

Hamilton, D. P., & Burns, J. A. 1991, Icarus, 92, 118

—. 1992, Icarus, 96, 43

Heggie, D. C. 1975, MNRAS, 173, 729

Heggie, D. C., Hut, P., & McMillan, S. L. W. 1996, ApJ, 467, 359

Hills, J. G. 1975, Nature, 254, 295

—. 1988, Nature, 331, 687

—. 1991, AJ, 102, 704

Hils, D., & Bender, P. L. 1995, ApJ, 445, L7

Holley-Bockelmann, K., Gültekin, K., Shoemaker, D., & Yunes, N. 2008, ApJ, 686, 829

Holley-Bockelmann, K., Mihos, J. C., Sigurdsson, S., Hernquist, L., & Norman, C. 2002, ApJ, 567, 817

Hopman, C. 2009, ApJ, 700, 1933

Hopman, C., & Alexander, T. 2005, ApJ, 629, 362

Hughes, S. A. 2003, Annals of Physics, 303, 142

Hughes, S. A., Drasco, S., Flanagan, É. É., & Franklin, J. 2005, Physical Review Letters, 94, 221101

Hulse, R. A., & Taylor, H. J. 1974, in Bulletin of the American Astronomical Society, Vol. 6, Bulletin of the American Astronomical Society, 453–+

Ivanov, P. B. 2002, MNRAS, 336, 373

Ivanova, N., Belczynski, K., Fregeau, J. M., & Rasio, F. A. 2005, MNRAS, 358, 572

Jackson, J. D. 1998

Kormendy, J., & Richstone, D. 1995, ARA&A, 33, 581

Kramer, M., Stairs, I. H., Manchester, R. N., McLaughlin, M. A., Lyne, A. G., Ferdman, R. D., Burgay, M., Lorimer, D. R., Possenti, A., D'Amico, N., Sarkissian, J. M., Hobbs, G. B., Reynolds, J. E., Freire, P. C. C., & Camilo, F. 2006, Science, 314, 97

Kroupa, P., & Weidner, C. 2003, ApJ, 598, 1076

Kubota, A., & Makishima, K. 2005, ArXiv Astrophysics e-prints

Kulkarni, S. R., Hut, P., & McMillan, S. 1993, Nature, 364, 421

Lee, Y.-W., Gim, H. B., & Chung, C. 2007, ArXiv e-prints

Lightman, A. P., & Shapiro, S. L. 1977, ApJ, 211, 244

Lipunov, V. M., Postnov, K. A., & Prokhorov, M. E. 1997, MNRAS, 288, 245

Liu, J., McClintock, J. E., Narayan, R., Davis, S. W., & Orosz, J. A. 2008, ApJ, 679, L37

Magorrian, J., & Tremaine, S. 1999, MNRAS, 309, 447

Magorrian, J., Tremaine, S., Richstone, D., Bender, R., Bower, G., Dressler, A., Faber, S. M., Gebhardt, K., Green, R., Grillmair, C., Kormendy, J., & Lauer, T.

1998, AJ, 115, 2285

Makino, J., Fukushige, T., Koga, M., & Namura, K. 2003, PASJ, 55, 1163

Matthews, L. D., & Gallagher, III, J. S. 1997, AJ, 114, 1899

McClintock, J. E., Shafee, R., Narayan, R., Remillard, R. A., Davis, S. W., & Li, L.-X. 2006, ApJ, 652, 518

Merritt, D. 2006, Reports on Progress in Physics, 69, 2513

Merritt, D., & Ferrarese, L. 2001, ApJ, 547, 140

Merritt, D., & Poon, M. Y. 2004, ApJ, 606, 788

Miller, J. M. 2007a, ARA&A, 45, 441

Miller, M. C. 2007b, in American Institute of Physics Conference Series, Vol. 924, The Multicolored Landscape of Compact Objects and Their Explosive Origins, ed. T. di Salvo, G. L. Israel, L. Piersant, L. Burderi, G. Matt, A. Tornambe, & M. T. Menna, 681–688

Miller, M. C., Freitag, M., Hamilton, D. P., & Lauburg, V. M. 2005, ApJ, 631, L117

Miller, M. C., & Lauburg, V. M. 2009, ApJ, 692, 917

Milosavljević, M. 2004, ApJ, 605, L13

Mirabel, I. F., Mignani, R., Rodrigues, I., Combi, J. A., Rodríguez, L. F., & Guglielmetti, F. 2002, A&A, 395, 595

Miralda-Escudé, J., & Gould, A. 2000, ApJ, 545, 847

Misner, C. W., Thorne, K. S., & Wheeler, J. A. 1973, Gravitation, ed. C. W. Misner, K. S. Thorne, & J. A. Wheeler

Nelemans, G., Yungelson, L. R., & Portegies Zwart, S. F. 2001, A&A, 375, 890

Oey, M. S., & Clarke, C. J. 2005, ApJ, 620, L43

O'Leary, R. M., & Loeb, A. 2008, MNRAS, 383, 86

O'Leary, R. M., O'Shaughnessy, R., & Rasio, F. A. 2007, Phys. Rev. D, 76, 061504

O'Leary, R. M., Rasio, F. A., Fregeau, J. M., Ivanova, N., & O'Shaughnessy, R.

2006, ApJ, 637, 937

Ott, C. D. 2009, Classical and Quantum Gravity, 26, 063001

Peters, P. C. 1964, Physical Review, 136, 1224

Peters, P. C., & Mathews, J. 1963, Physical Review, 131, 435

Pfahl, E. 2005, ApJ, 626, 849

Phinney, E. S. 1991, ApJ, 380, L17

Poon, M. Y., & Merritt, D. 2002, ApJ, 568, L89

Portegies Zwart, S. F., & McMillan, S. L. W. 2000, ApJ, 528, L17

—. 2002, ApJ, 576, 899

Quinlan, G. D., & Shapiro, S. L. 1989, ApJ, 343, 725

Rees, M. J. 1984, ARA&A, 22, 471

Rezzolla, L., Lamb, F. K., Marković, D., & Shapiro, S. L. 2001, Phys. Rev. D, 64, 104013

Rossa, J., van der Marel, R. P., Böker, T., Gerssen, J., Ho, L. C., Rix, H.-W., Shields, J. C., & Walcher, C.-J. 2006, AJ, 132, 1074

Ryan, F. D. 1995, Phys. Rev. D, 52, 5707

—. 1997, Phys. Rev. D, 56, 1845

Schinnerer, E., Böker, T., Emsellem, E., & Downes, D. 2007, A&A, 462, L27

Schutz, B. F. 1996, Classical and Quantum Gravity, 13, 219

—. 2003, Gravity from the Ground Up, ed. C. U. Press

Seth, A. C., Blum, R. D., Bastian, N., Caldwell, N., & Debattista, V. P. 2008, ApJ, 687, 997

Seth, A. C., Dalcanton, J. J., Hodge, P. W., & Debattista, V. P. 2006, AJ, 132, 2539

Shaddock, D. A. 2008, Classical and Quantum Gravity, 25, 114012

Shafee, R., McClintock, J. E., Narayan, R., Davis, S. W., Li, L.-X., & Remillard, R. A. 2006, ApJ, 636, L113

Sigurdsson, S., & Hernquist, L. 1993, Nature, 364, 423

Sigurdsson, S., & Phinney, E. S. 1993, ApJ, 415, 631

—. 1995, ApJS, 99, 609

Sigurdsson, S., & Rees, M. J. 1997, MNRAS, 284, 318

Sosin, C. 1997, AJ, 114, 1517

Spitzer, L. 1987, Dynamical evolution of globular clusters, ed. P. U. Press

Stiavelli, M., Miller, B. W., Ferguson, H. C., Mack, J., Whitmore, B. C., & Lotz, J. M. 2001, AJ, 121, 1385

Syer, D., & Ulmer, A. 1999, MNRAS, 306, 35

Taylor, J. H., Hulse, R. A., Fowler, L. A., Gullahorn, G. E., & Rankin, J. M. 1976, ApJ, 206, L53

Teukolsky, S. A. 1973, ApJ, 185, 635

Thorne, K. S. 1996, in IAU Symposium, Vol. 165, Compact Stars in Binaries, ed. J. van Paradijs, E. P. J. van den Heuvel, & E. Kuulkers, 153–+

Tremaine, S., Gebhardt, K., Bender, R., Bower, G., Dressler, A., Faber, S. M., Filippenko, A. V., Green, R., Grillmair, C., Ho, L. C., Kormendy, J., Lauer, T. R., Magorrian, J., Pinkney, J., & Richstone, D. 2002, ApJ, 574, 740

Tremaine, S. D., Ostriker, J. P., & Spitzer, Jr., L. 1975, ApJ, 196, 407

Volonteri, M. 2007, ApJ, 663, L5

Volonteri, M., Haardt, F., & Gültekin, K. 2008, MNRAS, 384, 1387

Walcher, C. J., Böker, T., Charlot, S., Ho, L. C., Rix, H.-W., Rossa, J., Shields, J. C., & van der Marel, R. P. 2006, ApJ, 649, 692

Walcher, C. J., van der Marel, R. P., McLaughlin, D., Rix, H.-W., Böker, T., Häring, N., Ho, L. C., Sarzi, M., & Shields, J. C. 2005, ApJ, 618, 237

Webbink, R. F. 1985, in IAU Symposium, Vol. 113, Dynamics of Star Clusters, ed. J. Goodman & P. Hut, 541–577

Wehner, E. H., & Harris, W. E. 2006, ApJ, 644, L17

Young, P. 1980, ApJ, 242, 1232

Yu, Q., & Tremaine, S. 2003, ApJ, 599, 1129